2023-08-01

Paradox Diapir Inclusions as a Window into Diapiric Processes in Proximity to the Uncompahgre Uplift and the Early History of the Paradox Basin, Utah and Colorado

Madison Clare Woelfel
University of Texas at El Paso

PARADOX DIAPIR INCLUSIONS AS A WINDOW INTO DIAPIRIC PROCESSES IN PROXIMITY TO THE UNCOMPAHGRE UPLIFT AND THE EARLY HISTORY OF THE PARADOX BASIN, UTAH AND COLORADO

MADISON CLARE WOELFEL

Master's Program in Geological Sciences

APPROVED:

Katherine Giles, Ph.D., Chair

Benjamin Brunner, Ph.D. Co-Chair

Cora E. Gannaway Dalton, Ph.D.

Stephen L. Crites, Jr., Ph.D.
Dean of the Graduate School

Dedication

To my family. Zachary, Dad, Mom, Destin, Kaley, Cresta, Chase, Asher, and Johnna.

I could not have asked for a better one.

PARADOX DIAPIR INCLUSIONS AS A WINDOW INTO DIAPIRIC PROCESSES IN PROXIMITY TO THE UNCOMPAHGRE UPLIFT AND THE EARLY HISTORY OF THE PARADOX BASIN, UTAH AND COLORADO

by

MADISON CLARE WOELFEL, B.S.

THESIS

Presented to the Faculty of the Graduate School of

The University of Texas at El Paso

in Partial Fulfillment

of the Requirements

for the Degree of

MASTER OF SCIENCE

Department of Earth, Environmental and Resource Sciences

THE UNIVERSITY OF TEXAS AT EL PASO

August 2023

Acknowledgements

First, Zachary. You never doubted me when I said I would go back and get my master's. Not after the first year off, or the fourth. Well, I finally did go back, and I did it! You have been with me through the end of my undergraduate degree, an incredible sabbatical to experience the life of a ski bum like only a twenty-something could, this master's degree, and now our transition to professional life. None of this would have been possible without your support, belief, and love. Thank you for making me eat, take breaks, and have fun where and when I could. I really could not have done this without you. Thanks for adventuring with me.

My Dad, the best field assistant in the southwest. Dad, thank you for giving up three weeks of your life to eat dust and look at cool rocks in the Paradox with me. More than that, thank you for inspiring me. I am a geologist today, in part, because of you. I have never forgotten our many camping trips and the incredible geologic interpretations you gave us. Even if I now know they are sometimes wild speculations, it always made me want to complete the puzzle. I am so happy that you got to play such a big part in the greatest geologic puzzle I have ever worked on.

Mi familia. Mom, thank you for supporting me, loving me, and commiserating with me, I am lucky to be your daughter. You always made me realize that women could achieve anything. Destin, my best friend, words cannot express. You are everything and you deserve a page in here. Kaley, thank you for the constant support and confidence and for becoming my second sister. Cresta, thank you for visiting me, the last-minute Ruidoso trips, and mostly for making me take breaks and days off, it was essential. Chasey, thank you for always believing in me, supporting me, and never seeming concerned I would finish, it meant the world. Asher, thanks for looking up to me. Having someone look up to you forces you to be the best version of yourself, so in a big way, I could not have done this without you. Johnna (nananafeefiforama), the sister I chose, thank

you for always touting me as the raddest geologist in town, I will always lick rocks with you, and thanks to Chris for putting up with our shenanigans, but even more, for becoming my fourth brother (I always thought I needed another one). Ciera, thanks for sticking with me, my O.G. geo-friend. I'm glad we went through it together, especially field camp. If you know, you know.

Finally, for the academia. To my co-advisors, and co-chairs of my committee, Dr. Katherine Giles, and Dr. Benjamin Brunner, thank you. It is a short two words, and I cannot put everything I want to say in here, but I would like to share a little something with both of you.

Kate, you are actually the reason I ended up at UTEP. I never even considered UTEP until Peter Mozley told me "Hey, you should really talk to my friend Kate." I remember thinking, "UTEP? My dad went there…" Yet, after speaking with you and hearing about what the project would be, the choice was clear. Working with you has been a pleasure and an experience only the very lucky get to enjoy. I am honored to have worked with such an accomplished, smart, and downright cool person. Your love for carbonates may have drawn me in, but I really must thank you for opening my eyes to the exceptionally interesting world of salt tectonics.

Ben, when I first began interacting with Kate, she quickly informed me that she would be co-advising me with her cohort, "geochemistry guru, Dr. Ben Brunner." Now, I know I have told you that geochemistry was never my favorite, but when I heard this, I started wondering if the project was really that cool. Well, I am glad I stuck it out and had the opportunity to not only meet you and work with you, but to get to know you. You truly have a gift for making geochemistry understandable! Additionally, thank you for being, what felt at times like, my personal editor. The quick responses and helpful insights did not go unnoticed.

Evey, thank you for the cold eyes on my research and writing. Also, thanks for helping me take a step back and look at everything from a different perspective.

Many thanks to the UTEP faculty and staff that helped along the way and taught me some really cool stuff: Dr. Richard Langford, Dr. Julien Chaput, Dr. Jason Ricketts, Dr. Laura Alvarez Rueda, Dr. Hernan Moreno, Dr. James Kubicki, and Dr. Annette Veilleux. Of course, thank you to my peers and friends for making this experience that much better: Judith, Nuria, Valeria, Jorge, Elizabeth, Steph, Santi, Becca, David, Rachelle, and Alan.

I would like to extend my gratitude to Dr. Peter Mozley for not only his help when I was applying to graduate school, but for inspiring me. I will never forget when you told me that I could one day be a sedimentary petrographer. I guess it really stuck. Thanks also to Dr. Dana Ulmer-Scholle who originally taught me about carbonates.

Financial support from research grants, scholarships, and the Institute of Tectonic Studies Salt-Sediment Interaction Research Consortium made this work possible. Funding for field work and laboratory analyses was made possible through research grants from the American Association of Petroleum Geologists, the Geological Society of America, and the Society for Sedimentary Geology as well as the George B. McBride Graduate Fellowship Endowment. I would also like to express my extreme gratitude for the following scholarships: the E. Russell Lloyd Memorial and WinGS (Women in Geological Sciences) scholarships from the West Texas Geological Society, 2022 and 2023 scholarships from the Permian Basin Section of SEPM, and 2022 and 2023 scholarships from the Southwest Section of AAPG.

Abstract

Layered evaporite sequences, cyclic, kilometer-thick deposits of salt, are among the most unusual and fascinating lithologies that geologists encounter. There is no recent analogue to their formation, and their ability to flow when subject to differential pressure makes them unique. Salt structures serve as sources for halite, bittern salts, metals, and hydrocarbons and can be used for storage of materials, including hydrocarbons, carbon dioxide, hydrogen, and nuclear waste. Basins in which layered evaporite sequences are deposited receive detrital input sporadically from adjacent areas, depositing inclusions of non-evaporite lithologies that are entrained when salt flows. These inclusions are exposed in a series of breached salt walls in the Paradox Basin and provide a window into the paleogeography and earliest stages of basin formation, for example if it was born as a uniform depression or as a series of indentations separated by steps.

Integrating field, microscopic, and geochemical observations, I have reconstructed the depositional setting of inclusions from three different sites: the Gypsum Valley, Salt Valley, and Sinbad Valley diapirs. I have used this information to elucidate the early history of detrital input into the Paradox Basin, and thereby gained insight into its paleogeography. Known non-evaporite lithologies in the Paradox Formation identified in this study include black shale, limestone, and sandstone. These lithologies are exposed in breached salt walls today as diapiric inclusions derived from the Paradox Formation layered evaporite sequence that were carried to the surface during diapirism. Conglomerate inclusions found in Paradox Basin diapirs, on the other hand, are not a known or recorded lithology of the Paradox Formation. This study reveals that they were part of the Paradox Formation and that the most likely detrital source was basement steps within the basin that were active during its deposition and contributed as a significant source of detritus in the Paradox layered evaporite sequence.

Table of Contents

Acknowledgements v

Abstract viii

Table of Contents ix

List of Tables xii

List of Figures xiii

List of Plots xv

Chapter 1: Introduction 1

1.1 Layered Evaporites, Salt Tectonics, and Inclusions of Non-Evaporite Lithologies 6

1.2 Geologic Background 9

1.2.1 Tectonics and Paleogeography 9

1.2.2 Pre-Salt Stratigraphy 17

1.2.2.1 Cambrian 18

1.2.2.2 Devonian 21

1.2.2.3 Mississippian to Early Pennsylvanian 22

1.2.3 Layered Evaporite Sequence (i.e., 'Salt') 26

1.2.3.1 Paradox Formation 27

1.2.4 Post-Salt Stratigraphy 28

1.2.4.1 Honaker Trail Formation 28

1.2.4.2 Cutler Group 30

1.2.4.3 Triassic and Younger Stratigraphy 30

1.3 Focus of Research 30

1.4 Hypotheses 31

1.4.1 Hypothesis A 31

1.4.2 Hypothesis B 32

1.5 Field Sites 32

1.5.1 Sinbad Valley 33

1.5.2 Salt Valley 35

1.5.3 Gypsum Valley 37

1.5.4 Onion Creek 37

1.5.5 Professor Valley 38
1.5.6 Moab Valley 38
1.6 Methodology 39
1.6.1 Field Work 39
1.6.2 Petrography 40
1.6.3 Isotope Analyses 40
Chapter 2: Results 42
2.1 Inclusion Lithologies: Description, Distribution, and Interpretation 42
2.1.1 BS: Black Shale (Black Laminated Mudstone) 47
2.1.2 SL: Sandy Limestone 50
2.1.2.1 SLnf: Non-Fossiliferous Sandy Limestone 51
2.1.2.2 SLmb: Mica-Bearing Sandy Limestone 55
2.1.2.3 SLf: Fossiliferous Sandy Limestone 60
2.1.2.4 SLo: Oolitic Sandy Limestone 63
2.1.3 SS: Sandstone 64
2.1.3.1 SSq: Quartz Sandstone 64
2.1.3.2 SScq: Carbonate-Quartz Sandstone 67
2.1.4 CG: Conglomerate 71
2.1.4.1 CGc: Carbonate-Clast Conglomerate 71
2.1.4.2 CGcs: Carbonate-Sandstone-Clast Conglomerate 86
2.2 Field Relationships 91
2.2.1 Sinbad Valley 91
2.2.2 Salt Valley 96
2.2.3 Gypsum Valley 100
2.3 Diagenesis 105
Chapter 3: Discussion 108
3.1 Where do Inclusions Come From? 108
3.2 Depositional Setting of Non-Evaporite Lithologies 108
3.2.1 Determination of Source of Inclusions 108
3.2.2 Derivation of Anomalous Conglomerates from Basement Steps 117
3.3 Using Inclusions to Determine the Timing and Evolution of the Paradox LES 119
3.3.1 Compaction and Diagenesis of Inclusions 119

3.3.2 History of the Deposition and Entrainment of Inclusions 124

Chapter 4: Conclusions 126

Chapter 5: Future Outlook 130

References 132

Vita 147

List of Tables

Table 1: Petrographic attributes of sandy limestone samples 43
Table 2: Petrographic attributes of sandstone samples 44
Table 3: Petrographic attributes of conglomerate samples 45
Table 4: Petrographic attributes of conglomerate clast samples 46

List of Figures

Figure 1: Map of the Paradox Basin and Uncompahgre uplift 2
Figure 2: Schematic cross section of the Paradox Basin with layered evaporite sequence basin fill 3
Figure 3: Typical Paradox Formation layered evaporite depositional cycle lithologies 4
Figure 4: Schematic cross-section of breached Paradox salt wall 5
Figure 5: Paradox Basin development 10
Figure 6: Stratigraphic and structural sections of the Paradox Basin with underlying basement steps 11
Figure 7: Diagram of major fault lineaments underlying the Paradox Basin 12
Figure 8: Paleogeography of the Paradox Basin area during Desmoinesian (Middle Pennsylvanian) time 14
Figure 9: Pre-salt strata of the Colorado Plateau area 18
Figure 10: Comprehensive stratigraphic column of the Paradox Basin area 20
Figure 11: Stratigraphic column of Devonian to Mississippian rocks in the Paradox Basin 23
Figure 12: Depositional facies and karsted surface of Leadville Limestone 24
Figure 13: Paradox Basin fill 27
Figure 14: Variety of clast lithologies in Sinbad Valley 34
Figure 15: Fossils in Sinbad Valley carbonate and chert clasts 35
Figure 16: Gastropod in chert 36
Figure 17: Outcrop photographs of inclusions 42
Figure 18: Gypsum Valley Image Map #1 49
Figure 19: Outcrop photographs of non-fossiliferous sandy limestone (SLnf) sample locations 52
Figure 20: Photomicrographs of microspar-dominated SLnf 53
Figure 21: Photomicrographs of micrite-dominated SLnf 54
Figure 22: Gypsum Valley Image Map #2 56
Figure 23: Gypsum Valley Image Map #3 57
Figure 24: Photomicrographs of mica-bearing sandy limestone (SLmb) 58
Figure 25: Photomicrographs of SLmb 59
Figure 26: Outcrop images of fossiliferous sandy limestone (SLf) sample locations and photomicrographs of SLf boundstones 61
Figure 27: Photomicrographs of SLf packstones 62
Figure 28: Outcrop image and photomicrograph of oolitic sandy limestone (SLo) 63
Figure 29: Outcrop images of quartz sandstone (SSq) sample locations 65
Figure 30: Photomicrographs of SSq 66
Figure 31: Outcrop images of a carbonate-quartz sandstone (SScq) sample locations 68
Figure 32: Photomicrographs of SScq 69
Figure 33: Photomicrographs of SScq 70
Figure 34: Carbonate-clast conglomerate (CGc) clast sample locations 72
Figure 35: Sandy pockets in CGc outcrops 73
Figure 36: Flute casts in Salt Valley CGc outcrop 73
Figure 37: Photomicrographs of CGc 75
Figure 38: Photomicrographs of CGc fossiliferous carbonate clasts 77
Figure 39: Photomicrographs of CGc fossiliferous carbonate clasts 78
Figure 40: Outcrop images of CGc sample locations and photomicrograph of chert clast 80

Figure 41: Photomicrographs of CGc non-fossiliferous carbonate clasts 81
Figure 42: Photomicrographs of CGc non-fossiliferous chert clasts 83
Figure 43: Photomicrographs of CGc fossiliferous chert clasts with silicification of grains 84
Figure 44: Photomicrographs of CGc fossiliferous chert clasts with silicification of matrix 85
Figure 45: Carbonate sandstone clast conglomerate (CGcs) outcrop images 87
Figure 46: Hand sample images and photomicrographs of CGcs matrix 88
Figure 47: Hand sample images and photomicrographs of CGcs sandstone clasts 90
Figure 48: Geologic map of inclusions in Sinbad Valley 92
Figure 49: Sandstone outcrop at Sinbad Valley 93
Figure 50: Sinbad Valley red conglomerate outcrop with sandstone clasts 95
Figure 51: Geologic map of inclusions in Salt Valley 96
Figure 52: Overview image of Salt Valley sandstone outcrop 97
Figure 53: Prominent conglomerate outcrop in Salt Valley 98
Figure 54: Salt Valley sandstone outcrop ridge former 99
Figure 55: Overview of Gypsum Valley 101
Figure 56: Stereonet and fold data from Gypsum Valley outcrop 103
Figure 57: Gypsum Valley stratigraphic column of inclusion outcrop 104
Figure 58: Sedimentary Processes in the Paradox Basin 114

List of Plots

Plot 1: Isotope analysis of carbonates in inclusions..... 107
Plot 2: Isotopic composition data for the Leadville Limestone 123

Chapter 1: Introduction

The Paradox Basin (PB) located in the Four Corners region of the southwestern United States (Fig. 1) is a salt basin that hosts significant resources of petroleum, potash, and ores and has potential as a source of lithium-rich brines and as a site for hydrogen gas (H_2) storage and carbon dioxide (CO_2) sequestration (e.g., Nuccio and Condon, 1996). Central to the framework and evolution of these resources is the Paradox Formation, a layered evaporite sequence (LES) deposited at the base of the basin that fed the growth of a series of salt walls (Fig. 2; Doelling, 1988; Raup and Hite, 1992; Williams-Stroud, 1994). This formation provides all elements of petroleum systems including organic-rich shales as source, permeable and porous siliciclastics as reservoirs, and mobile halite as the seal, altogether setting up diapirs as self-contained salt-tectonic hydrocarbon traps (e.g., Nuccio and Condon, 1996). Despite the importance of the Paradox LES to natural resources in the area, knowledge about what is in the diapirs besides evaporite minerals, as well as the depositional setting and early tectonic history of the proximal foredeep salt basin during deposition of the Paradox Formation is rudimentary. This deficit is due to the inability to directly access the deeply buried strata, limited wellbore data, and seismic resolution limitations in areas strongly affected by salt diapirism.

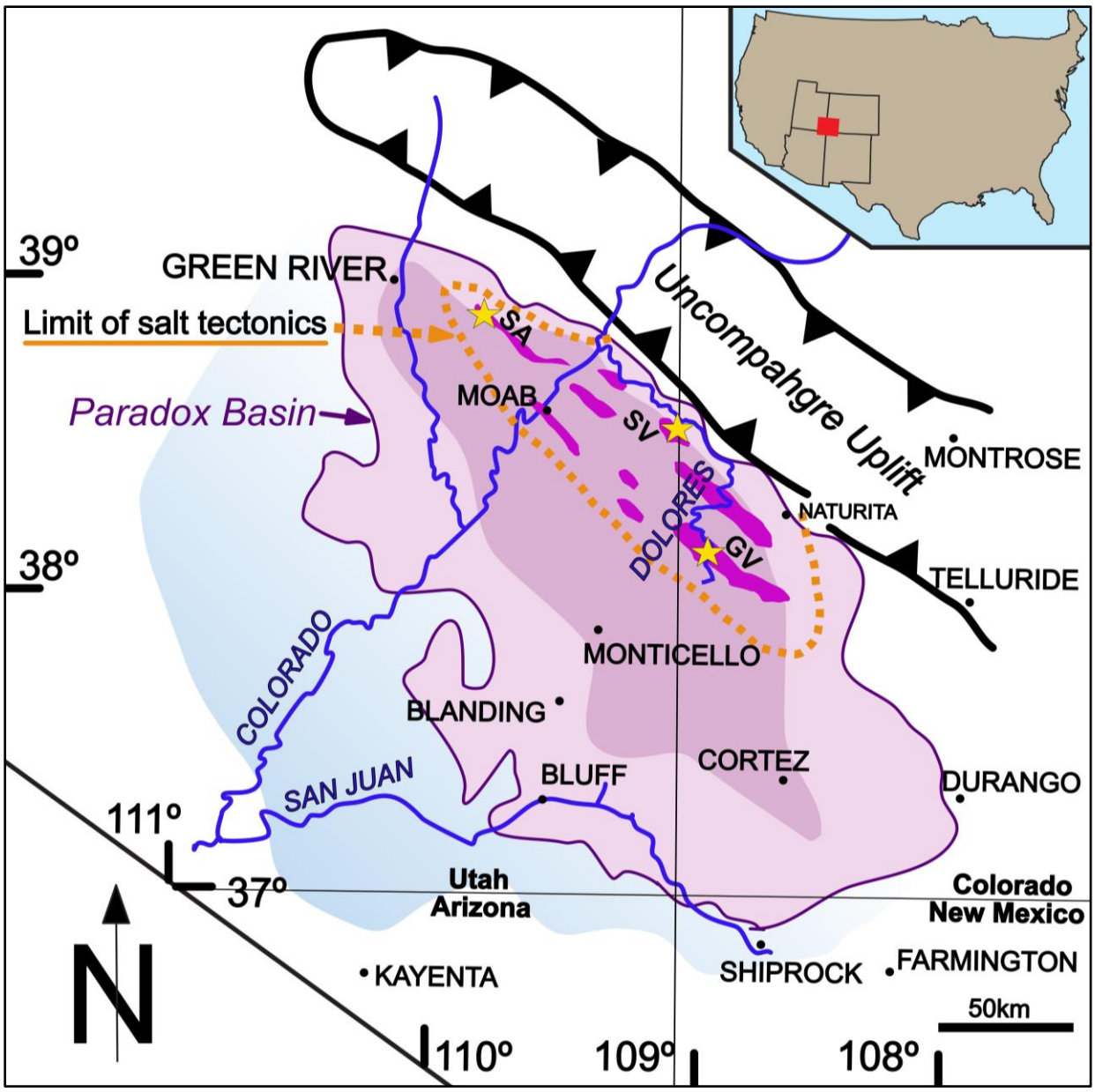

Figure 1: Map of the Paradox Basin and Uncompahgre uplift
Locations of breached salt walls shown in fuchsia. Yellow stars indicate targeted diapir exposures from west to east: Salt (SA), Sinbad (SV), and Gypsum (GV) valleys. Dashed orange line represents the extent of salt tectonics in the Paradox Basin, dark pink color indicates presence of potash salts in the subsurface, light pink color indicates presence of halite in the subsurface, dark purple line defines the limit of Paradox Formation salt, which defines the limit of the Paradox Basin, blue-gray color indicates presence of age-equivalent normal marine carbonates (Figure modified from Brunner et al., 2019).

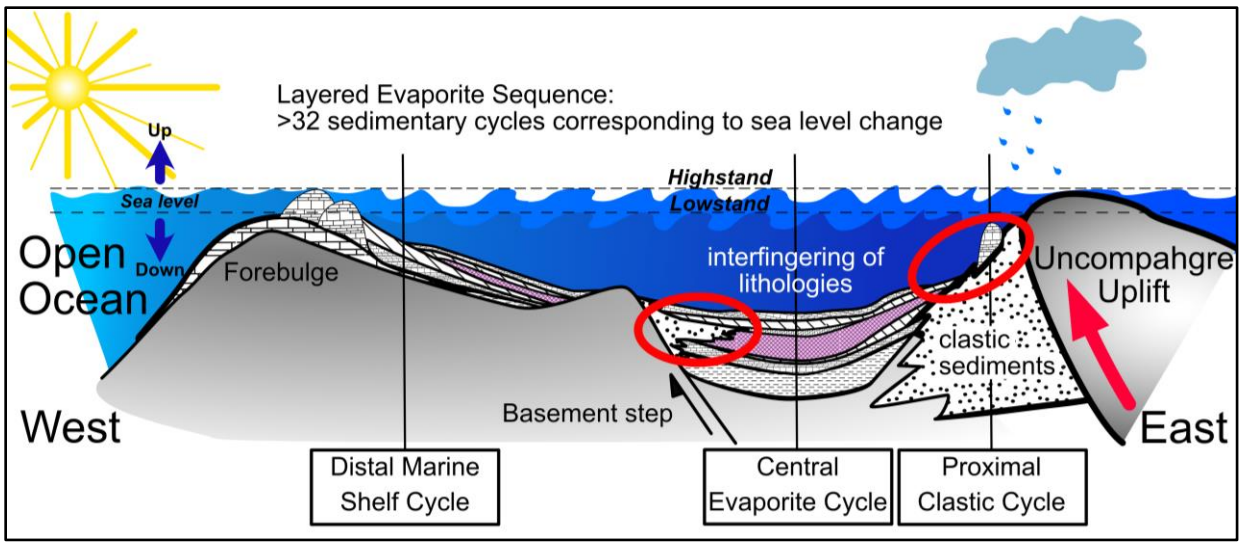

Figure 2: Schematic cross section of the Paradox Basin with layered evaporite sequence basin fill Red ovals show potential source of conglomerates with clastic wedges from the Uncompahgre uplift and basement steps. Pink indicates the presence of halite. Inclusions reflect a variety of siliciclastics and carbonates (Figure modified from Hite and Buckner, 1981; Williams-Stroud, 1994).

The PB salt walls contain non-evaporite inclusions, some of which crop out in a series of breached salt walls in the basin (Figs. 3, 4). Common diapiric inclusions are organic-rich carbonate mudstones (black shale) and sparsely fossiliferous dolostones derived from the Paradox LES that were transported upward during diapirism (Figs. 3, 4; Hite and Buckner, 1981; Rasmussen and Rasmussen, 2009). However, previous work and my reconnaissance studies document other types of inclusion lithologies as well (Dane, 1935; Gard, 1976; Hudson et al., 2017; Deatrick, 2019; Thompson Jobe et al., 2019; Lankford-Bravo, 2021; Scott, 2022). The exposed inclusions provide a unique opportunity to examine the lithologic detail of these otherwise inaccessible strata and provide new insight into the depositional and paleogeographic setting of the earliest phases of basin formation and salt tectonism.

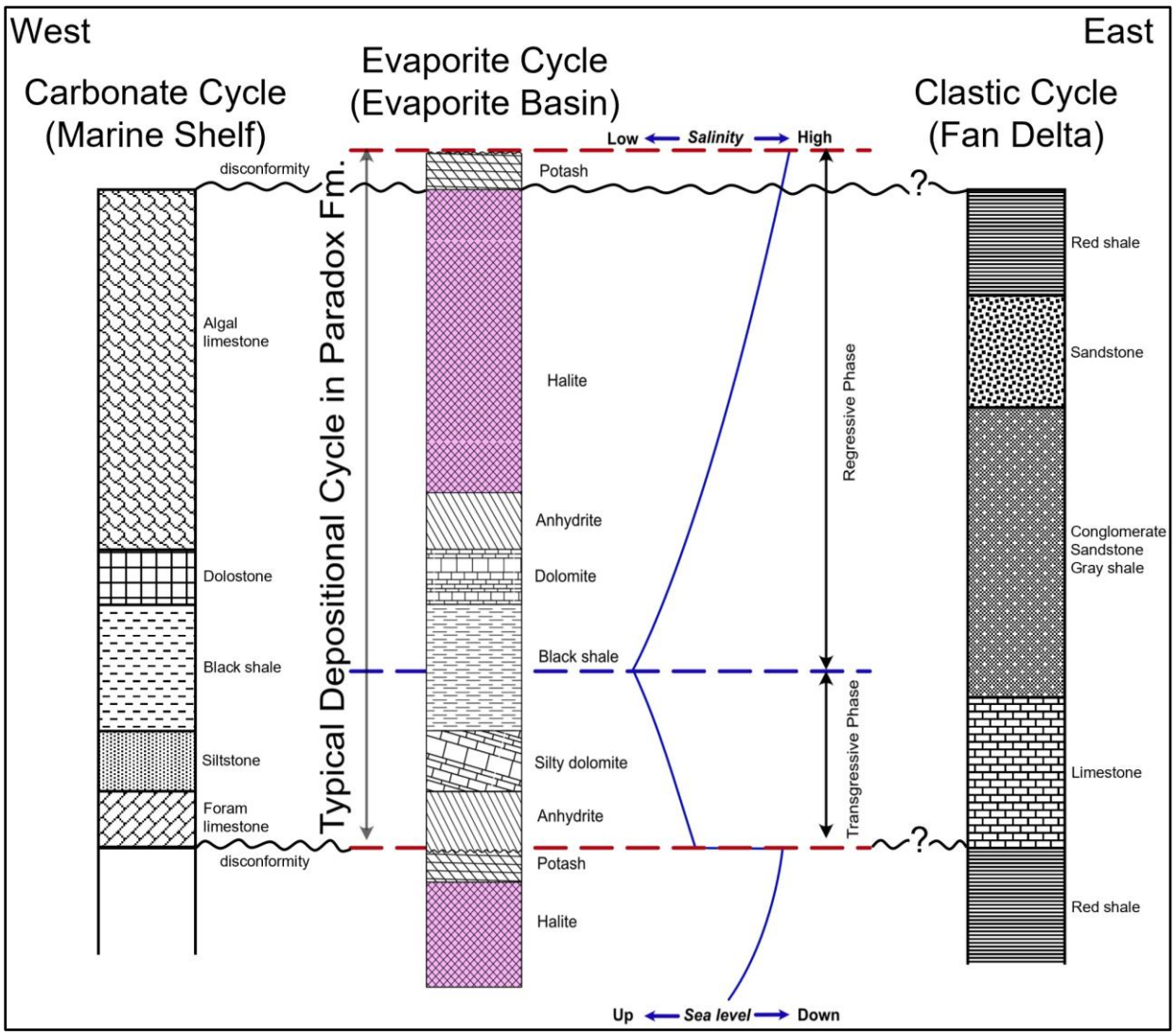

Figure 3: Typical Paradox Formation layered evaporite depositional cycle lithologies
Depositional cycle lithologies reflect sea level and salinity change in transgressive and regressive phases. Evaporite cycles correlate with carbonate cycles (distal/southwest) and clastic cycles (proximal/northeast) in the Paradox Basin. (Figure modified from Hite and Buckner, 1981; Hite et al., 1984; Raup and Hite, 1992; Williams-Stroud, 1994). The approximate location of typical cycle development is indicated in Figure 2. Note: deposition of clastics in the fan delta cycle does not correspond to deposition of clastic sediments as inclusions in the evaporite cycle, where coarsest sediment input is expected during lower sea level.

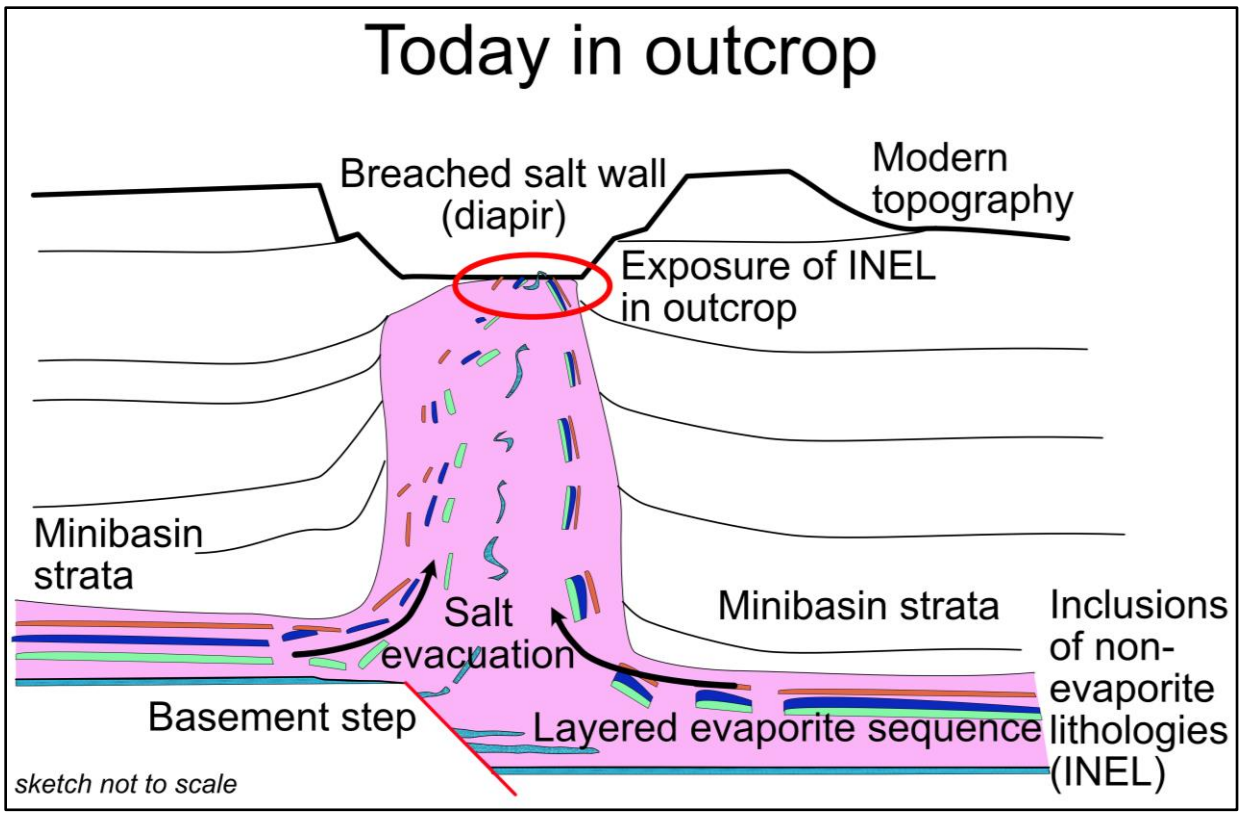

Figure 4: Schematic cross-section of breached Paradox salt wall
Showing salt in pink, diapiric pathway of inclusions in green, dark blue, and orange, and exposure site in modern outcrop in the red oval. Pathway of inclusions derived from basement steps shown in teal.

This study maps the surface distribution of the "other types" of inclusions present at three salt walls in the PB (Fig. 1), describes their lithologic, stratigraphic, and geochemical nature, and interprets their depositional setting. Two hypotheses related to the other types of inclusions are tested: 1) these inclusions are derived from the Paradox Formation LES, and 2) in addition to the Uncompahgre uplift, basement steps within the PB served as local detrital sources for the LES. These hypotheses are not mutually exclusive. If inclusions are derived from the Paradox Formation LES, they may or may not have been sourced from the basement steps. However, if the basement steps contributed clastic sediment as inclusions in the LES, then inclusions must also have been derived from the Paradox Formation LES. Thus, if the first hypothesis is supported, the second need not be, but, if the second hypothesis is supported, the first must also be supported.

1.1 Layered Evaporites, Salt Tectonics, and Inclusions of Non-Evaporite Lithologies

Cycles of sea level rise and fall may cause repeating periods of open marine circulation alternating with periods of restriction of ocean margin basins. When located in arid environments, periods of restriction can result in thick accumulations of evaporite minerals through evaporation of seawater. Cycles of open circulation and restriction result in basin fill of evaporite deposits depositionally interlayered with non-evaporite lithologies, such as carbonates and siliciclastics, and more rarely volcanics. The resulting cyclic sequences form LES consisting of layers of evaporite minerals, primarily anhydrite, gypsum, and halite and to a lesser degree potash/bittern salts, intercalated with the non-evaporite lithologies (Rowan et al., 2019). When exposed to differential pressure (via sediment loading or tectonics), evaporite layers as well as hydrated shale layers within the LES may become unstable and start to flow forming diapirs (Rowan et al., 2019). While halite and potash minerals are mobile, the more competent, intercalated non-evaporite layers can become entrained with the more mobile parts. These non-evaporite lithologies are carried into the rising diapir as disrupted but coherent packages encased in evaporites, i.e., diapiric inclusions, where they can undergo further deformation, such as folding and stretching (Fig. 4; Hudson et al., 2017; Rowan et al., 2019). The inclusions are transported upward during diapirism and can become exposed in breached salt walls (Fig. 4). Thus, deformation of inclusions could happen during entrainment into the diapir, during diapirism, or during later accretion in the caprock of the diapir. Such competent packages of lithologies have previously been referred to as intrasalt clasts, rafts, or stringers, all of which may carry a genetic connotation (Penge et al., 1999; Pratt, 2002; Hudson et al., 2017; Rowan et al., 2019). I simply use the term ‘inclusion’ in this study as it does not insinuate a known origin.

Previous studies focused on inclusions because they can serve as a hydrocarbon source or reservoir rock, but they can also be a hazard for hydrocarbon exploration or during mining of halite, bittern salts, and metals from diapirs (Kukla et al., 2011; Weijermars et al., 2014; Strozyk, 2017; Rowan et al., 2019). Additionally, inclusions can pose a hazard if a diapir is used to store materials (e.g., hydrocarbons, carbon dioxide, hydrogen, nuclear waste; Posey and Kyle, 1988; Hudson et al., 2017; Kernen, 2019; Rowan et al., 2019). Recent studies in the PB identified inclusions of lithologies other than previously recognized black calcareous mudstones and dolomite that hint at the possibility that the LES had different source areas for clastic detritus (Figs. 2, 4); these lithologies include limestones and siliciclastics in the form of carbonate-rich conglomerates and sandstones at Sinbad Valley (Thompson Jobe et al., 2020), Salt Valley (Rasmussen, 2014; Ritter et al. 2016), and Gypsum Valley (previously interpreted as caprock; Langford et al., 2022). This study aims to put inclusions found in PB diapirs into the greater salt-tectonic context of the PB as they may provide a unique view into otherwise inaccessible Paradox Formation strata by means of outcrop studies.

There are several ways in which non-evaporite lithologies can be incorporated into diapirs (Fig. 4). First, they could be deposited in the LES prior to salt movement (Goldhammer et al., 1991). Second is the possibility that they are pulled up from underlying strata during diapirism (Ala, 1974; Stern et al., 2011). Third, igneous intrusions into the diapir as dikes/sills (e.g., Black, 1953), perhaps even sediment injections as sedimentary dikes, are possible if the sediments are weakly consolidated and become “liquefied” (Cui et al., 2022). Fourth, diagenetic or microbial processes are also feasible where the non-evaporite lithologies are created from evaporite lithologies (e.g., as caprock carbonate from gypsum). Finally, these non-evaporites could also be younger strata deposited or karst-emplaced on the top of the breached diapir.

In the case of the PB, it is accepted that inclusions originated either syn- or post-depositionally to the LES. Non-evaporite carbonate and black shale lithologies were originally interbedded with evaporite lithologies deposited within the LES that later formed the diapirs (Fig. 3). Other non-evaporite lithologies (sandstones and conglomerates) could be younger strata deposited during or after the formation of the diapirs (Fig. 4). Previous geologic mapping of the Paradox salt diapirs has designated inclusions as outcrops of the Paradox Formation or the Honaker Trail Formation (Doelling, 1985; Doelling, 1988). Where inclusions are mapped as Paradox Formation, this implies synchronous deposition of these non-evaporites alongside evaporite lithologies as a part of the original LES stratigraphy. Where inclusions are mapped as Honaker Trail Formation, this instead suggests that younger strata were deposited onto the diapir. The coarse-grained siliciclastic inclusions are assumed to originate as detrital material shed from the Uncompahgre uplift into the Paradox evaporite basin (Fig. 2; Elston, et al., 1962; Doelling, 1988; Rasmussen and Rasmussen, 2009). There is also the possibility they were sourced from pre-salt strata uplifted on basement steps and syn-depositionally recycled, becoming a lithology of the Paradox Formation LES (Figs. 2, 4; Thompson-Jobe et al., 2019).

The determination of how clastic inclusions were incorporated into PB diapirs was one of the main goals of this study. If true, the hypothesis that inclusion lithologies exposed in breached PB salt walls formed as part of the LES would indicate that they are syn-depositional and could not have originated as younger strata. Further, if true, the hypothesis that inclusion sediments were sourced at least partly from basement steps in the basin would indicate that the Uncompahgre uplift was not the only source of siliciclastic deposition in the PB. By extension, this would mean that the investigated inclusions were deposited prior to initiation of salt tectonics.

1.2 GEOLOGIC BACKGROUND

1.2.1 Tectonics and Paleogeography

The PB is located in southeastern Utah and southwestern Colorado and is associated with Pennsylvanian tectonic loading by the Uncompahgre uplift (Figs. 2, 5). Today, the PB has an irregular oval shape with a maximum length of 306 km parallel to the Uncompahgre uplift and 153 km perpendicular to uplift (Fig. 1; Nuccio and Condon, 1996). The basin area is defined by the extent of Paradox Formation salt, while the extent of salt tectonics is defined by a series of breached salt walls that are confined to the proximal portion of the basin within 50 km from the Uncompahgre uplift (Fig. 1).

Before the formation of the PB and the subsequent deposition of the first layer of salt, the area in which the PB formed was a slowly subsiding Lower Paleozoic passive margin characterized by primarily carbonate platforms that deepened to the west and south (Doelling, 1988). During Pennsylvanian time, Laurentia and Gondwana collided, resulting in the Ouachita-Marathon orogeny and the formation of the Ancestral Rocky Mountains (ARM), including the Uncompahgre uplift, by the Middle Pennsylvanian (Kluth, 1986). During Pennsylvanian to Permian time, the PB underwent substantial paleogeographic changes triggered by ARM tectonic events that resulted in the deepest part of the PB against the Uncompahgre uplift progressively shallowing to the forebulge margin to the south (Figs. 5, 6; Barbeau, 2003). Kluth and DuChene (2009) note that the margins connecting the ARM uplifts and basins were tight, complicated areas. Moreover, the interpretation of the evolution of the PB is complicated by the presence of mobile salt (Kluth and DuChene, 2009; Trudgill and Arbuckle, 2009).

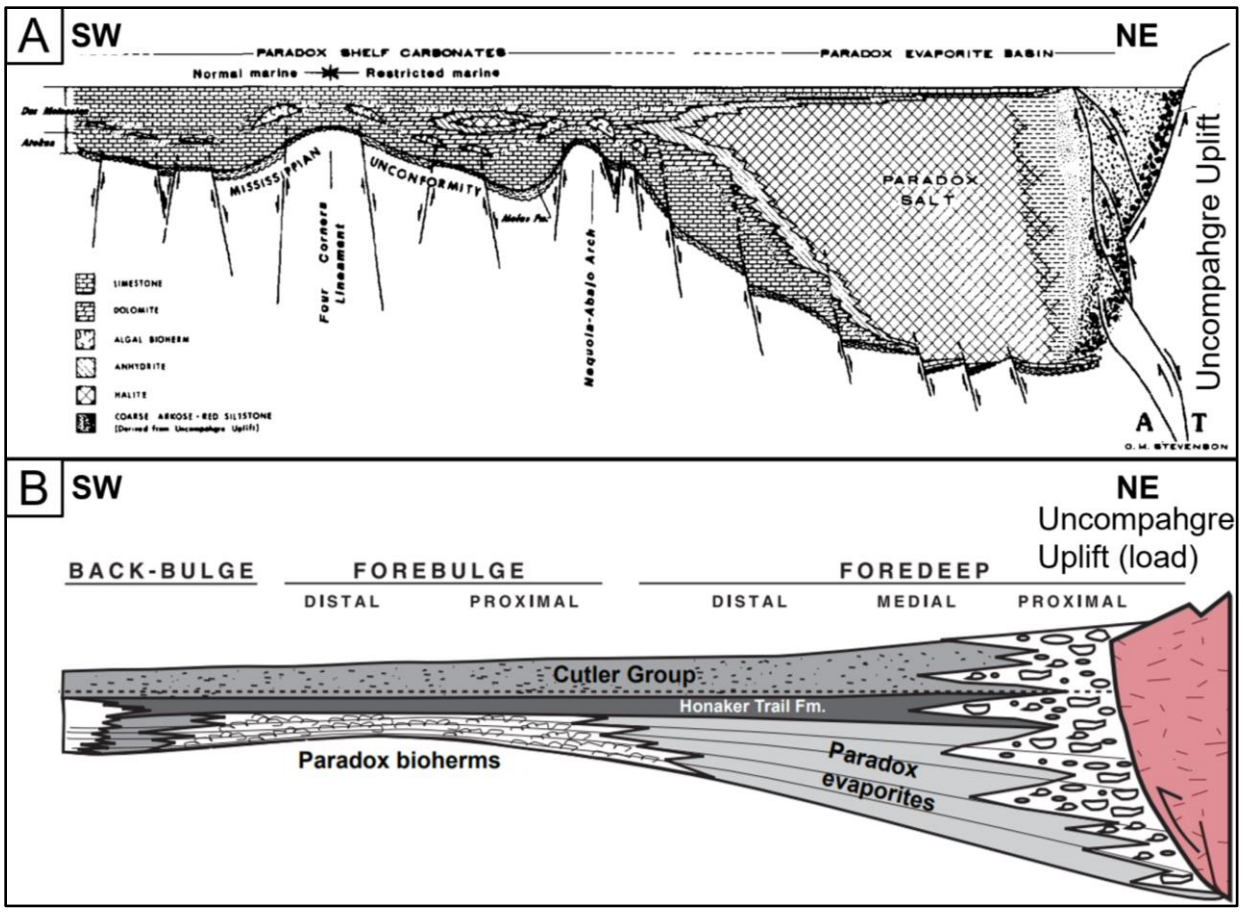

Figure 5: Paradox Basin development

Models for Paradox Basin development. A) Pull-apart model for the Paradox Basin showing deepest trough near the Uncompahgre uplift and basement steps at the base of the basin (Figure after Stevenson and Baars, 1986). B) Flexural model for the Paradox Basin showing gentler basin profile with deep trough in the foredeep near the Uncompahgre uplift (Figure after Barbeau, 2003; Trudgill and Paz, 2009; Trudgill, 2011).

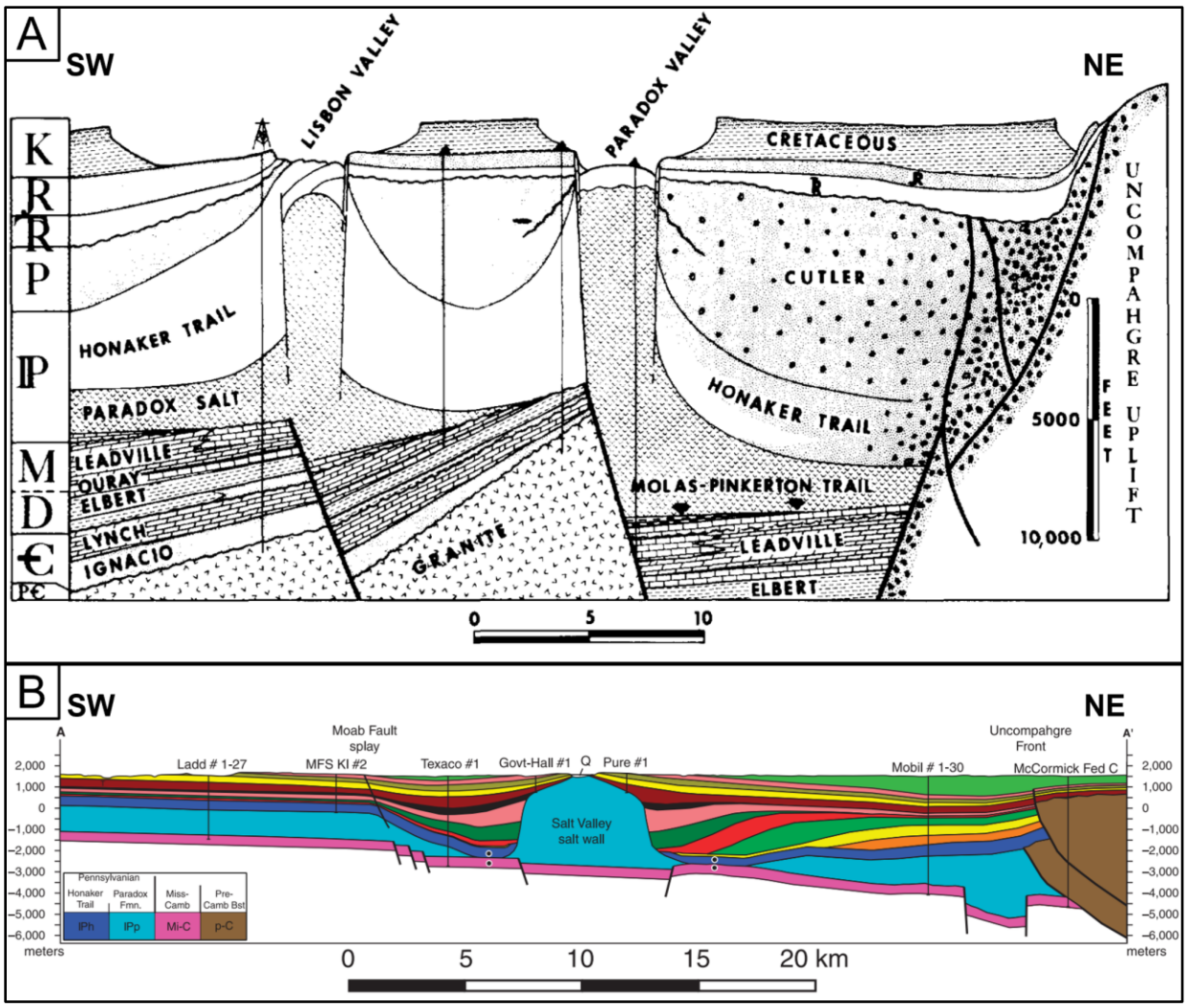

Figure 6: Stratigraphic and structural sections of the Paradox Basin with underlying basement steps

Basement steps show pre-Paradox Formation strata offset by basement faults. A) Structural cross-section showing a schematic view of the basement steps at the base of the Paradox Basin beneath the Paradox Valley and Lisbon Valley salt walls (Figure after Stevenson and Baars, 1986). Note inferred thickness change in pre-Paradox Molas-Pinkerton Trail and Ignacio formation, implying offset of steps prior to evaporite deposition. B) Structural cross-section interpreted from well, gravity, and seismic data showing geologic structure of Salt Valley salt wall and adjacent areas (Figure after Trudgill, 2011).

It is generally assumed that vertical and lateral movement during the Paleozoic followed ancient fracture systems in the Precambrian basement that developed during the Early Proterozoic (e.g., Maughan and Perry, 1986). The ancient fracture systems can be discerned as major intersecting lineaments (Fig. 7), the first occurring approximately 1700 Ma and trending

orthogonally northwest and northeast (N 30-40° W and N 50-60° E), the second occurring approximately 1675-1640 Ma and trending approximately east-west and north-south (N 75-85° W and N 5-15° E; Warner, 1978; Baars and Ellingson, 1984; Stevenson and Baars, 1986; Maughan and Perry, 1986). These ancient fracture systems underwent subsequent reactivation that regulated the distribution of facies in the Cambrian, Late Devonian, and Mississippian (Fig. 6; Baars, 1966; Baars and See, 1968; Stevenson and Baars, 1986).

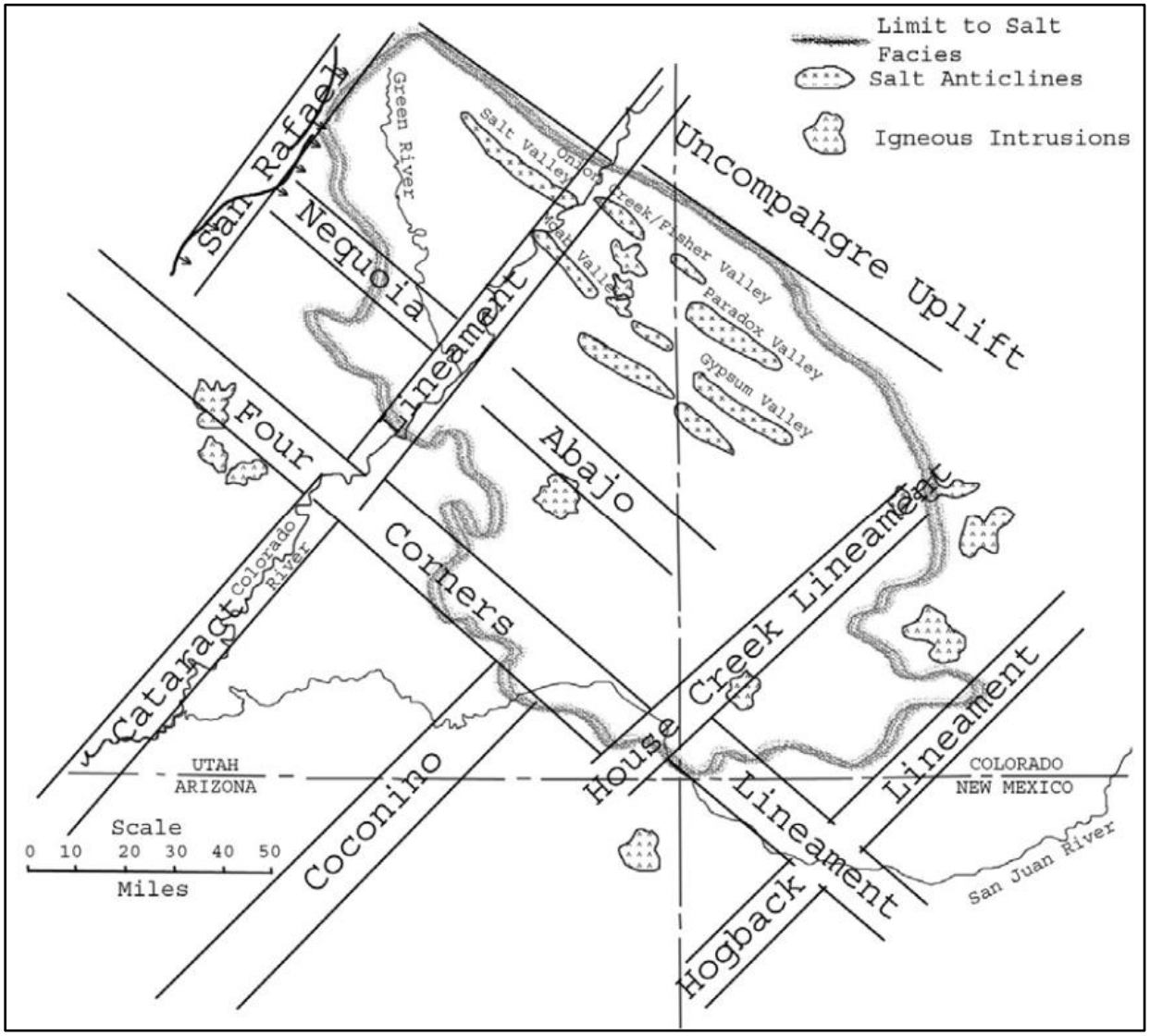

Figure 7: Diagram of major fault lineaments underlying the Paradox Basin
Major fault lineaments outlined in relation to the Uncompahgre uplift and the Paradox Basin salt walls (Figure from Arbuckle, 2008; Stevenson and Baars, 1986).

The PB has been interpreted as both a pull-apart basin (Stevenson and Baars, 1986) and as an ARM flexural foreland basin (Barbeau, 2003). Along the sides of the Uncompahgre uplift, reverse faults serve as evidence that the PB is a foreland basin (Fig. 5; Blakey, 2009). Trudgill (2011) observed that Barbeau's (2003) model appears to successfully represent the larger scale features of the Paradox Basin, but that interpretations of the Uncompahgre front across the Colorado-Utah state line (Kluth and DuChene, 2009) suggest a different geometry and timing for the evolution of the Uncompahgre front along strike. Trudgill and Arbuckle (2009) propose a combination of pull apart and flexural foreland basin, with a submerged Uncompahgre uplift for most of the duration of the deposition of the Paradox Formation (Fig. 2). During Atokan (Middle Pennsylvanian) time, the formation of a releasing bend along the either submerged (Trudgill and Arbuckle, 2009) or emergent (Stevenson and Baars, 1986) Uncompahgre highland was followed by extensional faulting defining the pull-apart geometry of the PB and confining the early phases of the Paradox LES deposition in the proximal PB (Fig. 8). Kluth and DuChene (2009) propose that the eastern half of the PB developed earlier and was deeper based on the sedimentation of the Paradox LES (Fig. 8-D).

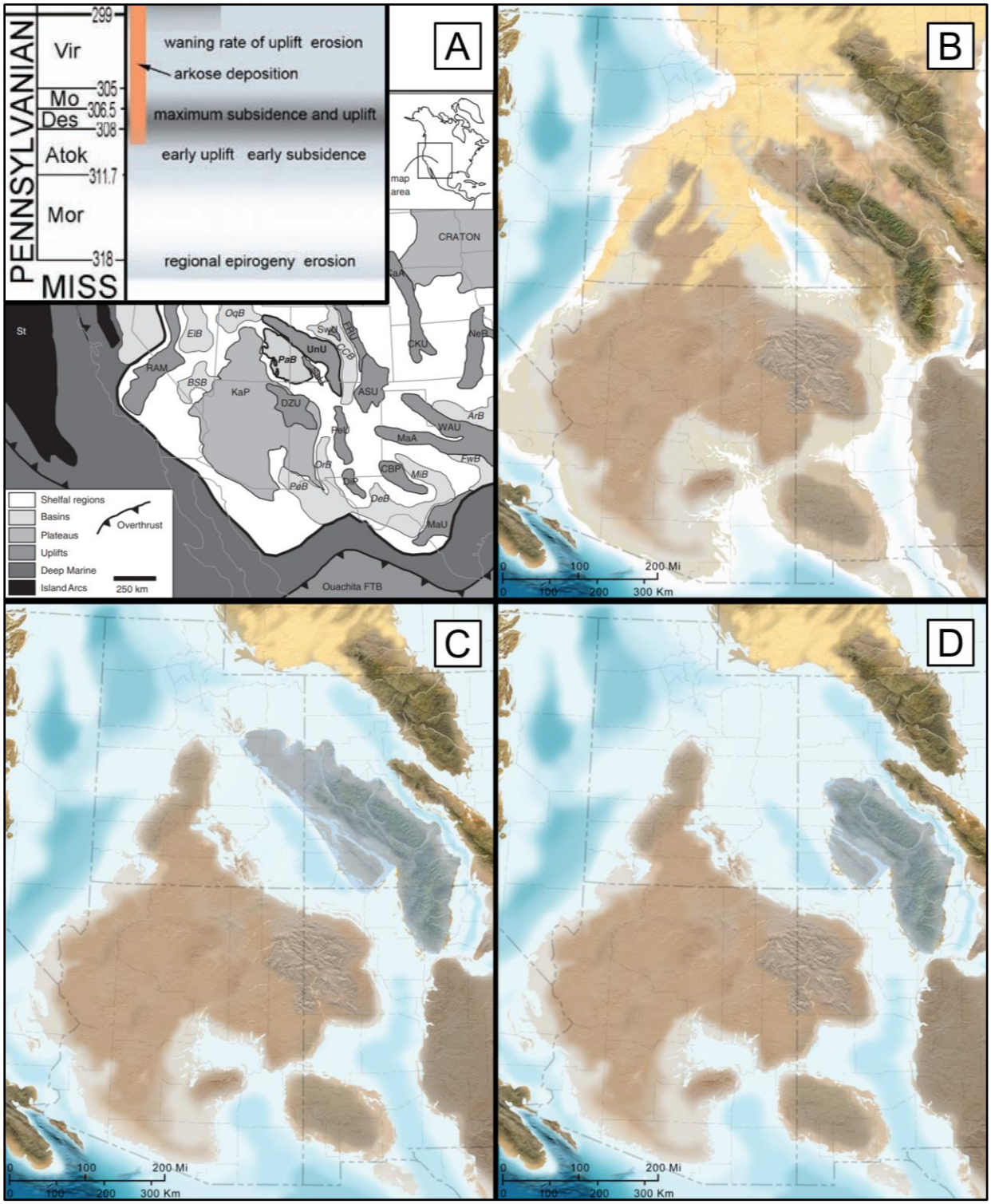

Figure 8: Paleogeography of the Paradox Basin area during Desmoinesian (Middle Pennsylvanian) time

A) Overall paleogeography of the Paradox Basin and surrounding areas with inset marking major events, UnU: Uncompahgre uplift, PaB: Paradox Basin (Modified from Trudgill, 2011). Paleogeography of the Paradox Basin (Modified from Blakey, 2009) during B) lowstand, C)

highstand shown with Uncompahgre uplift submerged D) highstand as proposed by Kluth and DuChene (2009).

A series of Cambrian, Devonian, Mississippian, and Early Pennsylvanian formations were deposited on a west-south facing passive margin prior to PB subsidence. Below this suite, there are Precambrian basement rocks. It is thought that normal fault steps in the basement existed before deposition of the Paradox LES, but after the deposition and subaerial exposure of the Mississippian Leadville Limestone, resultant Molas Formation, and Early Pennsylvanian Pinkerton Trail Formation (Fig. 6; Cross and Larsen, 1935; Merrill and Winar, 1958; Baars, 1966; Kluth and DuChene, 2009). The Paradox Formation was deposited on these southwest-oriented uplifts/steps that included basement and pre-orogenic Paleozoic rocks through the Early Pennsylvanian Pinkerton Trail Formations (Fig. 6; Kluth and DuChene, 2009). The Pennsylvanian marked the time of the most significant revival of these structures that resulted in the formation of the ARM uplifts and the PB, allowing for deposition of the LES under restricted conditions (Stevenson and Baars, 1986). During these periods of regression, the PB was isolated from the World Ocean and became an evaporite basin (Fig. 2; Huffman and Condon, 1993).

In the Early to Middle Desmoinesian (Late Pennsylvanian), continued extensional faulting resulted in the formation of subbasins during ongoing LES deposition and the beginning of clastic deposition from the Uncompahgre uplift (Stevenson and Baars, 1986; Trudgill and Arbuckle, 2009). This emergent deposition of the Cutler Group resulted in differential loading of the underlying Paradox LES, which initiated early diapirism in the proximal PB (Stevenson and Baars, 1986; Trudgill, 2011; Rowan, 2019). Basement-involved normal faults within the PB defined salt diapir configurations and ultimately resulted in the salt diapirs having wall-like geometries limited by the length of the basement faults (Baars, 1966; Doelling, 2001; Trudgill and Arbuckle, 2009; Trudgill, 2011). By Late Desmoinesian, extension and basin subsidence had slowed considerably

while diapirism accelerated in the proximal PB, where, closest to the Uncompahgre front, total subsidence was highest and clastic sediment deposition started earliest (Stevenson and Baars, 1986). The end of Desmoinesian time marked the return to normal marine conditions across the majority of the PB with the last phases of Paradox LES deposition and basin subsidence occurring in the northeast part of the basin (Stevenson and Baars, 1986).

While ARM tectonism slowed significantly by the end of the Middle Pennsylvanian, influx of coarse-grained arkosic sediments derived from the Uncompahgre uplift continued through the Permian (Kluth and Coney, 1981). The most active period of salt tectonics lasted about 75 million years spanning late Pennsylvanian to Permian time (Doelling, 1988; Thompson Jobe et al., 2020). The Uncompahgre uplift was buried during the Permian, which is evidenced by the uppermost Cutler Group onlapping and burying the ancient Uncompahgre Precambrian basement during the Permian (Cater and Craig, 1970; Soreghan et al., 2012). This indicates that by that time, ARM tectonics had ceased and the Uncompahgre highland and greater area including the proximal PB began sinking, at least at its southwest flank (Cater and Craig, 1970; Soreghan et al., 2012). Hydrocarbon generation due to burial by sediments began in the proximal PB during the Late Pennsylvanian and Early Permian and moved westward to the distal PB with the latest generation in the Early Triassic (Rasmussen and Rasmussen, 2009). This interpretation agrees with Kluth and DuChene (2009) who observe that salt walls grow younger in the southwest direction and surmised that deposition of sediments moved in that direction. Additionally, they conclude that the eroded material from the Uncompahgre uplift was deposited only in the proximal PB, and further distal sedimentation occurred by southwest-moving axial flow rather than directly from the Uncompahgre uplift (Kluth and DuChene, 2009). As sediment was deposited it would displace the salt until it reached the underlying rocks (Leadville Limestone) forming a primary weld (Kluth

and DuChene, 2009). This marked the termination of accommodation space generated by salt withdrawal, the sediment would then bypass that area and move to the next minibasin. Kluth and DuChene (2009) refer to this as “fill and spill” after workers in the Gulf of Mexico. This salt migration likely began early after deposition at high-angle basement faults, generating the large anticlines characteristic of the area during the Pennsylvanian through Triassic periods (Doelling, 1988, Chidsey, 2020).

The PB was modified by a series of tectonic events from the Mesozoic through the Cenozoic resulting in the geomorphology we see now (Nuccio and Condon, 1996; Thompson Jobe et al., 2020). Following the most active period of salt tectonics during Pennsylvanian to Permian (Doelling, 1988; Thompson Jobe et al., 2020), waning salt diapirism and progressive burial of the salt walls lasted another 125 million years (Langford et al., 2022). Deep burial of the diapirs occurred during the Cretaceous Sevier Orogeny (sediment accumulation thickness between 1.2 km and 2 km), the Late Cretaceous to Paleogene Laramide Orogeny, and by additional Tertiary sediments (accumulation thickness between 0.3 km and 0.8 km) toward the end of the Laramide Orogeny (Doelling, 1988; Rasmussen and Rasmussen, 2009; Trudgill, 2011). Reactivation of basement faults occurred in the Late Cretaceous to Paleogene Laramide Orogeny (Kluth and DuChene, 2009).

1.2.2 Pre-Salt Stratigraphy

The determination of how inclusion sediments were incorporated into PB salt walls was one of the main goals of this study. The hypothesis that the inclusions contain sediments derived from basement steps within the basin would indicate that inclusions were derived from rocks older than the Paradox Formation. The pre-salt stratigraphy is detailed below to compare inclusion sediments (grains/clasts) with basement step rocks.

Crystalline basement rocks underlying the sedimentary fill in the PB are Proterozoic in age and consist of medium to high grade metamorphic gneiss, quartzite, and schist, and plutonic granite, which are exposed in the Uncompahgre uplift today (Doelling, 1988; Nuccio and Condon; 1996). The Cambrian through Mississippian rocks overlying the basement tend to thin eastward as a whole (Parker and Roberts, 1966; Condon, 1995; Fig. 9).

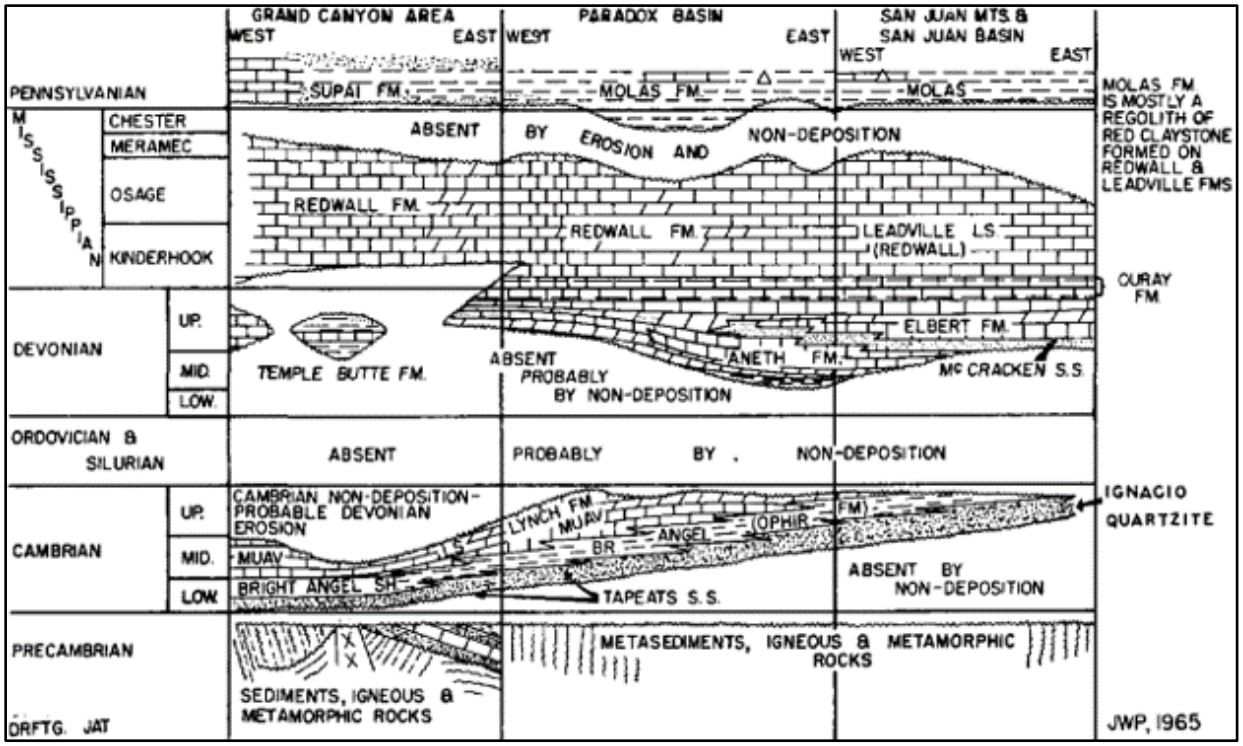

Figure 9: Pre-salt strata of the Colorado Plateau area
Pre-Paradox Formation simplified stratigraphic chart for the Grand Canyon area, the Paradox Basin, and the San Juan Mountains and Basin. Lateral distribution of known units shown with periods of erosion and non-deposition. Figure not to scale (Figure from Parker and Roberts, 1966).

1.2.2.1 Cambrian

The Cambrian Tintic Quartzite Formation (lithocorrelative with the Ignacio Quartzite Formation in the east; Ohlen and McIntyre, 1965) overlies Precambrian basement rocks (Condon, 1995; Figs. 9, 10). It is defined at its base by quartz pebble conglomerate, at its middle by cross-bedded quartzite, and at its top by thin green shales (Condon, 1995). Conformably overlying the

Tintic Quartzite Formation is the Cambrian Ophir Formation (Figs. 9, 10). The Ophir Formation is composed mainly of shale, with limestone beds in the middle of the unit (Condon, 1995). The lower shale unit is defined by interbedded greenish shale and sandstone, the middle unit is dark gray limestone with greenish shales interbedded, and the upper unit is light greenish shale with lenticular sandstone beds (Condon, 1995). The Ophir Formation is recognized as marine which is evidenced by trilobites in the lower unit (Condon, 1995). Locally, the upper unit may contain algae, oolites, and brachiopods (Condon, 1995). Above the Ophir Formation is the marine, Upper Cambrian Lynch Formation (Figs. 9, 10). The Lynch Formation is predominately (~75%) dark gray to black dolomite defined at its base by a dark blue limestone with very thin shale layers, and locally, it contains an upper shale unit. Beneath the PB, the Lynch Formation is much lighter in color, mostly tan limestone and dolomite interbedded with thin shale and sandstone, the upper part is slightly sandy with algae, oolites, and brachiopods (Condon, 1995).

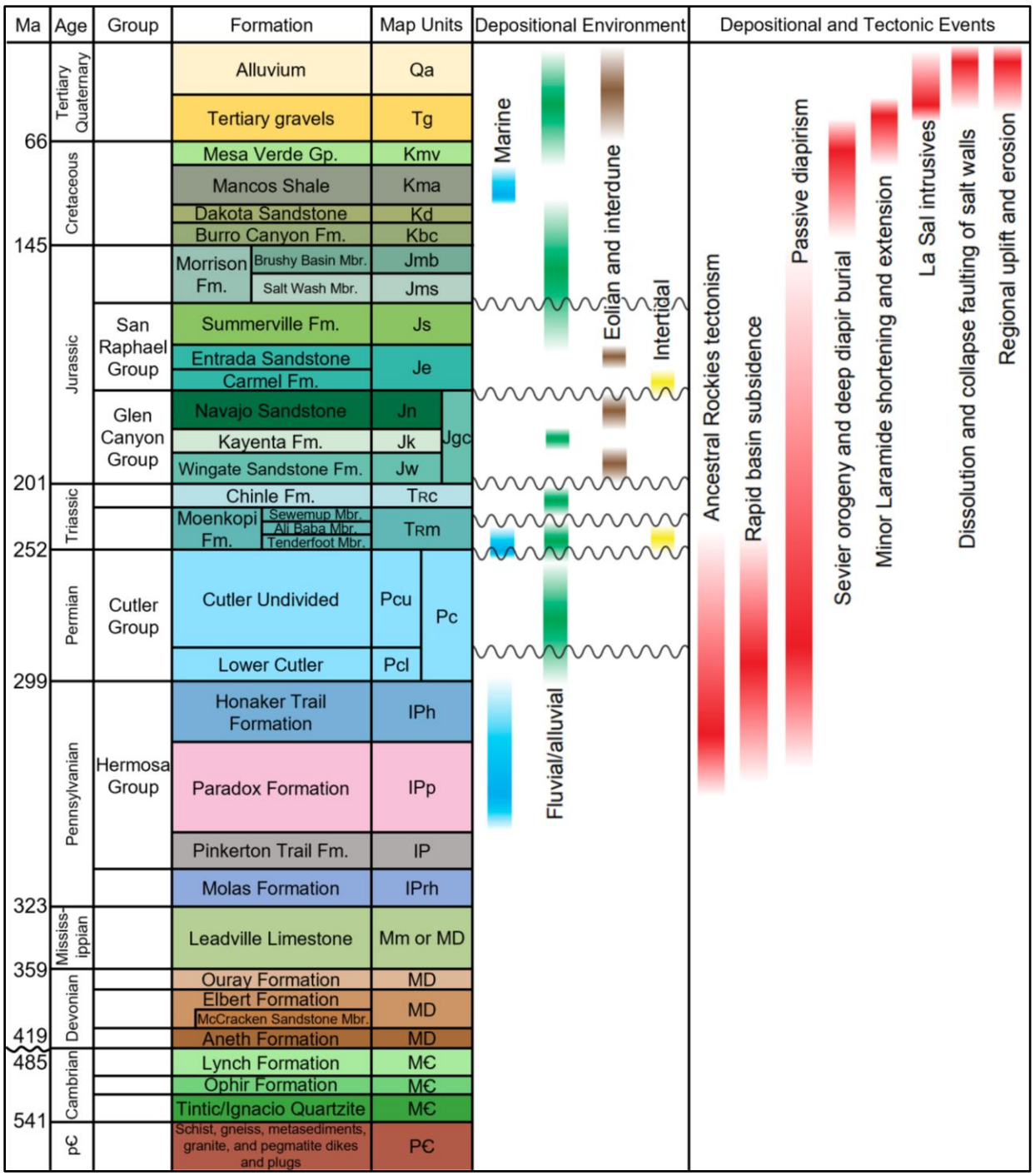

Figure 10: Comprehensive stratigraphic column of the Paradox Basin area
Stratigraphic column displaying major units from Precambrian through Quaternary, depositional environments, and major depositional and tectonic events associated with the Paradox Basin. The squiggly line between numerical ages indicates a period of either erosion or non-deposition, there are no rocks in the Paradox Basin during this time. Squiggly lines in depositional environments box indicate regional unconformities (Figure modified from Hintze and Kowallis, 2009; Thompson Jobe et al., 2020).

1.2.2.2 Devonian

There are no rocks in the PB region of Ordovician, Silurian, or Early Devonian age. There is little evidence to suggest the reason for this, though it could be due to erosion or non-deposition (Parker and Roberts, 1966; Condon, 1995). The Upper Devonian Aneth Formation unconformably overlies the Lynch Formation (Figs. 9, 10). The Aneth Formation is fossiliferous dark brown dolomite and gray to black shale and siltstone (Condon, 1995). Fossils within this formation include placoderm fish (scales and parts) and plant pieces (Parker and Roberts, 1966; Condon, 1995). The Aneth Formation is believed to have accumulated in local sags or basin areas in which euxinic (sulfidic) conditions prevailed intermittently (Parker and Roberts, 1966). The lowermost part of the overlying Devonian Elbert Formation toward the north and west may be contemporaneous with part of the Aneth Formation (Fig. 9; Parker and Roberts, 1966). The Elbert Formation is divided into the lower McCracken Sandstone Member and the upper Elbert Member separated by a gradational contact (Figs. 9, 10; Condon, 1995). The McCracken Sandstone Member is composed mainly of glauconitic sandstones that can be white to gray to green to pink, and can be fine to coarse grained (Condon, 1995). It also contains dolomite and some thin shales (Condon, 1995). Minor amounts of oil are produced from the McCracken Sandstone Member at Lisbon field (Parker and Roberts, 1966; Chidsey, 2020) The upper Elbert Formation is predominately dolomite with some minor shales and local stromatolites, fish fossils, and anhydrite clasts suggesting a shallow evaporite environment (Condon, 1995). The Devonian Ouray Formation conformably overlies the Elbert Formation and is composed of brown fossiliferous limestone and some shale beds (Figs. 9, 10; Condon, 1995). Locally, the Ouray Formation is oolitic, and may contain crinoids or brachiopods (Condon, 1995).

1.2.2.3 Mississippian to Early Pennsylvanian

The Leadville Limestone (Late Kinderhookian to Early Meramecian) is the only formation of Mississippian age in the PB region and is separated from overlying and underlying units by unconformities (Figs. 9, 10, 11; Condon, 1995). The age equivalent limestones are referred to as the Redwall Limestone (Grand Canyon area), the Joana Limestone (western Utah and Nevada), the Pahasapa Limestone (Black Hills), the Guernsey Limestone (Wyoming), and the Madison Formation (Rocky Mountains, Great Plains). The Leadville Limestone is one of two major oil and gas reservoirs in the PB, the other being the Pennsylvanian Paradox Formation (Chidsey, 2020). The Leadville Limestone is a massive shallow marine to lagoonal limestone that is gray and diversely fossiliferous (Fig. 12; Condon, 1995; Chidsey, 2020). Additionally, chert is a common occurrence in this formation and, most interestingly, preserves fossils much better than in the limestone or dolomite (Parker and Roberts, 1966). It is likely that the chert was primary and occurred prior to dolomitization of these rocks evidenced by the superb preservation of detail in fossils within the chert when compared to the lack of preserved detail in the adjacent carbonates (Parker and Roberts, 1966). Chert that is not fossiliferous is color-banded due to groundwater interactions, thus classifying it as secondary chert (Parker and Roberts, 1966).

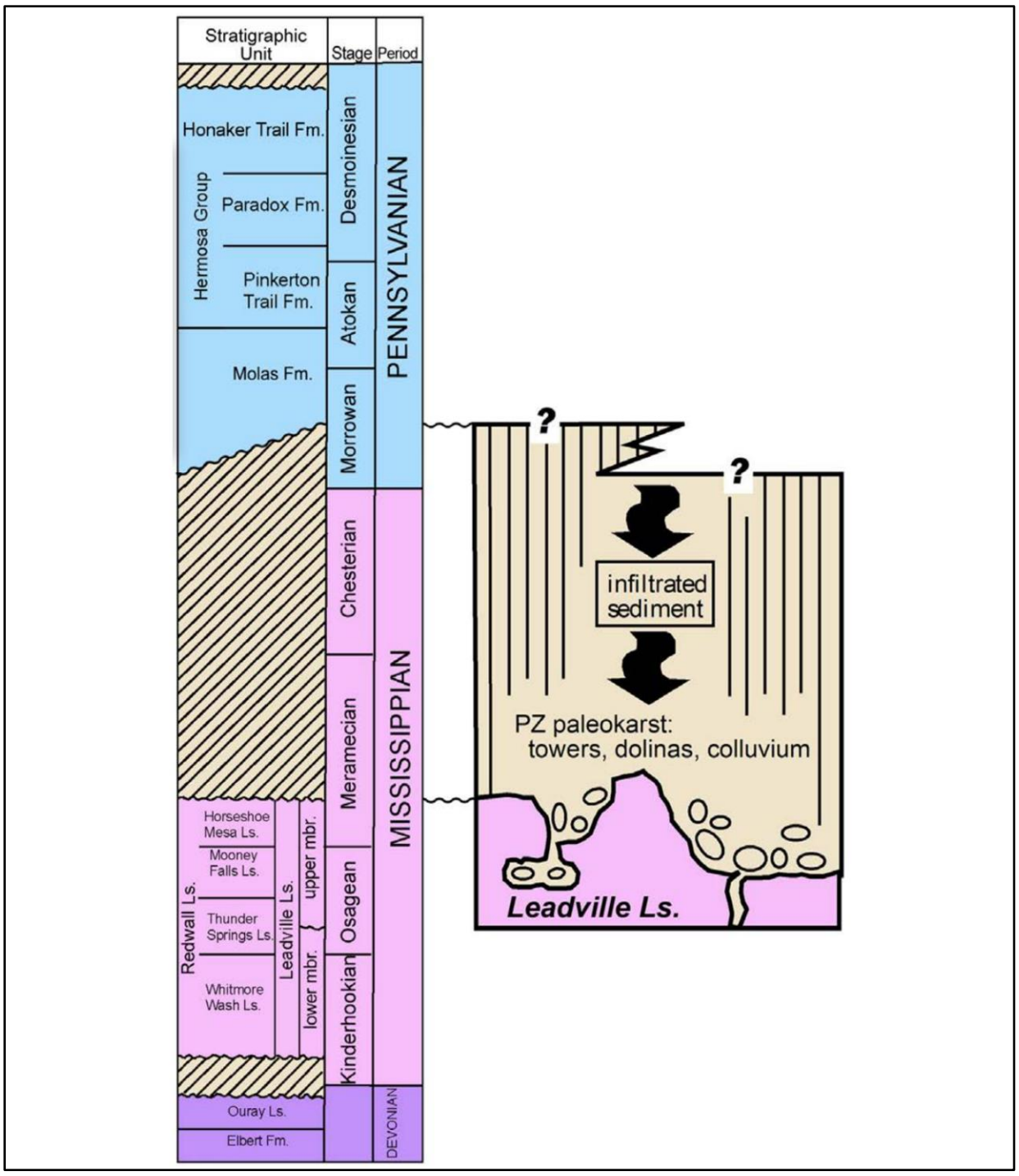

Figure 11: Stratigraphic column of Devonian to Mississippian rocks in the Paradox Basin
The stratigraphic column shows the major unconformity between the Leadville Limestone and the Molas Formation Coalbank Hill Member. Unconformity clarified showing karsted Leadville Limestone surface and infill of sediments belonging to the Coalbank Hill Member of the Molas Formation (Figure from Chidsey, 2020).

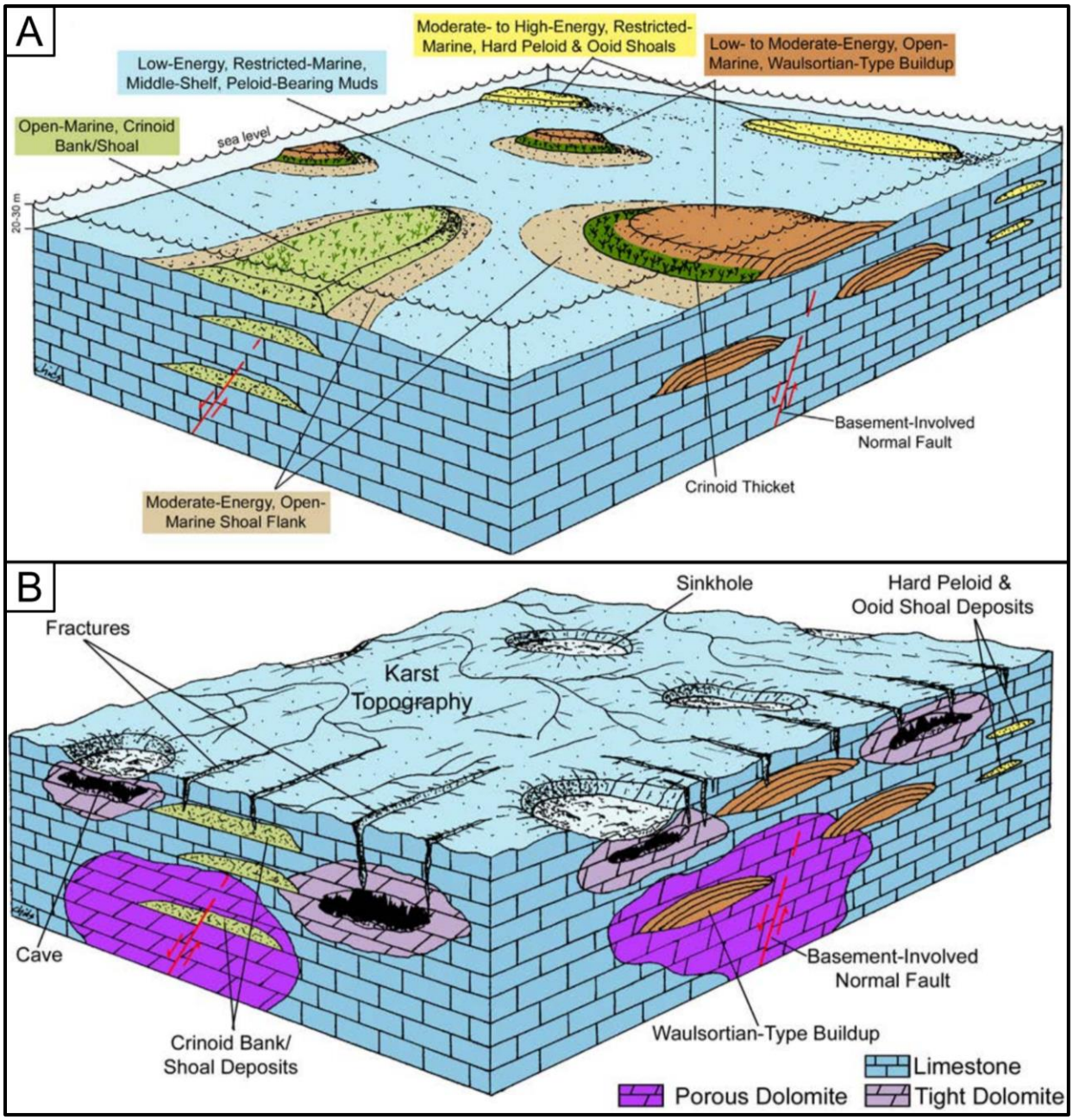

Figure 12: Depositional facies and karsted surface of Leadville Limestone

A) Major depositional facies of the widespread Leadville Limestone showing high variability in overall lithology of the Leadville Limestone, B) Post-depositional Leadville Limestone karsted and fractured surface. Karst later infilled with the lower Coalbank Hill Member of the Molas Formation (Figure after Chidsey, 2020).

The Leadville Limestone is separated from the overlying Early Pennsylvanian Molas Formation by a major subaerial unconformity with a chert clast lag over a karsted Leadville

Limestone top contact (Figs. 11, 12; Chidsey, 2020). Prior to initial subsidence of the PB which occurred in the Middle Pennsylvanian (Atokan; Stevenson and Baars, 1986), the Molas Formation and the lower member of the Hermosa Group, the Pinkerton Trail Formation, were deposited during transgression of the passive margin and the transition from restricted to normal marine conditions (Doelling, 1988; Goldhammer et al., 1991). Subsidence of the PB may not have started uniformly along the Uncompahgre uplift with the eastern, more proximal, PB being older and deeper (Stevenson and Baars, 1986; Kluth and Coney, 1981; Kluth and DuChene, 2009).

The Molas Formation is divided into lower (Coalbank Hill), middle, and upper members. The Coalbank Hill Member is noted as the "transition zone" bounded by unconformities with the underlying Leadville Limestone and overlying middle member of the Molas Formation and can be 1.5 to 17 m thick depending on locality (Merrill and Winar, 1958). This transition locally includes a red paleosol attributed to the deep alteration of the carbonate rocks belonging to the Leadville Limestone (Baars, 1966), and is noted by Cross and Larsen (1935) and Merrill and Winar (1958) as a dissolution-formed unit of the Leadville Limestone causing some disagreement as to whether it should be considered in the Molas Formation or the Leadville Limestone. The Coalbank Hill Member is defined by red mudstones and siltstones that include angular to rounded limestone pebbles to boulders and angular to rounded pebble sized chert fragments (Merrill and Winar, 1958). Chert pebbles are noted to contain Leadville aged fossils (Girty, 1903; Merrill and Winar, 1958). The middle member of the Molas Formation is 12 m thick on average and comprises transported non-marine interbedded massive siltstone, laminated shales, massive lenticular conglomerates (containing black chert, quartz, and limestone pebbles), and occasional sandstones (Merrill and Winar, 1958). The upper member of the Molas Formation is at least 7.5 m thick and is varied with transported marine sandstone, shale, siltstone, mudstone, breccia, and limestone

lithologies; silica cement is widespread in this member (Merrill and Winar, 1958). The most resistant beds are massive sandstones, grains within these beds are angular and coarse due to the silica cement, and chert, limestone, and red shale pebbles occasionally are present (Merrill and Winar, 1958). Present in the middle member and more abundant in the upper member are heavy minerals (Merrill and Winar, 1958). The Early Pennsylvanian Pinkerton Trail Formation was deposited above the Molas Formation under restricted marine conditions and is composed of thin limestone, siltstone, black shale, and anhydrite beds (Fig. 10; Doelling; 1988).

1.2.3 Layered Evaporite Sequence (i.e., 'Salt')

The sedimentary fill in the proximal portion of the PB consists of three distinct stratigraphic units deposited after PB subsidence initiated: in ascending order, the Paradox Formation, the Honaker Trail Formation, and the Cutler Group (Figs. 10, 13; Barbeau, 2003). The following sections discuss these three units with attention to non-evaporite lithologies previously identified within them.

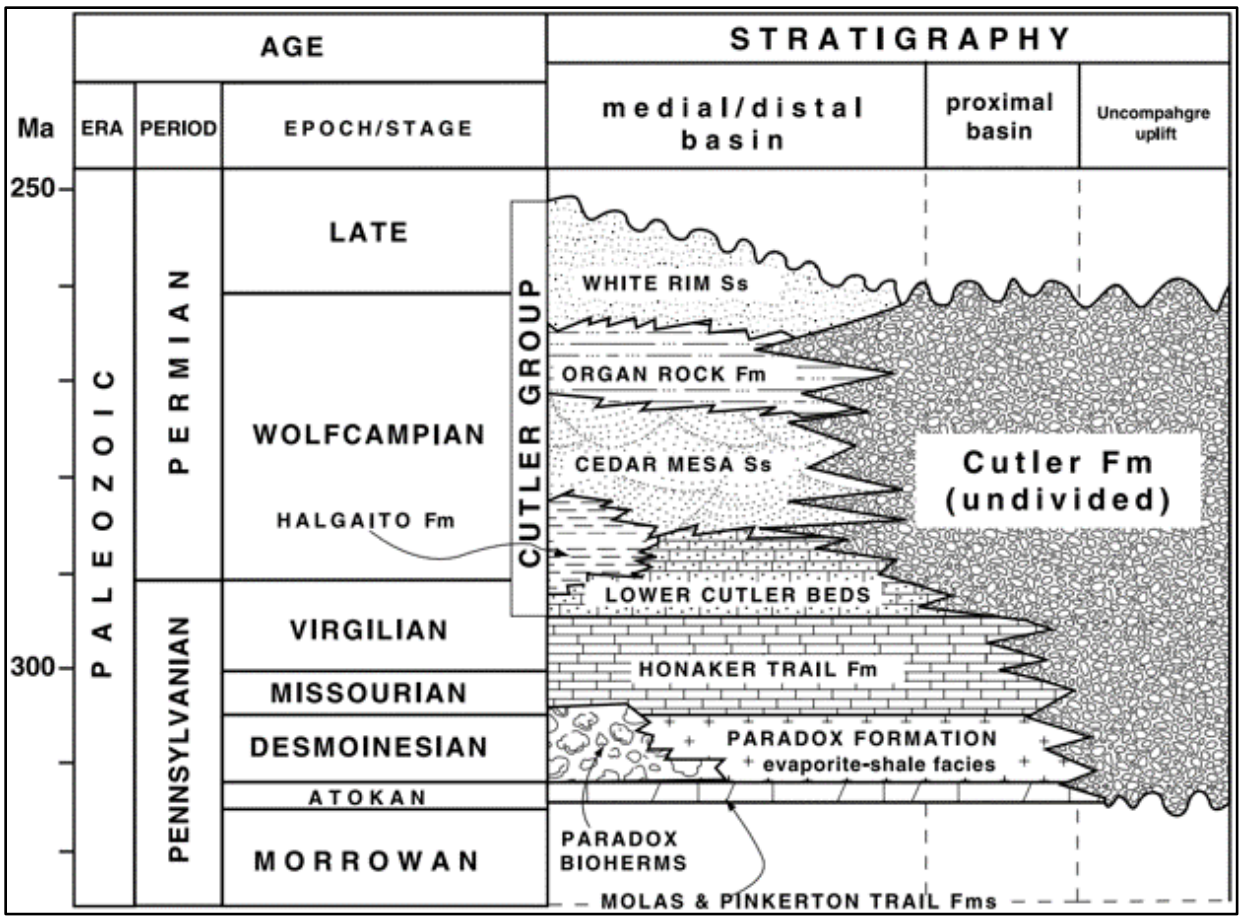

Figure 13: Paradox Basin fill
Stratigraphic column showing the basin fill in distal to proximal portions of the Paradox Basin (Figure from Barbeau, 2003).

1.2.3.1 Paradox Formation

The Pennsylvanian Paradox Formation is the middle member of the Hermosa Group and was deposited in the subsiding PB during glacio-eustatic cycles of sea level rise and fall during middle Pennsylvanian time (Figs. 2, 3). It is estimated that it was originally 2.0 to 2.6 km thick consisting of a cyclic LES with a majority of evaporite minerals intertonguing with clastics and carbonates and was deposited in an arid environment (Fig. 2; Rasmussen and Rasmussen, 2009; Trudgill, 2011).

Typical LES transgressive-regressive cycles include, in ascending order: anhydrite, silty dolomite, calcareous black shale, dolomite, halite, and potash salts (Fig. 3; Doelling, 1988; Raup

and Hite, 1992; Williams-Stroud, 1994). Cycles are marked by "sharp knife-edge contacts" at upper halite beds where rapid transgression resulted in dissolution of these beds forming marker bed disconformities (Raup and Hite; 1992). Above the base cycle disconformities, sea level continued to rise resulting in anhydrite deposition, followed by silty dolomite, culminating in black shale deposition at the height of sea level rise (Fig. 3; Raup and Hite, 1992). After deposition of the black shale, sea level began to drop, resulting in increasing salinity in the basin. The beginning of the regressive phase starts with dolomite deposition, followed by anhydrite as sea level continued to drop, and finally thick halite and thin potash beds during the periods of highest basin restriction, these beds eventually formed the next discontinuity when sea level began rising abruptly (Fig. 3; Raup and Hite, 1992; Williams-Stroud, 1994). While evaporite minerals anhydrite, halite, and potash salts mainly formed during periods of regression as the sea water evaporated from the basin, non-evaporite lithologies that belong to LES cycles were deposited during transgressive/regressive phases (carbonates, dolomite, gypsum) and highstands (black shales; Fig. 3). However, at any stage in the cycle, these typical LES lithologies could be interlayered with additional, clastic lithologies (Fig. 2). The deposition of these additional non-evaporite clastic lithologies was a result of fluvial, marine (turbidite, suspension), and colluvial (mass wasting) transport processes (Fig. 3).

1.2.4 Post-Salt Stratigraphy

1.2.4.1 Honaker Trail Formation

In the proximal PB, overlying the Paradox Formation is the upper member of the Hermosa Group, the Pennsylvanian Honaker Trail Formation (Fig. 10). It is up to 533 m thick, consists predominantly of carbonates, but also contains siltstones, sandstones, and cherts deposited in both fluvial and shallow-marine environments (Wengerd and Matheny, 1958; Wengerd, 1963).

Notably, inclusions are often mistaken as this formation (Doelling, 1985; Thompson Jobe et al., 2020).

The Honaker Trail Formation can be described by its carbonate and clastic facies. The carbonate facies include pedogenic carbonate, microbiotic boundstone laminites, micritic mudstones, dolomitic mudstones, peloid/foraminifera grainstones, phylloid bafflestones, skeletal grain-supported limestones, skeletal mud-supported limestones, sandy fossiliferous packstones, and evaporite associated carbonate (Gianniny and Miskell-Gerhardt, 2009). These facies include many marine fossils: ostracodes, gastropods, foraminifera, stromatolites, oncolites, phylloid algae, crinoids, brachiopods, rugose corals, fusulinids, bryozoans, bivalves, and zoophycus (Condon, 1997; Gianniny and Miskell-Gerhardt, 2009). These carbonate facies represent depositional environments from supra- to subtidal as well as sabkha and the K paleosol horizon (Gianniny and Miskell-Gerhardt, 2009). Clastic facies include dark-gray shales, micaceous mudstones, clinoform sandstones, channelized mud-rich sandstones, channelized conglomeratic sandstones (occasionally containing angular, non-fossiliferous chert), and thin-bedded sandstones with interbedded red mudstones (Gianniny and Miskell-Gerhardt, 2009). Thick sandstone beds are gray to tan and can range from fine-grained to transitioning to conglomerates with subarkosic to arkosic composition (Condon, 1997). Calcareous sandstones are frequently cross-stratified and often include ooids/coated grains (Kim, 1996; Barbeau, 2003). Siltstones and mudstones are present in a variety of colors, usually forming slopes (Barbeau, 2003). These facies often have plant debris and casts and represent depositional environments from offshore marine to fluvial (Gianniny and Miskell-Gerhardt, 2009).

1.2.4.2 Cutler Group

In the proximal part of the PB, the Permian Cutler Formation Undivided (Barbeau, 2003), also referred to as the Cutler Group Undivided, intercalates with and overlies the Honaker Trail Formation (Figs. 10, 13). It consists locally of up to approximately 5000 m of arkosic sandstones and siltstones with Proterozoic-clast conglomeratic channel horizons (Condon, 1997). The entire section fines upwards and outwards from the Uncompahgre uplift front, its original source of detritus (Barbeau, 2003). The lower section of the Cutler Group Undivided is also intercalated with the Paradox Formation LES that forms basal basin fill (Fig. 13; Barbeau, 2003).

1.2.4.3 Triassic and Younger Stratigraphy

Unconformably overlying the Cutler Group is the Triassic Moenkopi Formation, which consists of up to approximately 760 m of sandstones and shales deposited in a marginal marine environment (Fig. 10; Trudgill, 2011). An upper unconformity separates the Moenkopi Formation from the overlying Triassic Chinle Formation, which is up to approximately 230 m thick, and consists of orange to red sandstones, siltstone, shales, and pebble conglomerates deposited in a fluvial environment (Fig. 10; Cater and Craig, 1970; Doelling, 1988). An upper unconformity separates the Chinle Formation from the overlying Triassic-Jurassic Glen Canyon Group (Fig. 10; Doelling, 1985; Doelling, 1988). The Glen Canyon Group is divided into three formations: in ascending order, the eolian Triassic Wingate Sandstone, the fluvial Jurassic Kayenta Formation, and the eolian Jurassic Navajo Sandstone (Fig. 10; Doelling, 1985; Doelling, 1988).

1.3 FOCUS OF RESEARCH

The accessibility of inclusions cropping out at the salt walls in the PB provides a unique opportunity to study otherwise inaccessible strata in detail. Prior to this study, inclusions in the PB had not been extensively mapped, described, or their age and origin determined. Based on a

literature review and a reconnaissance field excursion in November 2021 visiting the Sinbad Valley (CO), Salt Valley (UT), Gypsum Valley (CO), Onion Creek (UT), and Moab (UT) diapirs, I came to two key findings. First, at each site I was able to identify large blocks of inclusions with a variety of lithologies including black shales, mudstones, siltstones, sandstones, carbonates, and conglomerates. Black shales have been identified as black laminated mudstones (Goldhammer et al., 1991; Rasmussen and Rasmussen, 2009), but for consistency with existing literature I will refer to them as black shales in this study. Second, all conglomerates contain primarily carbonate clasts. This finding was intriguing, because carbonate rocks weather (both chemically and mechanically) and breakdown quickly during hydrologic transport (Folk, 1959), implying a relatively short travel distance between the location from which those clasts were sourced and the site where they were deposited. These insights raised many questions about the origin of the inclusions leading to two distinct hypotheses, which I then tested utilizing field work, petrographic, and geochemical analyses.

1.4 HYPOTHESES

1.4.1 Hypothesis A

The initial question arose immediately. Are the outcrops at my selected sites inclusions from the Paradox Formation? I hypothesized that the selected sites are outcrops of inclusions derived from the Paradox LES.

I tested this hypothesis by determining the lithologies and fossil content of inclusions. If the outcrops are inclusions derived from the Paradox LES, the age determined from lithology/fossil content must not be younger than the Paradox Formation. However, lithologies and fossils derived from older strata may be present as recycled clasts/bioclasts into younger Paradox Formation LES depositional facies and therefore be included in inclusions derived from the Paradox Formation.

1.4.2 Hypothesis B

The second hypothesis builds on Hypothesis A as it assumes that inclusions were deposited as lithologies of the Paradox Formation. The observation that conglomerate inclusions contain many carbonate clasts, which are not expected to survive transport from a distant source (i.e., Uncompahgre uplift) suggests that a more local source was present. A potential local source of the carbonate clasts could be the basement steps present in the PB salt tectonics region. Were PB basement steps shedding debris into the PB during the deposition of the LES? I hypothesized that in addition to the Uncompahgre uplift, basement steps within the PB served as local detrital sources for the LES. If this hypothesis is proven true, then my first hypothesis must also be true.

I tested this hypothesis by comparing the crystalline basement components to the sedimentary rock components in conglomerates and sandstones. Additionally, the distance from the source area was tested by investigating the shape (roundness), preservation (indicators for weathering, rinds), and relative abundance of clasts that typically would be attributed to a major uplift where crystalline basement is exposed (i.e., Uncompahgre uplift) relative to sedimentary rocks that could also be exposed at a basement step. I also tested Hypothesis B by exploring the relationships established in the paleogeographic concept of proximity to the Uncompahgre uplift. If inclusions from more distal sites show a higher abundance of sedimentary rock clasts or if the composition of those clasts differs from the crystalline basement, my hypothesis would be supported.

1.5 Field Sites

The PB is host to multiple salt walls (Fig. 1), some of which have been previously identified to contain inclusions at easily accessible locations: Sinbad Valley (Thompson Jobe et al., 2019), Salt Valley (Gard, 1976; Dane, 1935; Rasmussen, 2014), Gypsum Valley (Deatrick, 2019),

Professor Valley (Scott, 2022), and Onion Creek (Hudson et al., 2017; Lankford-Bravo, 2021). Due to the unprecedented nature of this research, initial reconnaissance of five potential field sites (Sinbad Valley (CO), Salt Valley (UT), Gypsum Valley (CO), Onion Creek (UT), and Moab Valley (UT) diapirs) was necessary to determine the suitability of these areas for my project. From this reconnaissance field excursion, three sites Sinbad Valley (CO), Salt Valley (UT), and Gypsum Valley (CO) diapirs, were selected for further research because they contain unusual clastic facies not common in the Paradox Formation cycles. These facies provided the best opportunity to provide insight into the two hypotheses I was testing. The following are observations made at each of the salt walls reviewed on the reconnaissance trip (and Professor Valley (UT) which was visited later) and reasoning on why the salt wall was chosen or rejected for more in-depth analysis.

1.5.1 Sinbad Valley

The Sinbad Valley diapir is host to previously characterized conglomeratic inclusion outcrops (Thompson Jobe et al., 2020). Of particular interest is an outcrop of an extremely resistant, compacted conglomerate found in a streambed (38°29'9.67"N, 108°58'31.34"W). This conglomerate has predominantly carbonate clasts with fossils, but also includes clasts of black and white (often fossiliferous) chert, and quartz sandstone (Fig. 14). Within the carbonate and chert clasts, crinoid, fusulinid, fenestrate bryozoan, sponge, and ooids were identified by Thompson Jobe et al. (2020) and I further identified gastropod, tabulate coral, and brachiopod fossils during my reconnaissance excursion (Fig. 15). One of the outcrops of conglomerate was found to be fining upwards with rip up clasts. This site was thus selected as a study site with the main goal of determining if basement steps served as a source of detrital material found in these conglomerates.

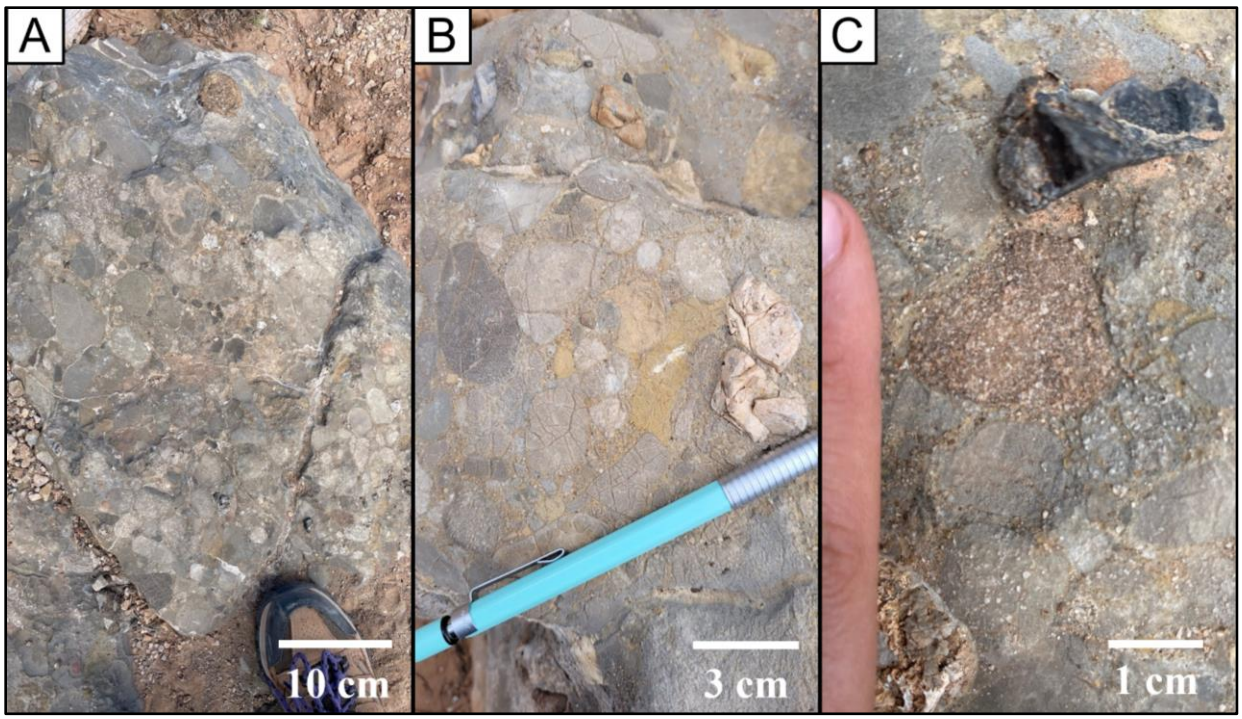

Figure 14: Variety of clast lithologies in Sinbad Valley
Pictures show the variety of clast lithologies found within the Sinbad Valley conglomerates. Clasts impinge on each other indicating compaction of conglomerate.

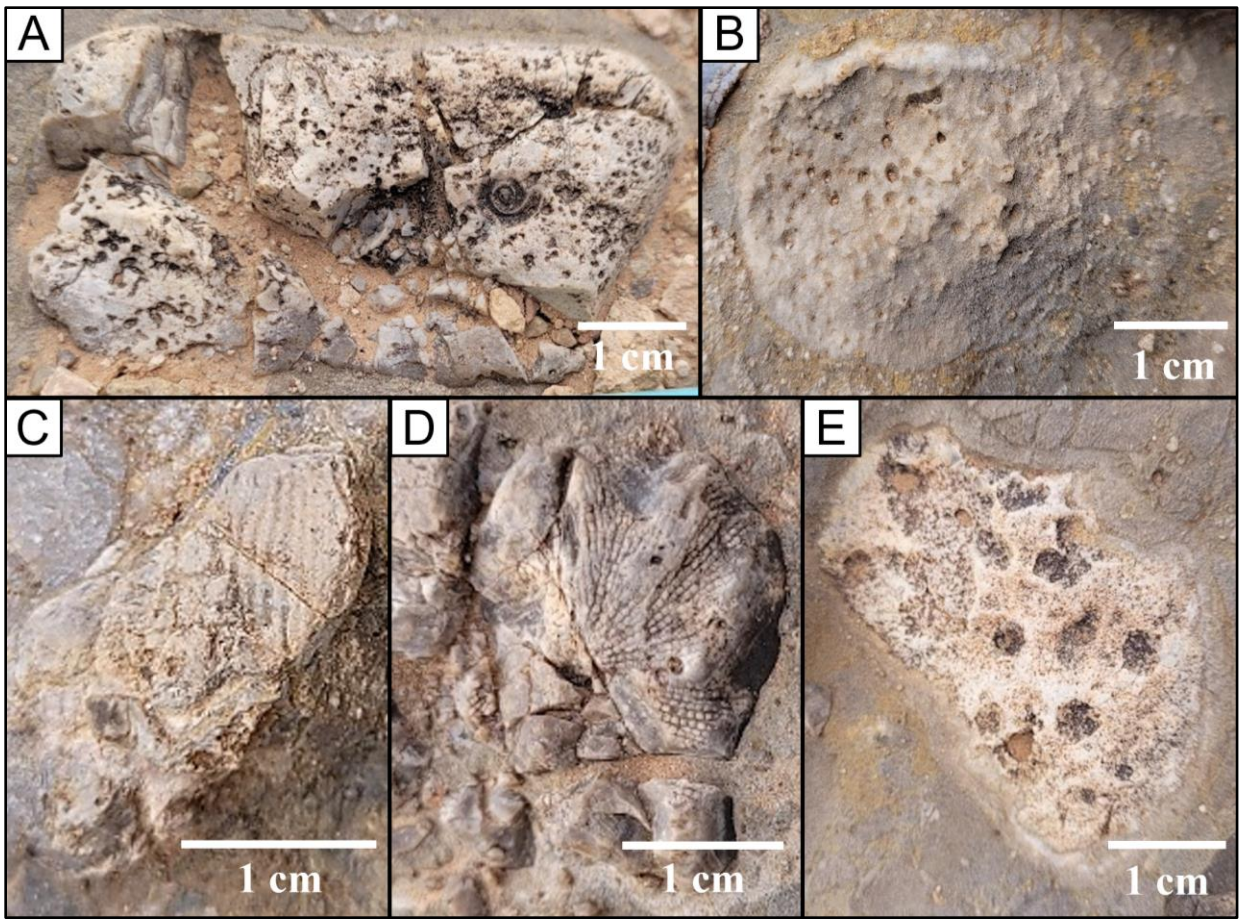

Figure 15: Fossils in Sinbad Valley carbonate and chert clasts
Pictures show the many varieties of fossils identified in outcrop within the carbonate and chert clasts in the Sinbad Valley conglomerate (A: gastropod, B: sponge, C: bivalve, D: fenestrate bryozoan, E: tabulate coral).

1.5.2 Salt Valley

Within the part of the Salt Valley diapir that lies northwest of the limits of Arches National Park and just inside the northwest corner of the park, I discovered the most interesting outcrops of inclusions similar to those identified at Sinbad Valley. This diapir is host to many inclusions with a wide variety of lithologies, but most striking among them is a large, faulted outcrop of conglomerate with clasts varying in both lithology and size. This outcrop contains fossils which have been researched by Dane (1935), Gard (1976), Rasmussen, 2014; and Ritter (conodonts; 2021, personal communication). This elongate, faulted conglomeratic outcrop is located east of

the Klondike Bluffs along Salt Valley Road (38°49'20.08"N, 109°42'4.14"W) and is one of the northernmost and largest contiguous inclusion outcrops identified within the Salt Valley diapir. Bordered by the Cedar Mesa Hill dome to the north and by the Chinle Caprock dome to the southeast, there are many smaller conglomerate and carbonate outcrops identified with an outcrop separation of as low as ~5 m between conglomerate and carbonate. Additionally, a chert block with a gastropod was identified (Fig. 16). Due to the incredible exposure of large blocks of inclusions, Salt Valley was selected as a study site.

Figure 16: Gastropod in chert

Picture shows a well-preserved gastropod in chert found in float near a Salt Valley outcrop.

1.5.3 Gypsum Valley

The Gypsum Valley diapir hosts many geological features critical to the modern understanding of salt diapirism, for example the megaflap and radial faults in Big Gypsum Valley (Mast, 2016; Deatrick, 2019; Escosa et al., 2019) and the burial wedges (Langford et al., 2022) and atypical carbonate caprock in Little Gypsum Valley (Lerer, 2017; Poe, 2018; Brunner et al., 2019; Labrado, 2021). While inclusions have been observed in Gypsum Valley, they have been previously considered as relatively small and poorly exposed (Deatrick, 2019; Giles and Brunner, personal communication, 2021). During the November 2021 visit to the Bridge Canyon location (38° 9'16.69"N, 108°52'51.34"W) at the Gypsum Valley field site, adjacent to a salt shoulder (McFarland, 2016), we identified an inclusion block with a wide variety of lithologies at the contact between diapiric caprock and outlying strata. Due to the expected scarceness of inclusions, Gypsum Valley originally was not considered as a target for my project, but after discovering this interesting, folded outcrop of inclusions, it was selected as a study site in the hopes of discovering how inclusions are affected by diapirism.

1.5.4 Onion Creek

Onion Creek diapir is host to many inclusion outcrops including lithologies of black shales, fossiliferous sandstones and limestones, quartz sandstones, and mudstones (Hudson et al., 2017). Our reconnaissance of the field area confirmed this finding. However, with one exception, the encountered lithologies have also been identified at my other field sites, where they are better exposed. The exception is a crinoid- and brachiopod-rich limestone outcrop (38°41'49.98"N, 109°15'15.74"W). However, there is considerable debate about the origin of this rock package (Lankford-Bravo, 2021) and it was determined that within the framework of a master’s thesis it

would not be possible to come to a conclusive answer to the question of if this is an inclusion. So, the Onion Creek Diapir was not further investigated in this study.

1.5.5 Professor Valley

The Professor Valley diapir has been extensively studied by Scott (2022) where he identified sandstone and conglomerate inclusion outcrops. Scott (2022) describes inclusion facies (which he referred to as lithosomes) of calcareous sandstone, quartz sandstone, carbonate mudstone, calcite recrystallized dolomite, stromatolitic dolomicrite, carbonate-matrix conglomeratic sandstone, and sandy carbonate lithoclast wackestone. The area of inclusion exposure within Professor Valley is relatively small, the inclusions have been carefully described and mapped by Scott (2022), and outcrop conditions are not optimal. I visited this site in May 2022 to assess the inclusions and recognized lithologies similar to inclusions I had previously studied at other sites (with the exception that some inclusions at Professor Valley contain feldspars), so, this site was omitted from further study, but results from Scott (2022) were incorporated into the discussion of the origin of PB inclusions.

1.5.6 Moab Valley

So far, the Moab Valley diapir has not been intensely studied by our group (Brunner et al., 2019). After a personal communication (2021) with Dr. Benjamin Brunner and Dr. Katherine Giles and review of a geologic map including the Moab Valley anticline (Doelling, 1985), this location was assessed as a potential study area. At the northwestern side of the Moab diapir (38°34'13.05"N, 109°34'13.18"W), a prominent band of carbonate rocks that are associated with some black shales and sandstones, crops out at or near the diapir margin. Visiting this site, we assessed the potential that these carbonates are inclusions and determined that many of the exposed features (types of carbonates, interbedding with shales, continuity of outcrop) are strongly reminiscent of megaflap

strata found at Big Gypsum Valley (Mast, 2016), highlighting the potential that these outcrops do not represent inclusions. Thus, this site was omitted from my study.

1.6 METHODOLOGY

1.6.1 Field Work

Field work consisted of the initial reconnaissance field excursion in November 2021 to determine suitable field sites, and then a primary field excursion in May 2022 to research these field sites. Field work was a prime component in the research of inclusions as the spatial variability and distribution of outcrops was necessary to reconstruct the depositional setting and history of the Sinbad Valley, Salt Valley, and Gypsum Valley salt walls.

At all three sites, field work during the primary field excursion was comprised of geologically mapping inclusions, determining sedimentary facies and their distribution, and collecting samples for laboratory analyses. Geologic mapping was completed using the StraboSpot app to outline surficial exposures of inclusions. StraboSpot data was imported into ArcGIS Pro for final map production. At the Gypsum Valley site, a stratigraphic section was measured using a Jacob's staff and many strikes and dips were taken with a quadrant notation Brunton compass on limbs and hinges of folds. Measuring sections at the other two field sites was unsuccessful due to the disrupted nature of the inclusions. Gard (1976) came to a similar conclusion at the Salt Valley salt wall, attributing the issue to the convoluted nature and high variability in lithologies at the exposed outcrops (Doelling, 1988).

Due to the small scale of the Gypsum Valley outcrop and its near-vertical exposure, traditional mapping methods were substituted by annotating photographs of the outcrop to outline various lithologies and folds. As the Gypsum Valley outcrop hosts four measurable folds, stereonet

analysis was applied to determine the nature of these folds and find interlimb angles as well as the trends and plunges of the fold axes.

1.6.2 Petrography

For petrographic analyses, samples collected in the field were cut into billets using a tile saw, then sent to petrographic services companies to be made into thin sections. Associated hand samples, billets, and thin sections were given matching labels relating to the location where the sample was obtained. All thin sections were half stained with a combination Alizarin Red S and potassium ferricyanide solution to aid in the differentiation between calcite and dolomite as well as ferrous carbonate minerals. Glass cover slides were utilized for each thin section to protect the integrity of the thin section and staining. Vacuum impregnation processes were utilized for samples that were fractured or porous. The initial reconnaissance field excursion resulted in 35 samples, which were sent to Spectrum Petrographics, Inc. in Vancouver, WA, and the primary field excursion resulted in 73 samples, which were sent to Texas Petrographic Services in Houston, TX. Thin sections were petrographically analyzed using a Leica DM750P polarizing microscope. Observations in outcrop, hand specimen and thin sections focused on color, composition, grain/clast size, matrix material, and textures to aid in the description of various lithologies and to identify diagenetic alterations for inclusions at the three field sites.

1.6.3 Isotope Analyses

Carbon and oxygen isotope analysis ($\delta^{13}C$ and $\delta^{18}O$) of carbonate was conducted for select inclusion samples utilizing the billets cut from field-obtained hand samples where possible and uncut hand samples when a billet was not available. Samples were chosen to analyze conglomeratic clast lithologies, matrix material, and similar lithologies displaying different diagenetic alterations, such as different types of cements. The selection resulted in 71 of the 105

available billets and six uncut hand samples being used for isotope analysis. Powders were drilled with a Dremel microdrill and the resulting 90 samples were sent to the W.M. Keck Paleoenvironmental and Environmental Stable Isotope Laboratory (KPESIL) at the University of Kansas for carbon and oxygen isotope analyses. The KPESIL uses a ThermoFinnigan MAT253 IRMS isotope ratio mass spectrometer in continuous-flow mode for the analysis.

Chapter 2: Results

2.1 Inclusion Lithologies: Description, Distribution, and Interpretation

The Sinbad Valley, Salt Valley, and Gypsum Valley salt walls have various inclusion lithologies present, some of which are present at all three diapirs (Fig. 17). The following sections describe these various lithologies, their similarities and variations in comparison to each other, and their distribution within the salt walls and the PB, as well as interpret their depositional setting. Tables 1-4 provide descriptions from petrographic analysis of all inclusion samples collected at my three field sites and includes locations where these lithologies were observed.

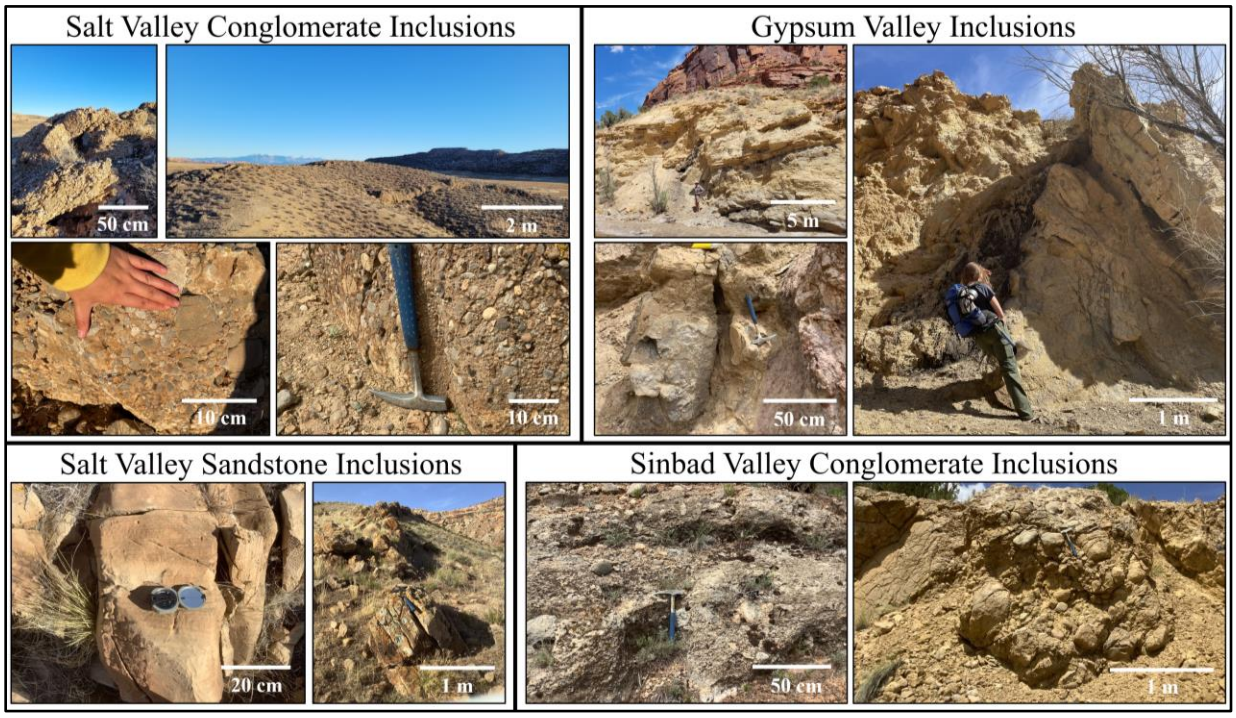

Figure 17: Outcrop photographs of inclusions
Outcrops in the Gypsum Valley, Salt Valley, and Sinbad Valley diapirs. Smaller-scale pictures for reference where conglomerate clasts are too small to see in large-scale pictures.

Table 1: Petrographic attributes of sandy limestone samples

Tabulated data from petrographic analysis of sandy limestone samples. F: ferroan.

Sandy Limestones

	Location			Grains								Matrix			Fossils				Cement		Diagenetic Alterations			
TS #	Gypsum Valley	Salt Valley	Sinbad Valley	Chert	Dolomite	Fossil	Glauconite	Mica	Micrite	Ooids	Quartz	Dolomite	Micrite	Microspar	Brachiopods	Bryozoans	Echinoderms	Sponges	Calcite	Calcite (Ferroan)	Dolomitization	Fractures	Fracture fill	Pyrite
Non-Fossiliferous Sandy Limestone																								
60																							most	
61																							most	
30																								
5																								
29																								
47																							most	
58																								
Oolitic Sandy Limestone																								
23																								
25																								
Fossiliferous Sandy Limestone																								
33																								
34																								
46																								
55																								
57																								
Mica-Bearing Sandy Limestone																								
62																								
63																								
64													F											
65																								
66																								
67													F											
68													F											
69																								
70																								
71																							most	
72																								
73																								

Table 2: Petrographic attributes of sandstone samples
Tabulated data from petrographic analysis of sandstone samples. F: ferroan.

Sandstones																				
	Location		Grains							Fossil Grains			Cement			Diagenetic Alterations				
TS #	Salt Valley	Sinbad Valley	Chert	Dolomite	Carbonate/Fossil	Glauconite	Micrite	Ooids	Quartz	Brachiopods	Echinoderms	Peloids	Calcite	Calcite (Ferroan)	Silica	Dolomitization	Dedolomitization	Fractures	Fracture fill	Pyrite
Quartz Sandstone																				
28																				
45																F				
Carbonate-Quartz Sandstone																				
27																				
32																				
35																				
26																				
36																				
37																				
Sinbad Valley CGcs Sandstone Clasts (TS# 48, 49) and Matrix (TS# 50)																				
48																				
49																				
50																				

Table 3: Petrographic attributes of conglomerate samples

Tabulated data from petrographic analysis of conglomerate samples. Thin sections of conglomerate samples with pebble sized clasts were utilized for analysis of conglomerate fabrics and matrix material.

Conglomerates:																				
	Location		Matrix							Fossils/Grains					Cement		Diagenetic Alterations			
TS #	Salt Valley	Sinbad Valley	Chert grains	Dolomite	Fossil Grains	Glauconite	Micrite	Microspar	Quartz grains	Brachiopods	Bryozoans	Echinoderms	Ooids	Peloids	Calcite	Calcite (Ferroan)	Dolomitization	Fractures	Fracture fill	Pyrite
Calcite Cement Only																				
40																				
43																			most	
44																				
52																				
54																				
Calcite and Ferroan Calcite Cement																				
4																				
22																				
24																				
51																				
53																				
59																			most	

Table 4: Petrographic attributes of conglomerate clast samples
Tabulated data from petrographic analysis of conglomerate clast samples. F: ferroan. HS: fossil identified in hand sample that thin section was derived from, but not analyzed or seen in the thin section itself.

Conglomerate Clasts:																
	Location		Fossils/Grains							Cement			Diagenetic Alterations			
TS #	Salt Valley	Sinbad Valley	Bivalves	Brachiopods	Bryozoans	Echinoderms	Ooids	Ostracodes	Sponges	Calcite	Calcite (Ferroan)	Silica	Dolomitization	Dedolomitization	Fractures	Fracture fill
Fossiliferous Carbonate Clasts																
3																
8																
9																
10																
11									HS							
21																
1																
7																
13																
17																
18																
12																
20																
38																
39																
56																
42			unidentifiable													
Non-Fossiliferous Dolomicrite Clasts																
6														F		
15																
2																
19																
41																

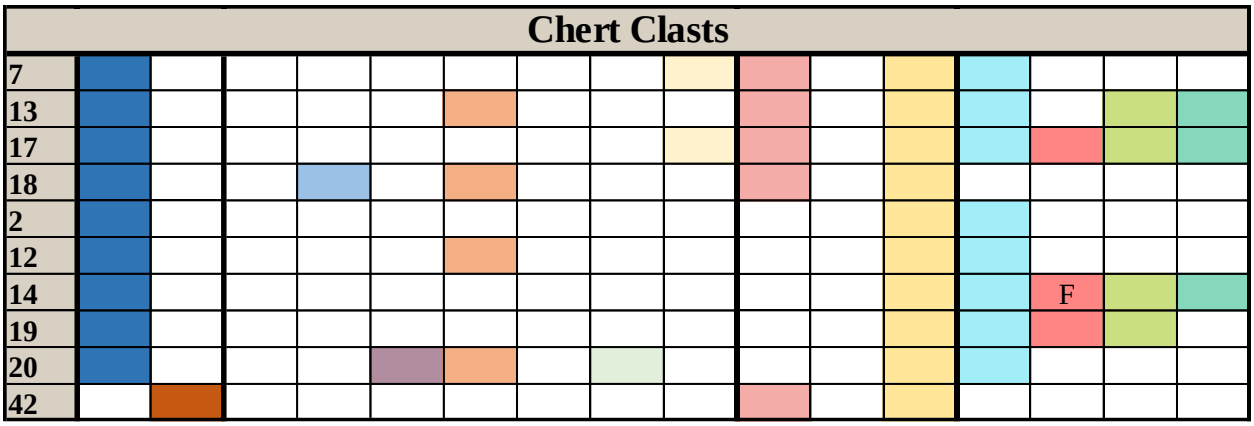

The inclusions studied fall into four main lithologies: black shale, sandy limestone (Table 1), quartz sandstone (Table 2), and carbonate-clast conglomerate (Tables 3, 4). Each of these lithologic groups represent different sedimentary facies and their attributes are used to determine their depositional environments. Due to the general lack of sedimentary structures in most inclusions, depositional facies are based mainly on constituents and their fabrics. However, due to the uncertainty involved in age constraints and clastic source areas associated with this research, they are not grouped into definitive geologic formations. The carbonate-clast conglomerates provide the most information for elucidating the depositional history of inclusions in the PB.

2.1.1 BS: Black Shale (Black Laminated Mudstone)

Black shale (BS) inclusions have only been evaluated in this study from two beds cropping out in Gypsum Valley, though this inclusion lithology is the most common in the Paradox Formation LES. It was not possible to make thin sections with samples retrieved from the Gypsum Valley beds because samples crumbled while attempting to cut billets, so descriptions are limited to outcrop observations.

Observations: The BS are light gray or light brownish-gray on weathered surfaces and black on fresh surfaces. The two BS beds at Gypsum Valley range in thickness from 0.2 m to 0.8 m and these thicknesses are variable along the length of each bed because of the intense folding of

this outcrop (Fig. 18). BS locally form resistant beds (Lb3b, Lb3ai; Fig. 18) or weathered recessive beds (Lb3a; Fig. 18). BS are thinly, planar laminated with common silt-sized grains. The BS lack visible fossils or trace fossils and emit a fetid odor when cleaved suggesting they are high in organic content.

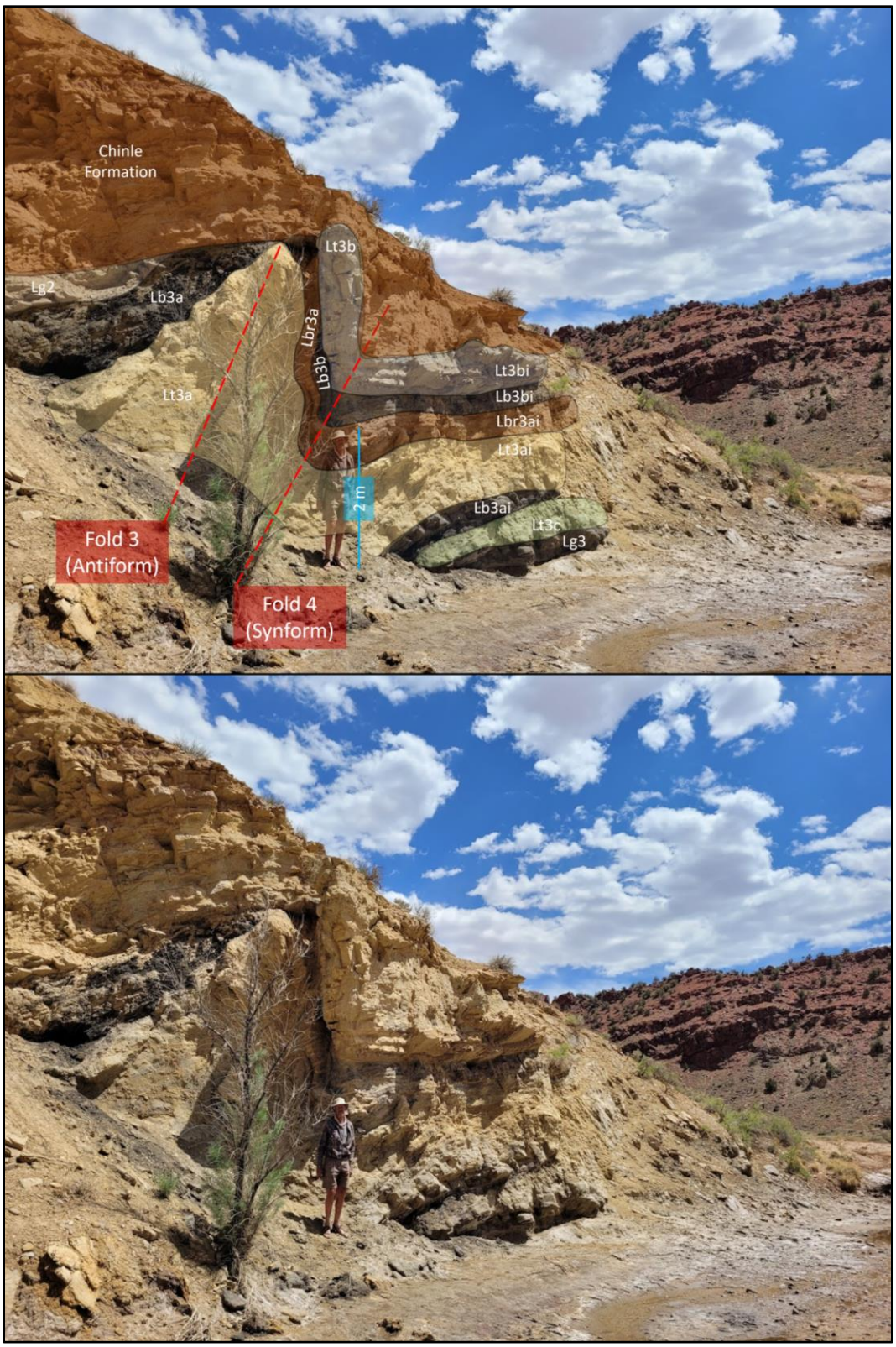

Figure 18: Gypsum Valley Image Map #1
Southernmost outcrop exposure at Gypsum Valley, view #1.

Interpretations: The BS were deposited in a quiet, anoxic/anaerobic most likely deep marine environment (Choquette and Traut, 1963; Peterson and Hite, 1969; Byers, 1977; Goldhammer et al., 1991). This is evidenced by thin, planar laminae reflecting a low-energy environment and suspension deposition. Additionally, the dark, black color and fetid odor reflects reducing conditions of organic-rich sediments (Choquette and Traut, 1963; Peterson and Hite, 1969; Byers, 1977; Goldhammer et al., 1991).

The BS inclusions lithologically match previous descriptions of the Paradox Formation black laminated mudstone facies (Hite et al., 1984; Raup and Hite, 1992; Goldhammer et al., 1991; Grammer et al., 2000; and Rasmussen and Rasmussen, 2009). Additionally, blocks of black shale would not have survived any length of sedimentary transport, so the shale must have been deposited in situ as a component of the LES. From this follows that deposition in the Paradox Formation LES and subsequent translation during diapirism is the only plausible source of BS inclusions.

2.1.2 SL: Sandy Limestone

Sandy limestone (SL) lithologies were identified at all three sites (Sinbad Valley, Salt Valley, and Gypsum Valley; Table 1). SL inclusion facies can be non-fossiliferous (SLnf), mica-bearing (also non-fossiliferous; SLmb), fossiliferous (SLf), or oolitic (SLo). Relative sandiness (amount of quartz grains) is variable within all facies.

SL inclusion facies match Paradox Formation limestone facies described by Choquette and Traut (1963), Pray and Wray (1963), and Goldhammer et al. (1991). The SL inclusion facies comprise traits described for the intermediate and sponge facies of Goldhammer et al. (1991), which are stratigraphically related (the intermediate facies overlying the sponge facies). Goldhammer et al. (1991) interprets the sponge facies deposition in a reducing environment during

the shift from transgressive to regressive phases, marked by the deposition of the overlying oxygenated intermediate facies. The SL inclusion facies represent shallow marine deposition under differing flow regimes and variable restricted to oxygenated conditions, which agrees broadly with these interpretations by Goldhammer et al. (1991).

2.1.2.1 SLnf: Non-Fossiliferous Sandy Limestone

Observations: SLnf are yellowish-tan, bright brownish-tan, tannish-gray, or gray on weathered surfaces and light brownish-tan or light to dark gray on fresh surfaces, with planar, laminated bedding (Fig. 19). All SLnf have silt to very fine sand size, subangular to subrounded, moderately sorted, compacted (Fig. 20-A,B) quartz grains (abundance is variable; Figs. 20, 21). SLnf are dominated by either micrite (Fig. 21) or microspar (Fig. 20) matrix. SLnf are cemented by calcite, have calcite fracture fill, and most have some dolomitization. Additionally, SLnf may have glauconite grains and pyrite crystals (some altered to hematite; Fig. 20-A,B).

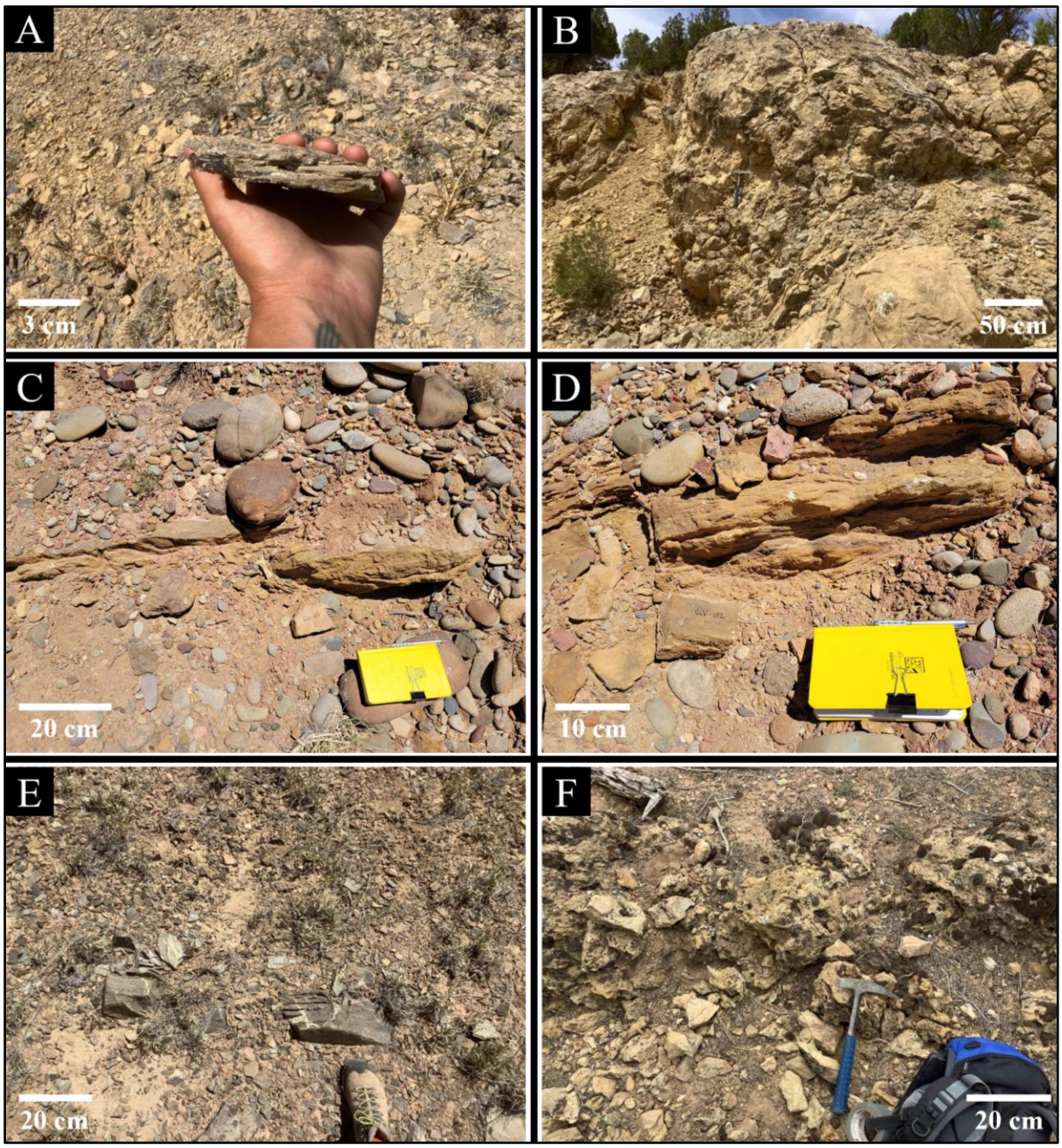

Figure 19: Outcrop photographs of non-fossiliferous sandy limestone (SLnf) sample locations Images of outcrops where SLnf samples were gathered. A) Image shows hand sample taken in Salt Valley. B) Image show overview of CGc outcrop in Sinbad Valley where SLnf sample was taken. C-D) Images show bright brownish-tan SLnf outcrops in Gypsum Valley with thin, planar bedding. E) Image shows small SLnf outcrop in Salt Valley with planar, laminated bedding. F) Image shows SLnf outcrop in Sinbad Valley.

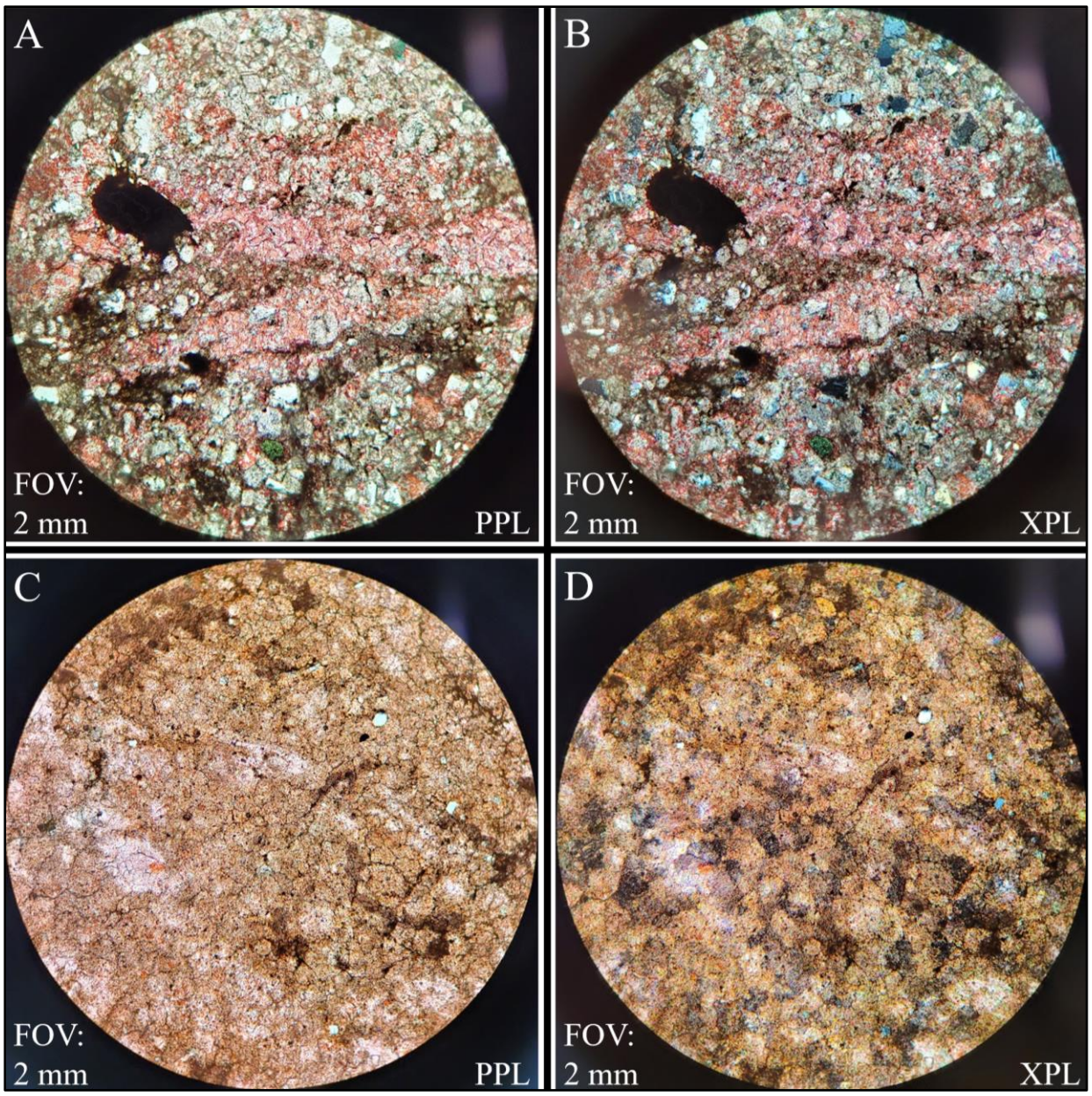

Figure 20: Photomicrographs of microspar-dominated SLnf
Photomicrographs of microspar-dominated SLnf endmembers. A) Plane-polarized light and B) cross-polarized light thin section photomicrographs of SLnf with higher amount of quartz grains. C) Plane-polarized light and D) cross-polarized light thin section photomicrographs of SLnf with minor amount of quartz grains.

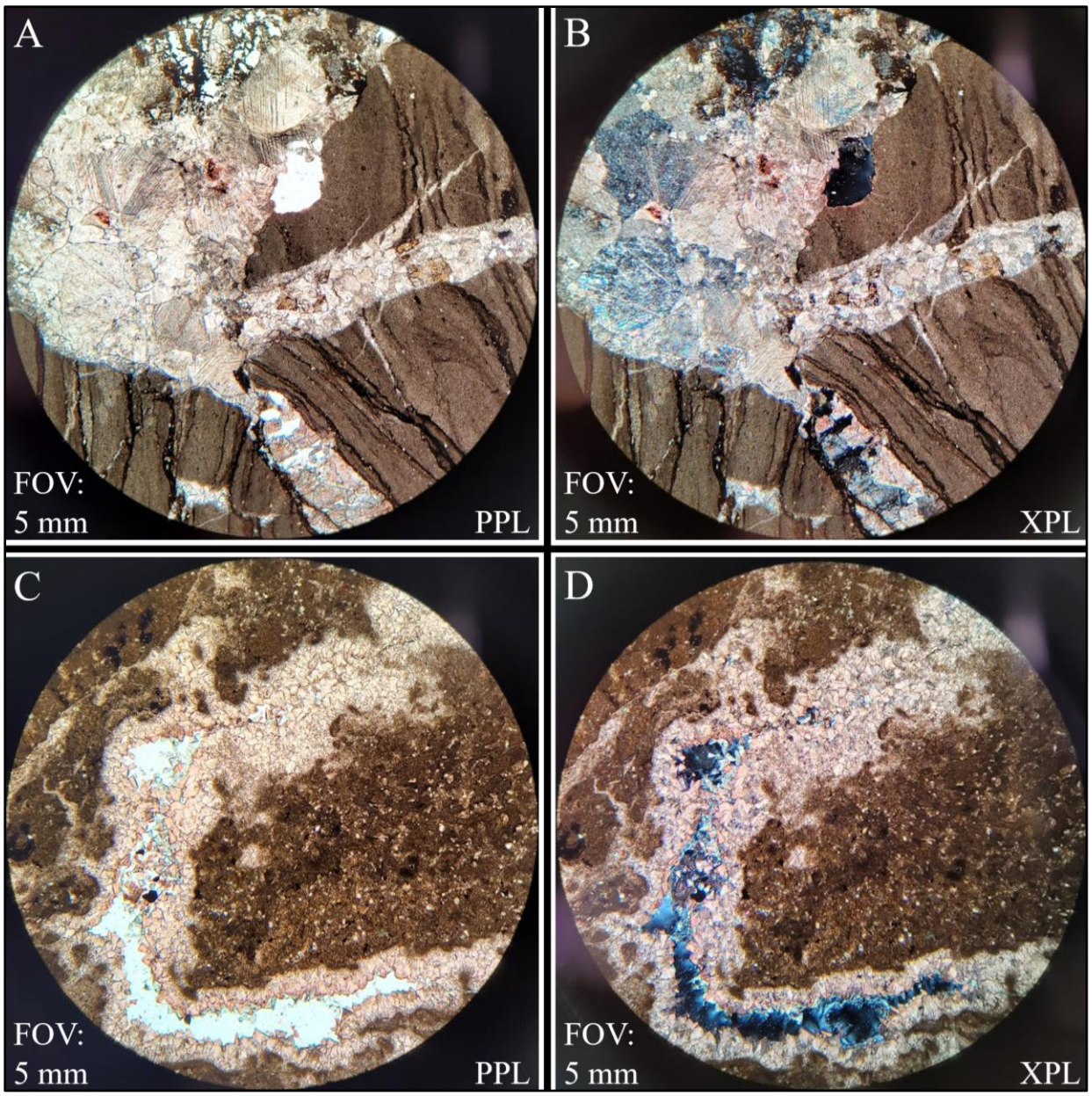

Figure 21: Photomicrographs of micrite-dominated SLnf
Photomicrographs of micrite-dominated SLnf endmembers. A) Plane-polarized light and B) cross-polarized light thin section photomicrographs of SLnf brecciated sample. Note large, blocky calcite cement. C) Plane-polarized light and D) cross-polarized light thin section photomicrographs of SLnf. Note isopachous calcite cement.

Interpretations: SLnf are deposited in quiet water from suspension settling interpreted from the micritic, planar-laminated bedding which indicates calm water allowing fine grains to settle without being disturbed (Shinn, 1983; Pratt, 2010). The micrite-dominated SLnf signify a

short distance of travel and reflect deposition in low-energy, relatively calm waters. Pyrite indicates reducing conditions (Scholle and Ulmer-Scholle, 2003). The microspar-dominated SLnf reflect later neomorphic recrystallization possibly from an early influx of meteoric water during glacioeustatic fluxes (Folk, 1959; Scholle and Ulmer-Scholle, 2003). Where pyrite is altered to hematite, oxidizing conditions are interpreted as occurring near the surface during meteoric diagenesis.

2.1.2.2 SLmb: Mica-Bearing Sandy Limestone

Observations: Mica-bearing sandy limestones (SLmb) are gray, tan, pink, and red on weathered surfaces and light gray, light greenish-gray, light tannish-gray, light tan, purple, dark gray, and dark greenish-gray on fresh surfaces. SLmb beds, with the exception of thick wedges in folds, are 0.17 m to 1.21 m thick with laminated to thin, planar bedding (Figs. 18, 22, 23). SLmb samples show a remarkable similarity in constituents with all containing silt to very fine sand (with rare fine) size, subangular to subrounded, moderately sorted quartz grains (Figs. 24, 25). Quartz grains exhibit compaction and occasionally have suture contacts (Fig. 24). SLmb contain silt and sand size muscovite (mica) flakes. This lithology has a micrite matrix, and contains replacive dolomite rhombs, pyrite, and calcite cement. The main deviations between samples show a difference in amount of dolomitization and quartz grains, randomness (Fig. 25) versus coherent layering of quartz grains (Fig. 24), and presence or absence of glauconite and ferroan calcite cement or micrite matrix (Fig. 25-C,D).

Figure 22: Gypsum Valley Image Map #2
Northernmost outcrop exposure in Gypsum Valley.

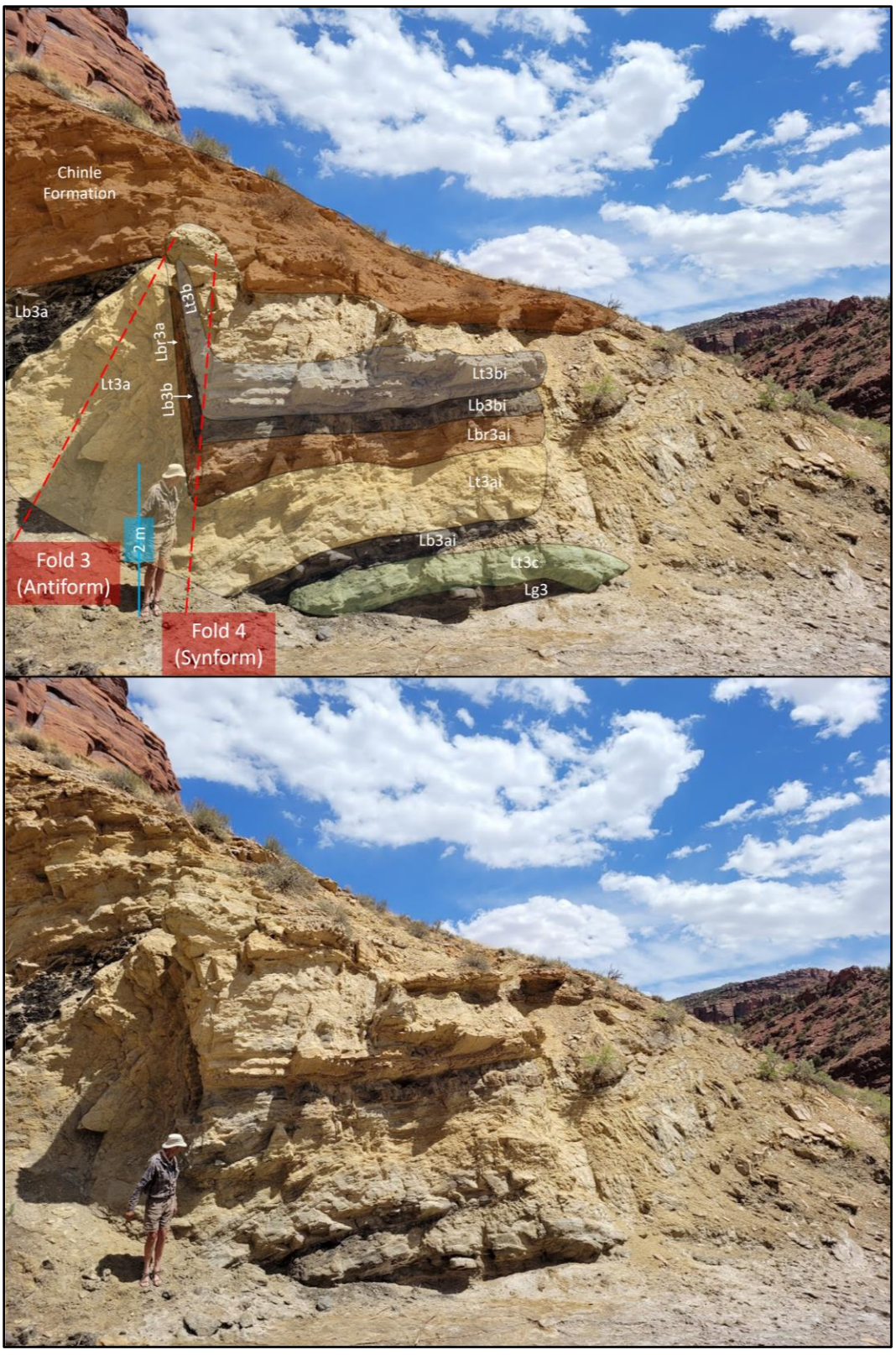

Figure 23: Gypsum Valley Image Map #3
Southernmost outcrop exposure at Gypsum Valley, view #2.

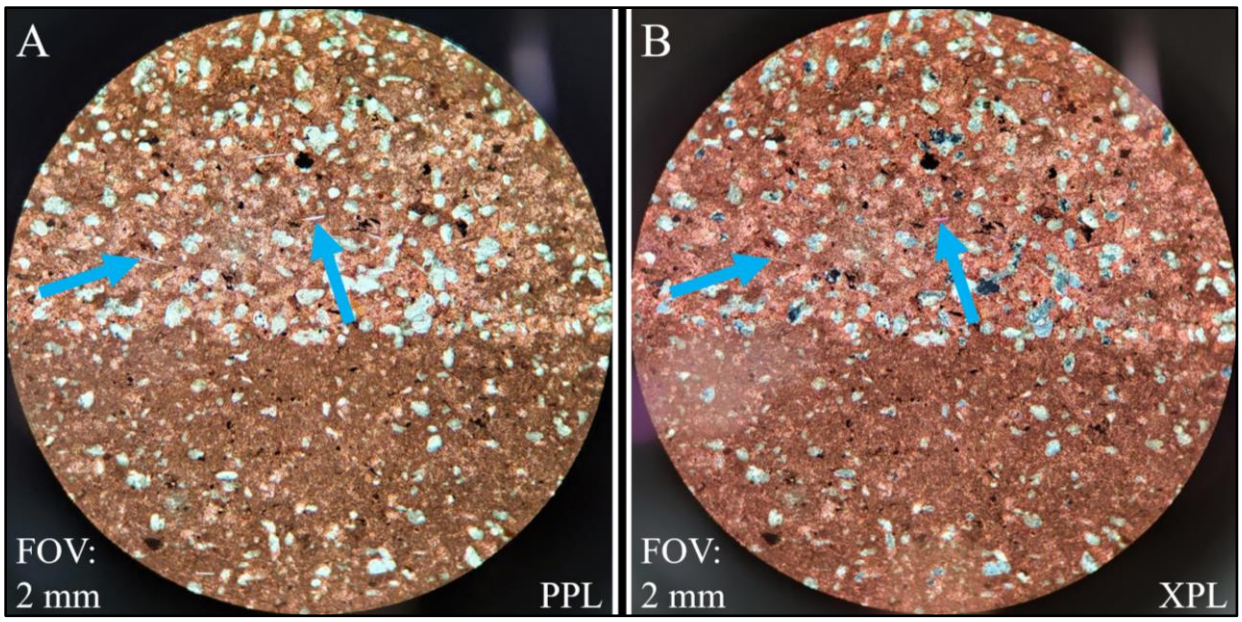

Figure 24: Photomicrographs of mica-bearing sandy limestone (SLmb)
Photomicrographs of SLmb endmember. A) Plane-polarized light and B) cross-polarized light thin section photomicrographs of SLmb with coherent layering of quartz grains. Blue arrows point to mica flakes.

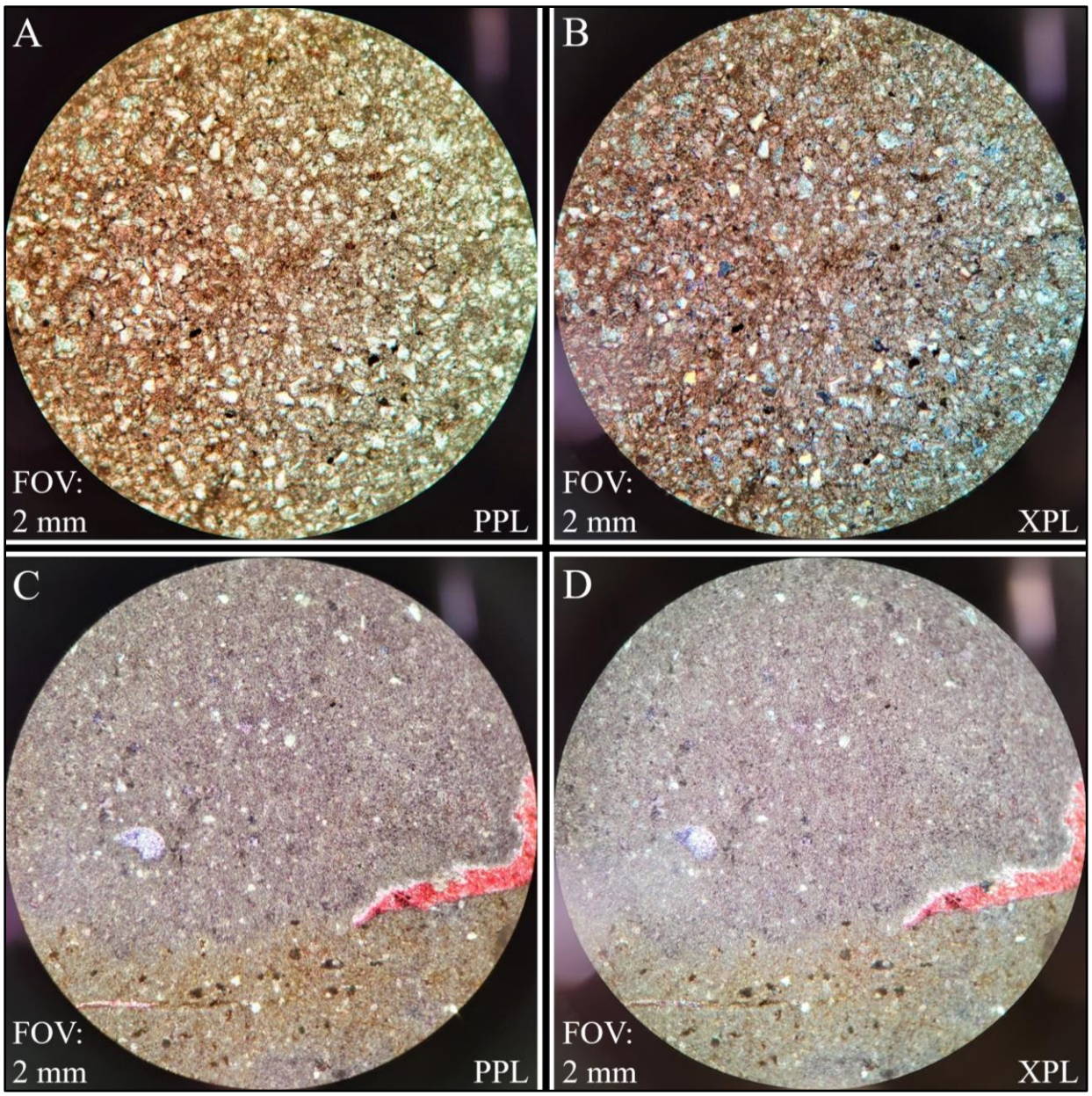

Figure 25: Photomicrographs of SLmb
Photomicrographs of SLmb endmembers. A) Plane-polarized light and B) cross-polarized light thin section photomicrographs of SLmb. Note randomness of quartz grains. C) Plane-polarized light and D) cross-polarized light thin section photomicrographs of SLmb with non-ferroan (red) and ferroan (purple) calcite cement and micrite. Note minimal sandiness.

Interpretations: SLmb is interpreted to be deposited in a lower energy environment evidenced by the fine size of grains and laminated to thin, planar bedding (Shinn, 1983; Pratt, 2010). Additionally, the presence of micrite bedding indicates suspension deposition in calmer

waters. Deposition in a marine environment, slow sedimentation, and reducing conditions are indicated by the presence of glauconite and restriction of this environment under reducing conditions is further evidenced by a lack of normal marine fossils, pyrite, and ferroan calcite cements and matrix (Scholle and Ulmer-Scholle, 2003).

2.1.2.3 SLf: Fossiliferous Sandy Limestone

Observations: SLf are light gray on weathered surfaces and light gray to light brownish-tan on fresh surfaces, with thin, planar bedding (Fig. 26-A,B). SLf have a micritic, sandy matrix with very fine to medium sand size, subangular to subrounded, moderately sorted quartz grains (Figs. 26-C,D, 27). SLf are cemented by calcite and underwent partial dolomitization (often forming rhombs). Slf can be either mixed-grain packstones (Fig. 27) or boundstones (Fig. 26-C,D) defined by encrusting sponges. The mixed-grain packstone SLf contain echinoderms and may contain chert, peloids, brachiopods, bryozoans, and ooids. Fossils are disarticulated and abraded fragment grains and grains are compacted and occasionally have suture grain boundaries in mixed-grain SLf (Fig. 27-A,B). SLf usually have pyrite crystals and commonly contain glauconite.

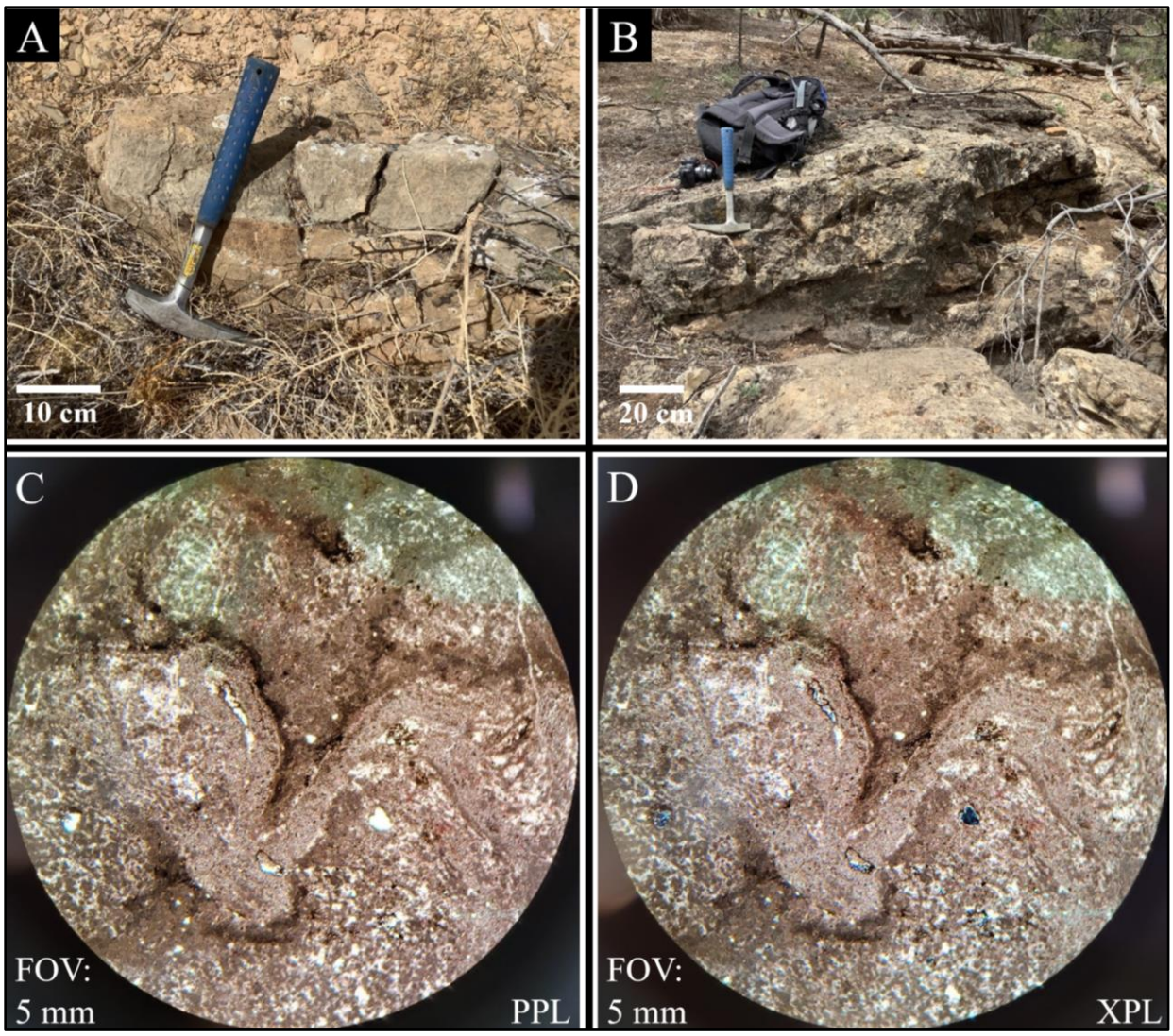

Figure 26: Outcrop images of fossiliferous sandy limestone (SLf) sample locations and photomicrographs of SLf boundstones

Images of outcrops in A) Salt Valley and B) Sinbad Valley where SLf samples were gathered. C) Plane-polarized light and D) cross-polarized light thin section photomicrographs of SLf micritic (sponge) boundstone endmember with extremely low sand content.

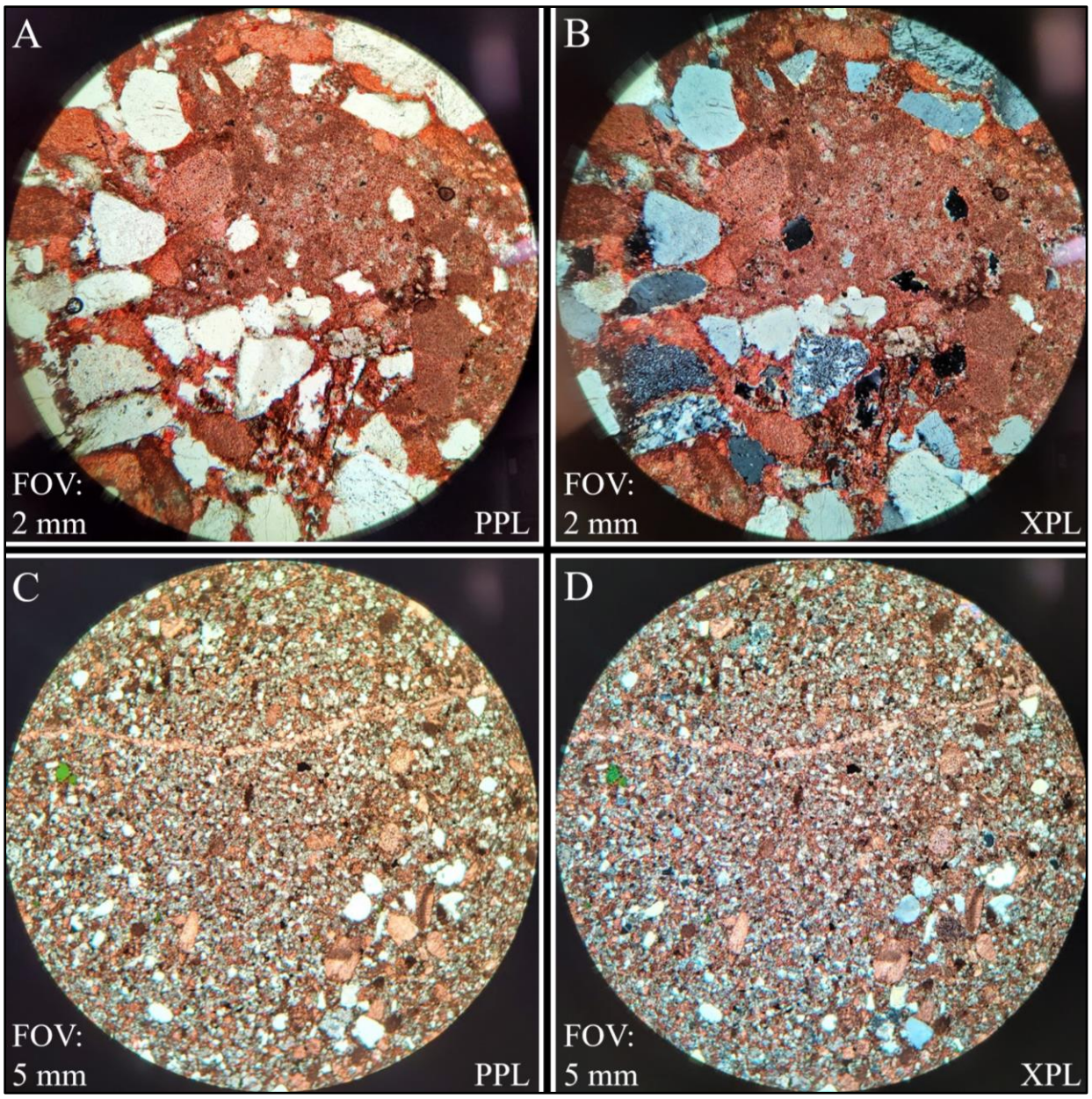

Figure 27: Photomicrographs of SLf packstones
Photomicrographs of SLf mixed-grain packstone endmember. A) Plane-polarized light and B) cross-polarized light thin section photomicrographs of SLf with micritic fossil fragments and matrix. Note chert replacing quartz grains. C) Plane-polarized light and D) cross-polarized light thin section photomicrographs of SLf with higher sand content.

Interpretations: SLf is interpreted to be deposited in a normal marine environment based on the fine to medium sand grains, normal marine fossils, and sponges. The disarticulation and abrasion of fossil grains and presence of variable sand sizes indicate a higher energy environment,

and the presence of normal marine fossils is evidence of oxygenated conditions. (Shinn, 1983; Pratt, 2010).

2.1.2.4 SLo: Oolitic Sandy Limestone

Observations: SLo are light to dark gray on weathered surfaces and light gray on fresh surfaces, with thin, planar bedding (Fig. 28A). SLo are micritic oolitic packstones (Fig. 28-B), that contain silt-sand size, subangular to subrounded quartz grains. SLo are cemented by calcite (some ferroan) and are partially dolomitized. Ooids display a compaction fabric.

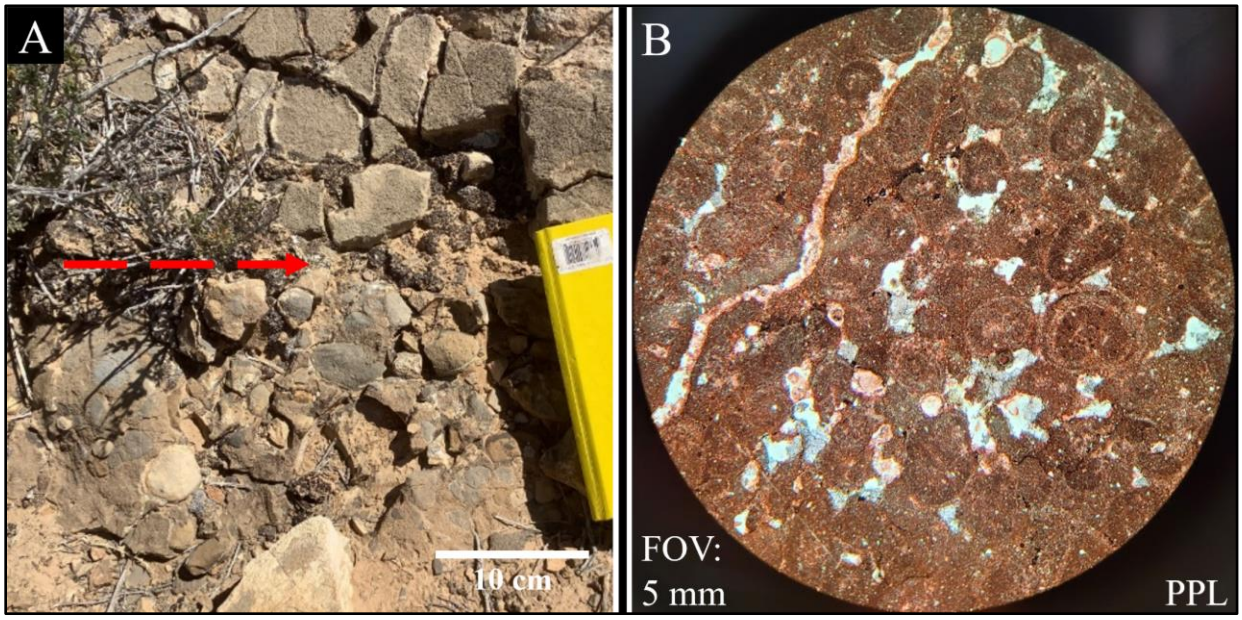

Figure 28: Outcrop image and photomicrograph of oolitic sandy limestone (SLo)
A) Image shows outcrop of SLo in Salt Valley where sample was gathered. Red dashed arrow outlines and points to contact with CGc. B) Plane-polarized light thin section photomicrograph of SLo micritic oolitic packstone. Note dolomitization of some calcite cement.

Interpretations: SLo is interpreted to be deposited in a current agitated, normal marine environment based on presence and abundance of ooids (Pratt, 2010). The lack of pyrite is evidence of oxygenated conditions (Scholle and Ulmer-Scholle, 2003).

2.1.3 SS: Sandstone

Sandstone (SS) inclusions were identified at Sinbad Valley and Salt Valley (Table 2). The SS inclusion facies include quartz sandstone (SSq) and carbonate-quartz sandstone (SScq). SS inclusions are interpreted as deposited in coastal depositional environments based on carbonate grain types, sizes, sorting, and roundness. As such, interpretations are general to avoid misrepresenting depositional environments.

SS inclusion facies match the Paradox Formation quartz sandstone facies summarized by Goldhammer et al. (1991) based on the size, sorting, shape, and abundance of quartz grains as well as the planar and local crossbedding. Goldhammer et al. (1991) classifies the quartz sandstone facies as deposited in a high energy, shallow marine shoreface environment.

2.1.3.1 SSq: Quartz Sandstone

Observations: SSq are light tannish-white on weathered surface and white on fresh surfaces, with thin, planar beds (Fig. 29-A) and are locally cross-bedded (Fig. 29-B,C). SSq is composed predominantly of fine to medium sand size, subrounded to rounded, well-sorted compacted quartz grains (Fig. 30). These SSq occasionally contain chert grains and have minor amounts of calcite cement. Porosity can range from very low up to ~30%. Quartz grains have quartz overgrowths in low-porosity SSq (Fig. 30-C,D) and are heavily fractured in higher-porosity SSq (Fig. 30-A,B). Higher-porosity SSq may contain small amounts of organic material. SSq may contain some pyrite crystals.

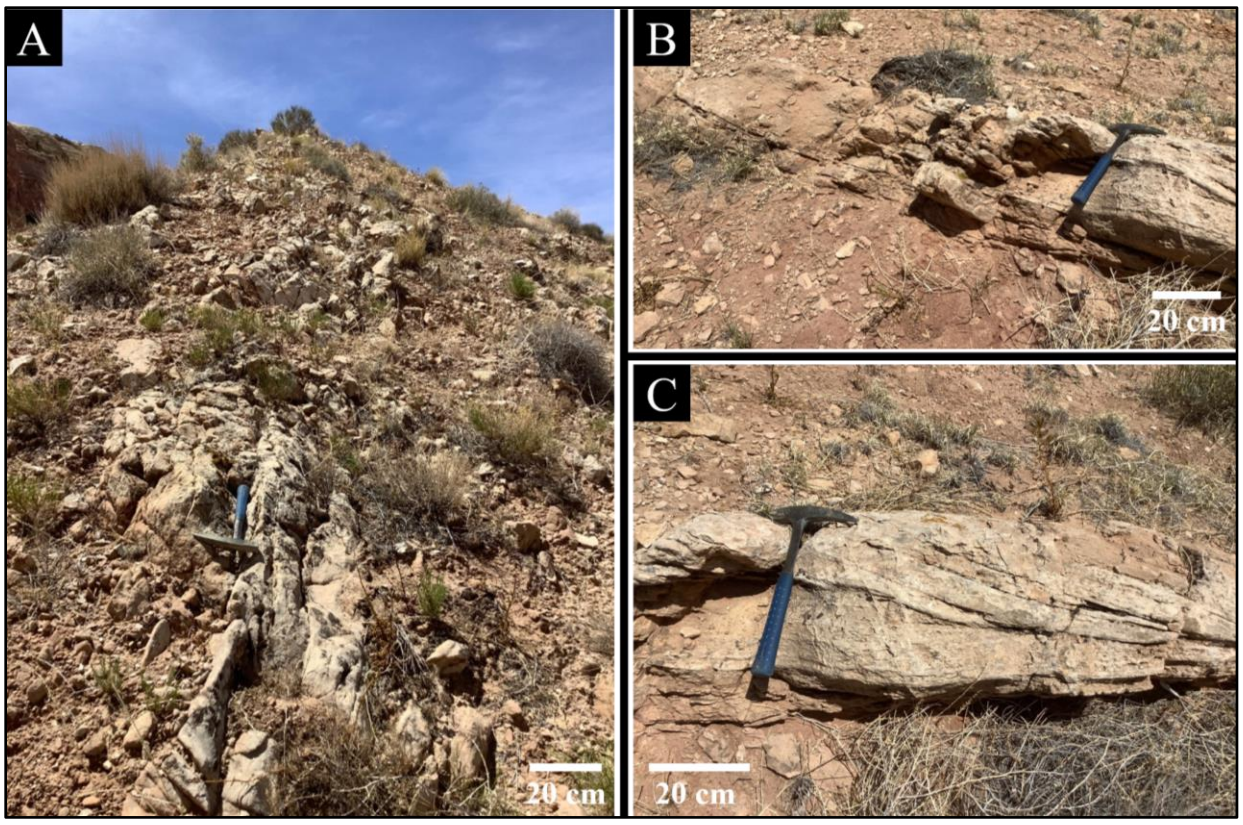

Figure 29: Outcrop images of quartz sandstone (SSq) sample locations
Images of Salt Valley outcrops where SSq samples were gathered. A) Image shows overview of a Ssq outcrop with thin, planar bedding. B-C) Images show SSq outcrop with crossbedding.

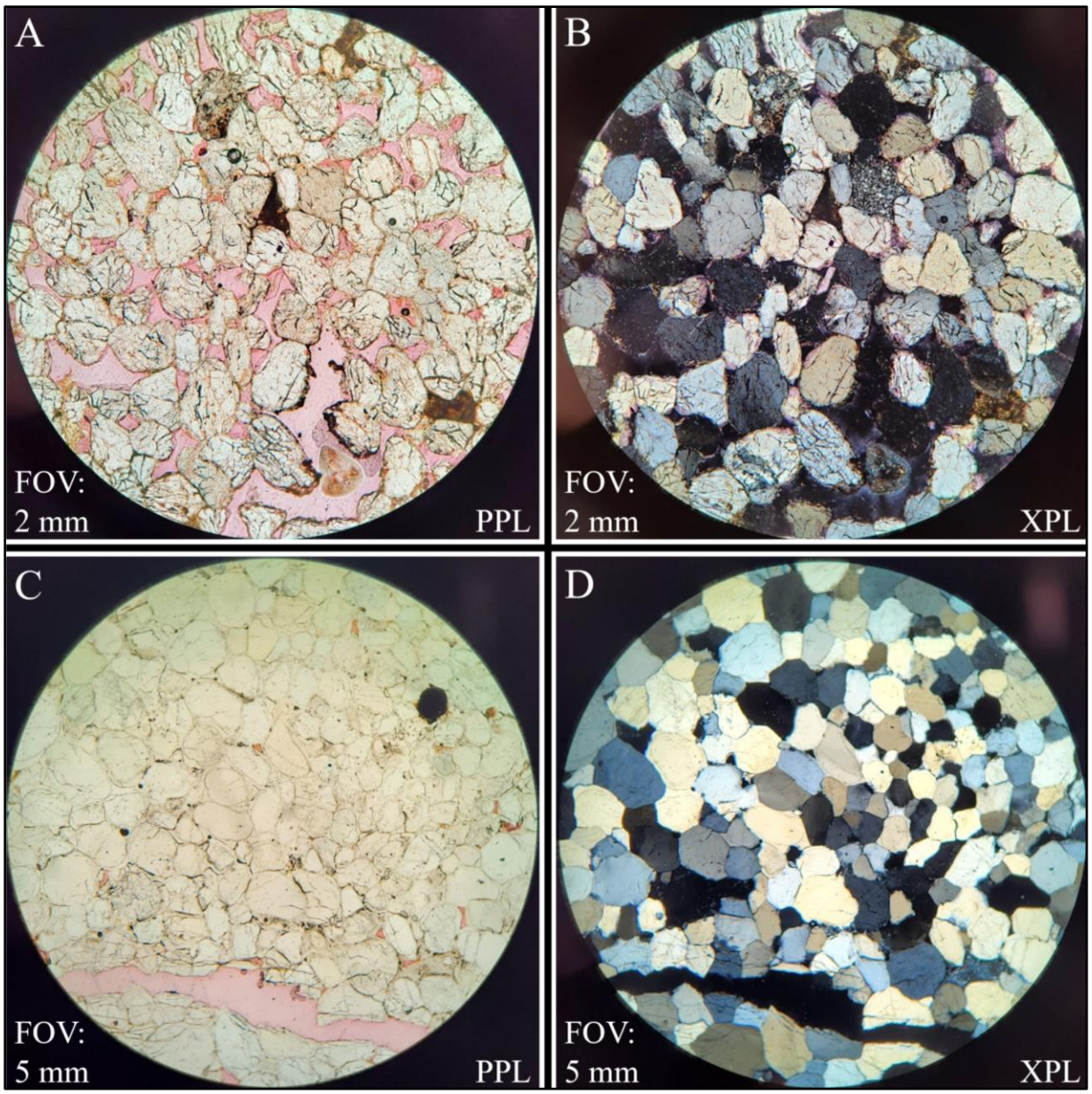

Figure 30: Photomicrographs of SSq
Photomicrographs of SSq endmembers. A) Plane-polarized light and B) cross-polarized light thin section photomicrographs of high-porosity SSq sample showing extreme fracturing of individual quartz grains. C) Plane-polarized light and D) cross-polarized light thin section photomicrographs of low-porosity SSq sample with quartz overgrowths.

Interpretations: SSq is interpreted to be deposited in a higher energy environment, likely an upper shoreface environment based on cross-beds, grain size, sorting, and roundness (Inden and Moore, 1983).

2.1.3.2 SScq: Carbonate-Quartz Sandstone

Observations: SScq are light brown to light (sometimes pinkish/reddish-) tan on weathered surfaces and light tan on fresh surfaces, with thin, planar bedding (Fig. 31). SScq contain abundant either very fine to fine (Fig. 32-C,D), or fine to medium sand size (Figs. 32-A,B, 33), subangular to subrounded, moderately-sorted compacted carbonate and quartz grains. SScq may also contain grains of chert, micrite, fossils, and glauconite. Fossil fragment grains identified in SScq include echinoderm and brachiopod (Table 2). A silicified ooid was found in one SScq sample (Fig. 33). SScq are cemented by calcite, and occasionally by ferroan calcite. Some dolomitization is seen with occasional rhombs. Small quantities of pyrite crystals are common.

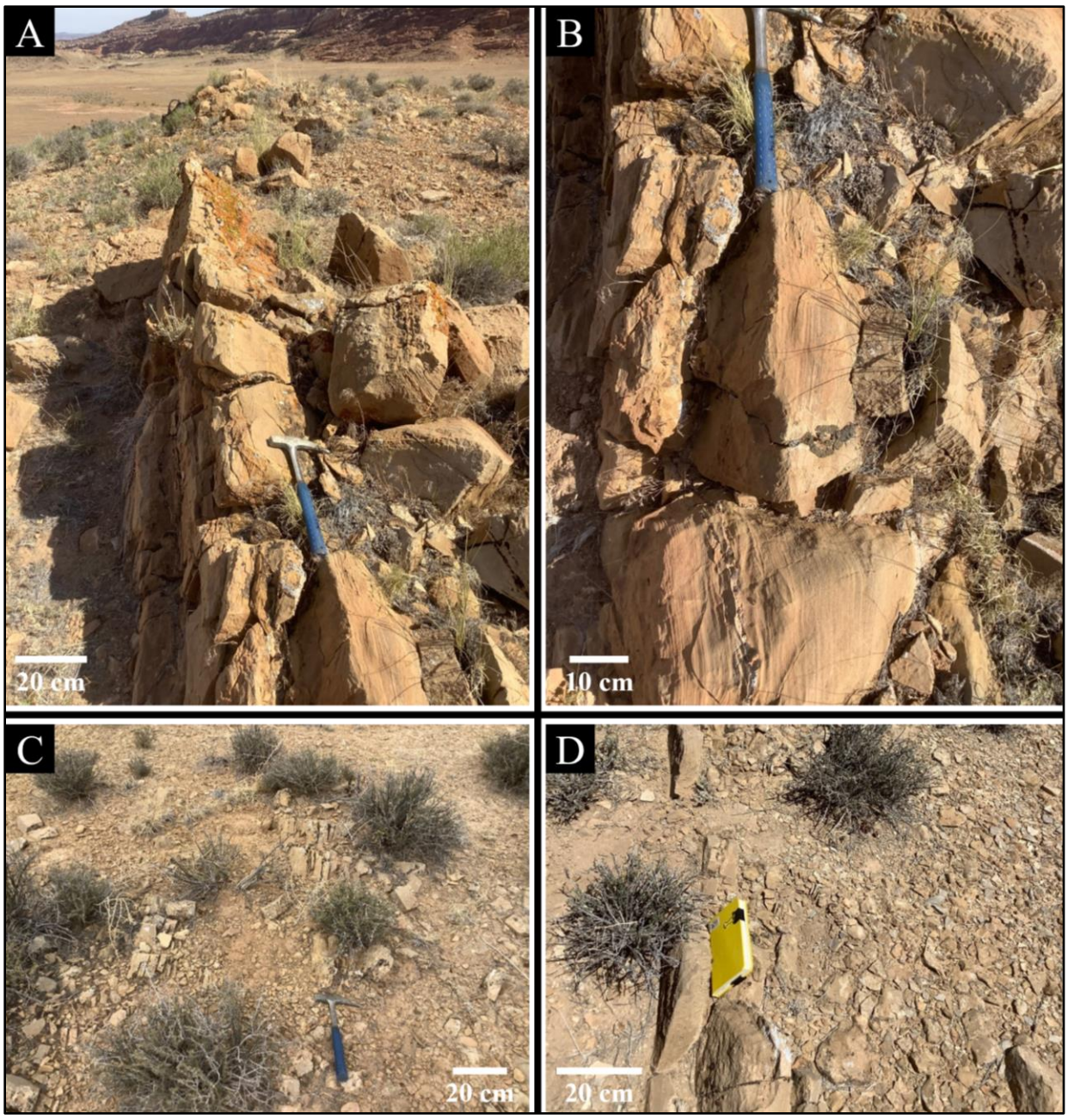

Figure 31: Outcrop images of a carbonate-quartz sandstone (SScq) sample locations
Images of Salt Valley outcrops where SScq samples were gathered. A) Image shows overview and B) close up view of the same SScq outcrop with thin, planar bedding. C-D) Images show overviews of SScq outcrops with thin, planar bedding.

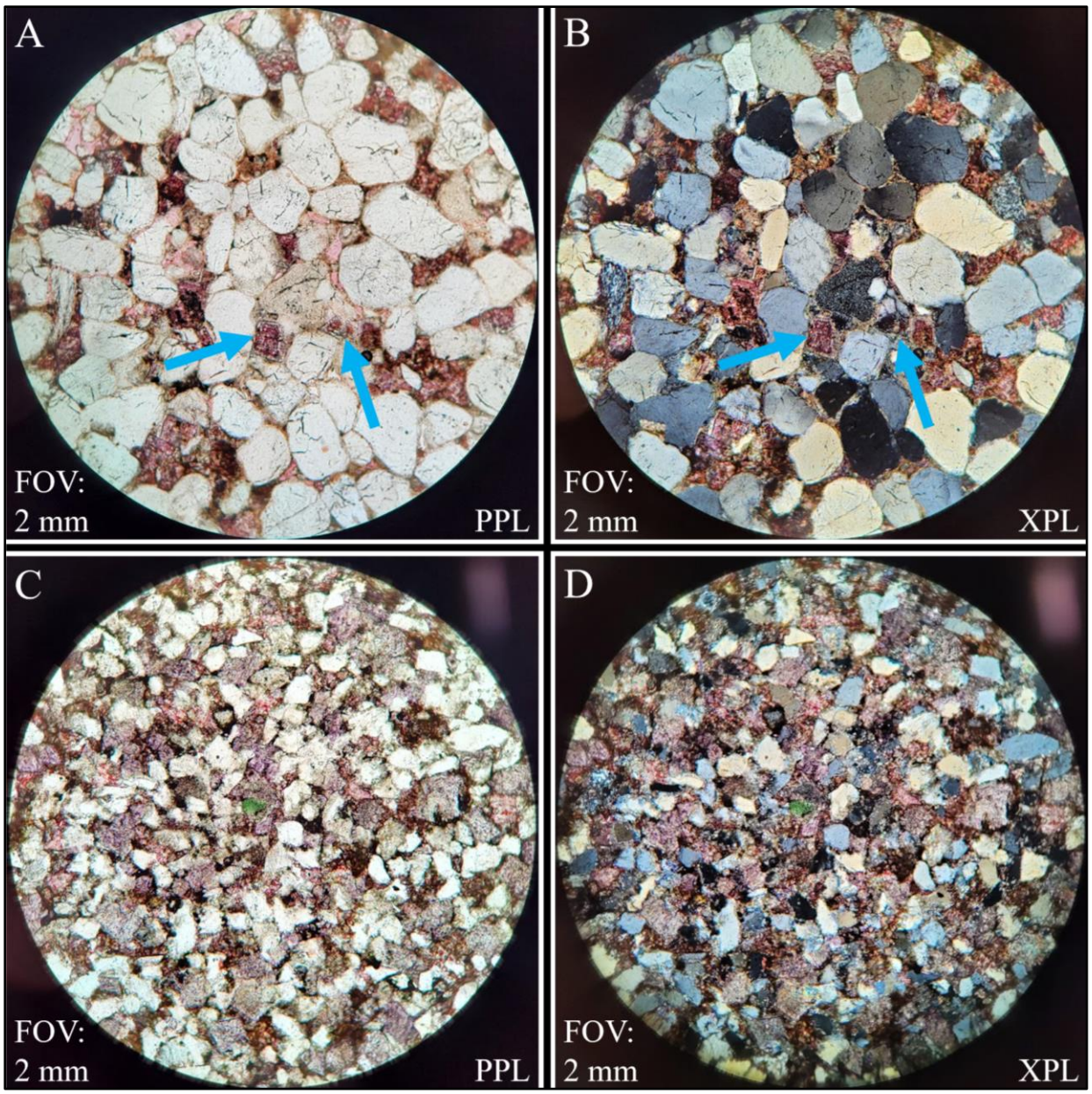

Figure 32: Photomicrographs of SScq
Photomicrographs of SScq endmembers. A) Plane-polarized light and B) cross-polarized light thin section photomicrographs of SScq with fine to medium size quartz grains, blue arrows point to dedolomitized rhombs. Note fractured quartz grains. C) Plane-polarized light and D) cross-polarized light thin section photomicrographs of SScq with fine to medium size quartz grains. Note ferroan calcite cement (purple).

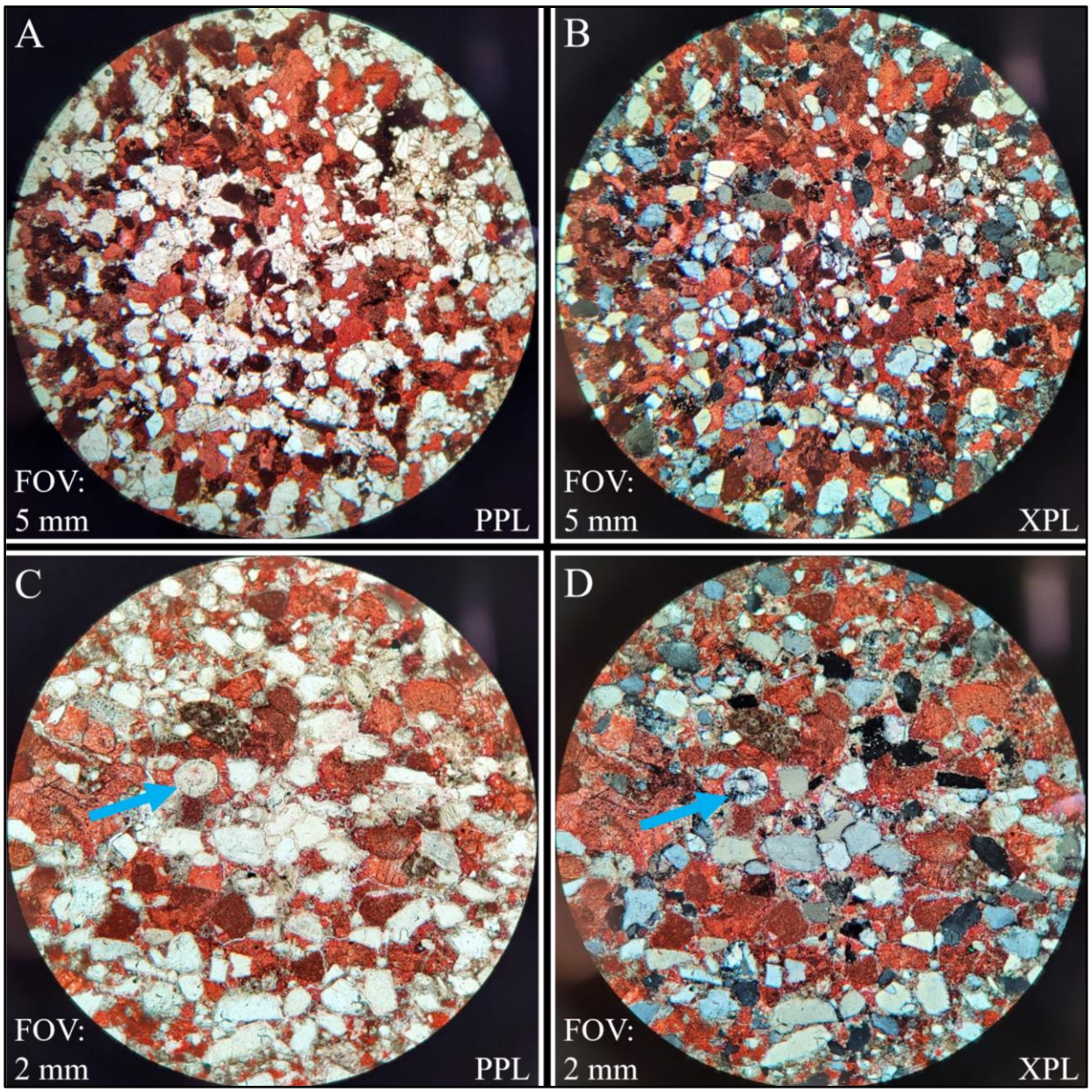

Figure 33: Photomicrographs of SScq
Photomicrographs of SScq endmember. A) Plane-polarized light and B) cross-polarized light thin section photomicrographs of SScq. C) Plane-polarized light and D) cross-polarized light thin section photomicrographs of SScq, blue arrows point to silicified ooid.

Interpretations: SScq is interpreted to be deposited in high energy marine environment, likely an upper shoreface environment based on disarticulated fossil fragments, grain size, sorting, and roundness (Inden and Moore, 1983).

2.1.4 CG: Conglomerate

Conglomerate (CG) inclusions were identified at Sinbad Valley and Salt Valley (Tables 3, 4). The main lithology of clasts is carbonate (CGc) as limestone and dolomitized limestone (both fossiliferous and non-fossiliferous) with occasional chert (often fossiliferous) clasts. One location at Sinbad Valley revealed an unusual outcrop of carbonate and sandstone clast conglomerate (CGcs) with a distinctive red color that is described separately. Based on clast constituents, clast lithologies are interpreted as representing deposition in normal marine shallow shelf environments. The conglomerates themselves are interpreted as subaqueous debris flow deposits based on matrix content, lack of clast sorting, and sedimentary sole marks.

2.1.4.1 CGc: Carbonate-Clast Conglomerate

Observations: Carbonate-clast conglomerates (CGc) are predominantly matrix-supported, usually with unsorted, compacted clasts that are pebble to boulder in size in massive bedding with no sedimentary structures (Fig. 34). Occasionally, beds are of moderate thickness and display grading (Fig. 34-B). Locally, CGc have sand pockets or thin, sandy interbeds (Fig. 35). CGc is dominated by carbonate clasts, which are often fossiliferous, but also contains chert clasts that often have well preserved fossils as well (Fig. 15). While CGc outcrops generally show a lack of sorting, they occasionally display basin-scale trends in clast sizes usually identifiable by the presence or lack of boulder-sized clasts (e.g., boulder-sized clasts exist at Sinbad Valley, but not at Salt Valley). The Salt Valley location hosts a unique CGc outcrop where CGc is filling large-scale (15-40 cm across) flute marks cut into the underlying sandy limestone facies (Fig. 36).

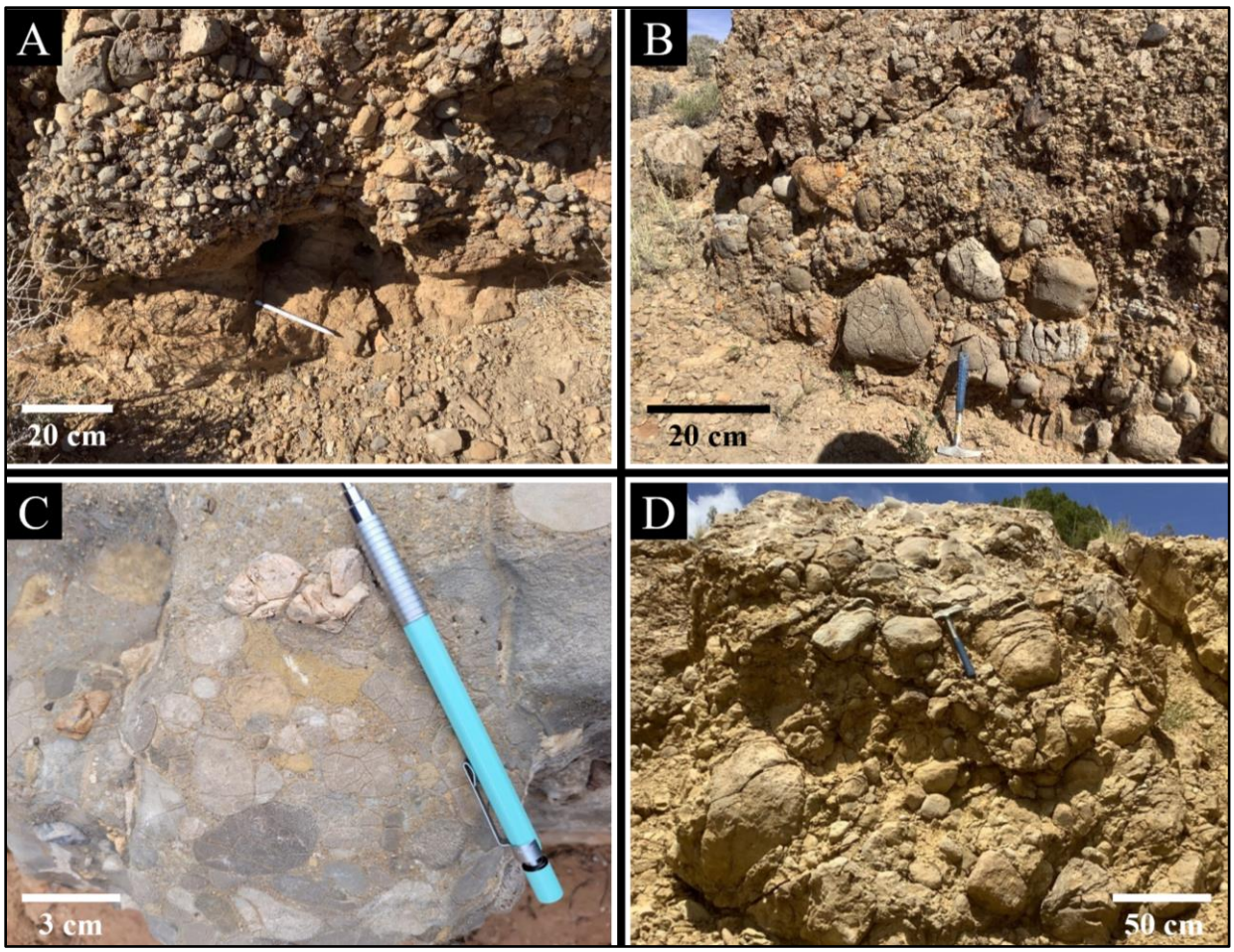

Figure 34: Carbonate-clast conglomerate (CGc) clast sample locations
Images of CGc showing locations where fossiliferous/non-fossiliferous carbonate and chert clast samples were gathered. A) Salt Valley conglomerate outcrop image showing smaller clasts. B) Salt Valley conglomerate outcrop image showing larger clasts with rare grading. C) Sinbad Valley outcrop image showing smaller clasts. D) Sinbad Valley outcrop image showing larger clasts.

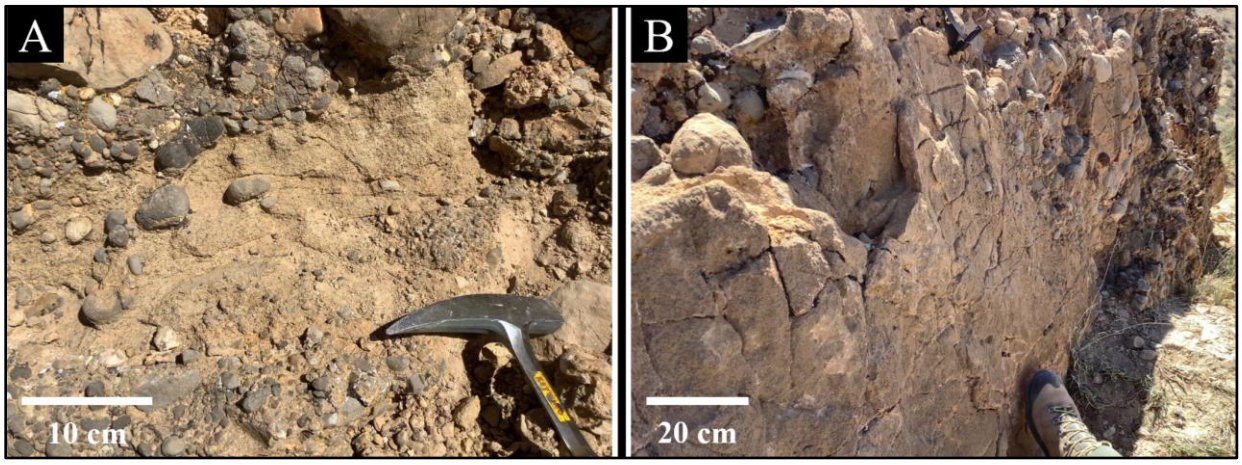

Figure 35: Sandy pockets in CGc outcrops
Images of A) small-scale sandy pocket showing random clast sizes alongside sand and B) large-scale sandy pocket.

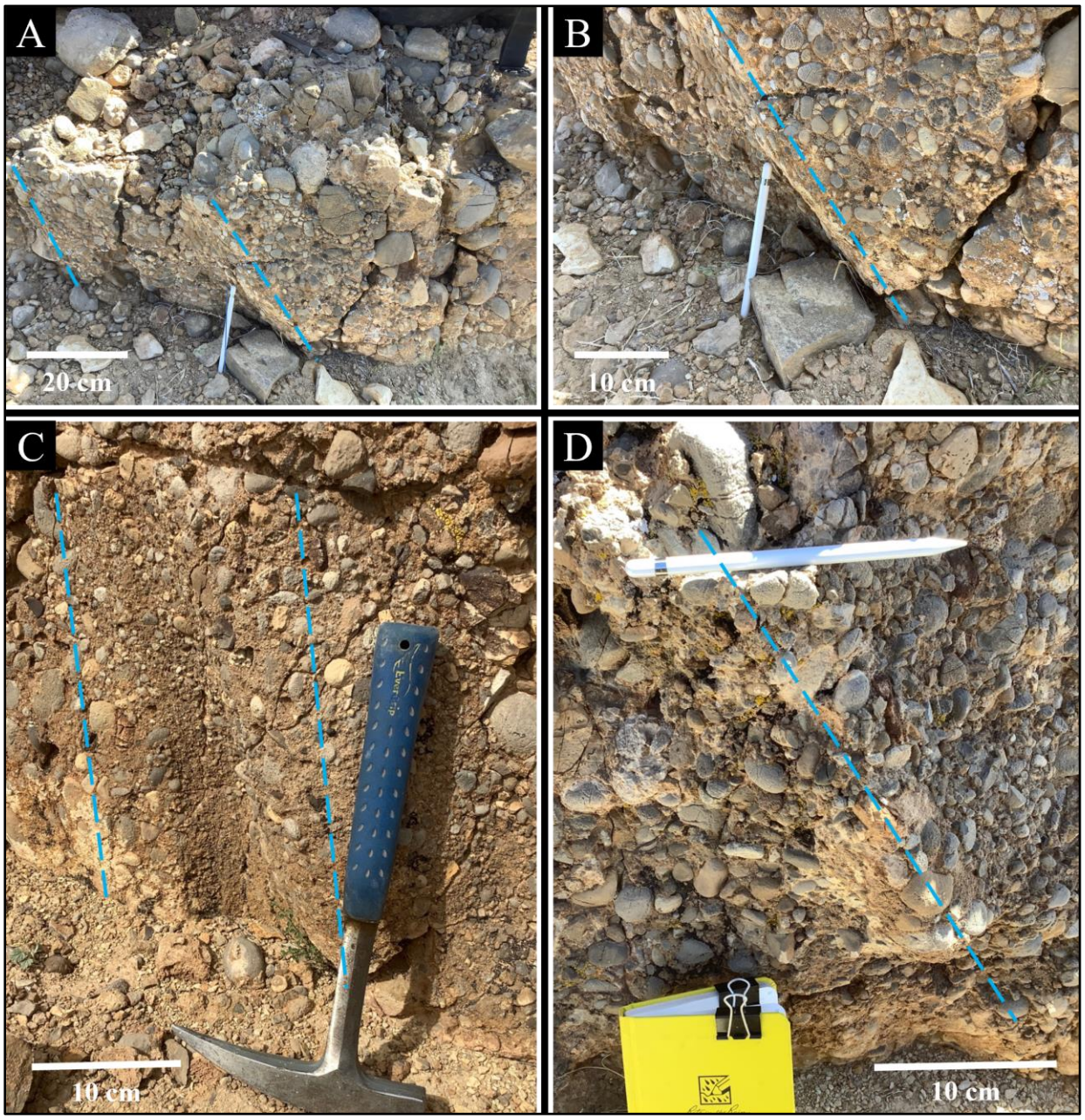

Figure 36: Flute casts in Salt Valley CGc outcrop
Images of flute casts with axial planes outlined with blue dashed lines. A) Overview image of ~40 cm wide flute cast and B) zoomed in view of axial plane of the same flute cast. C) Smaller, ~15cm wide, flute cast. D) Large flute clast.

Matrix composition of CGc contains very fine to medium sand size predominantly carbonate and quartz grains, with common fossil fragment grains. Silt and sand sized grains of chert and glauconite are common in the matrix as well as microspar and pyrite crystals. Crinoid pieces are the most common fossil grains in CGc matrix, but pieces of brachiopods, bryozoans, echinoderms, ooids, and micrite peloids are present as well. Fossil grains are disarticulated and abraded suggesting they were reworked into the conglomerate and were not alive. The CGc is calcite (commonly ferroan) cemented and is commonly partially dolomitized (Fig. 37).

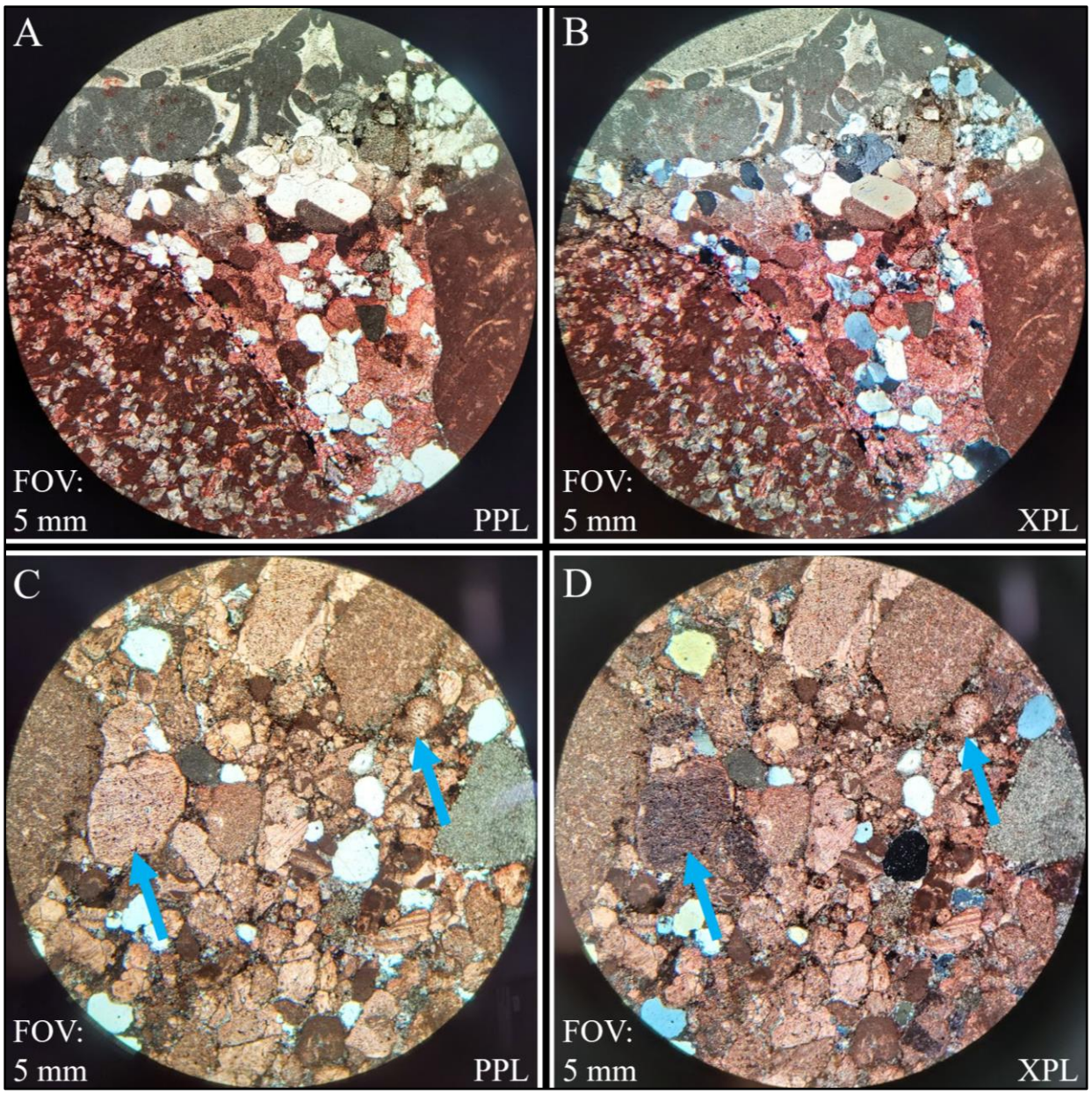

Figure 37: Photomicrographs of CGc
Photomicrographs of CGc samples showing clasts and matrix. A) Plane-polarized light and B) cross-polarized light thin section photomicrographs of CGc showing fossiliferous carbonate clasts, a partially dolomitized carbonate clast, and matrix. C) Plane-polarized light and D) cross-polarized thin section photomicrographs showing carbonate clasts and matrix, blue arrows pointing to fossil fragments in the matrix.

Interpretations: CGc is a carbonate clast-dominated, pebble-cobble, paraconglomerate (Boggs, 2006). CGc is interpreted as a shallow subaqueous cohesive debris flow that originated from slope failure mass wasting of clay to boulder sized grains/clasts (Rodine and Johnson, 1976;

Enos, 1977; Lowe, 1982, Elverhøi et al., 2000). CGc matrix material is similar in composition to the carbonate clasts within it indicating it originated from the same source. The mass wasting resulted in extremely small to extremely large material mixing with the water to create a buoyant cohesive sediment-water matrix that suspended even the largest clast sizes (Rodine and Johnson, 1976; Lowe, 1982). Subsequent deposition of this sediment resulted in a matrix-supported freeze unit containing all clast sizes (Lowe, 1982), like most outcrops of CGc in Sinbad Valley and Salt Valley.

Deposits of this nature may become turbulent at some point in their evolution (Enos, 1977). Turbulent phases occurring during sediment debris flow (Enos, 1977) could explain the occasional grading seen in outcrop and could explain the unique outcrop at Salt Valley where CGc is filling flute casts as this structure is evidence of subaqueous turbulent flow (Hsu, 1959). More likely, the subaqueous flow began as turbulent, initially carving flute marks into the sandy limestone now underlying CGc. As this flow began, it would become channelized and deposit the sparse, loose material accessible from early erosion into sorted beds. The turbulent flow would be overtaken as the mass wasting event occurred and the debris flow was deposited. Potentially, there were several amalgamated flows that had intervening turbulent flows that deposited the sandy patches between the conglomerates.

CGc Clast Lithologies

CGc contains three distinct clast lithologies: fossiliferous carbonate, non-fossiliferous dolomicrite, and chert. The fossiliferous carbonate clast lithology is interpreted to have originated in a normal marine, shelf environment. The non-fossiliferous dolomicrite clast lithology is interpreted to have originated in a restricted marine environment in the middle shelf. The chert clast lithology is interpreted to have originated in a normal marine shelf environment. It is further

interpreted to have formed penecontemporaneous with the aforementioned fossiliferous carbonate lithology.

Fossiliferous Carbonate Clasts:

Observations: Fossiliferous carbonate clasts are limestones that are light gray to dark gray on weathered and fresh surfaces and are pebble to boulder in size. Clasts are usually well-rounded to subrounded displaying a compacted fabric (Fig. 34). Fossiliferous carbonate clasts are packstones (Figs. 38, 39-A,B) and occasionally wackestones (Fig. 39-C,D) containing crinoids, ooids (usually micritized), brachiopods, bryozoans, echinoids, bivalves, Chaetetid sponges, and peloids. Fossils and ooids are generally well-preserved and crinoid plates are the largest fossils seen in these clasts, commonly an order of magnitude larger than ooids and other fossils (Figs. 38, 39-A,B). Calcite cement is common, though not always present. Non-fabric selective dolomitization is common.

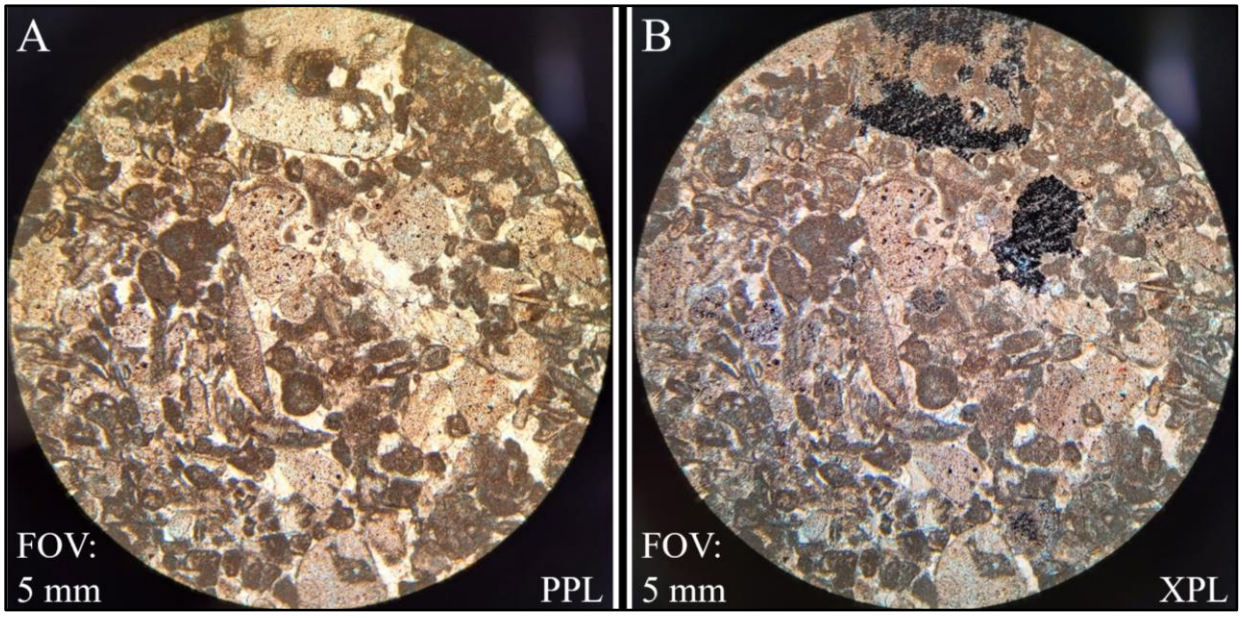

Figure 38: Photomicrographs of CGc fossiliferous carbonate clasts
Photomicrographs of CGc packstone clasts. A) Plane-polarized light and B) cross-polarized light thin section photomicrographs of a clast taken from CGc.

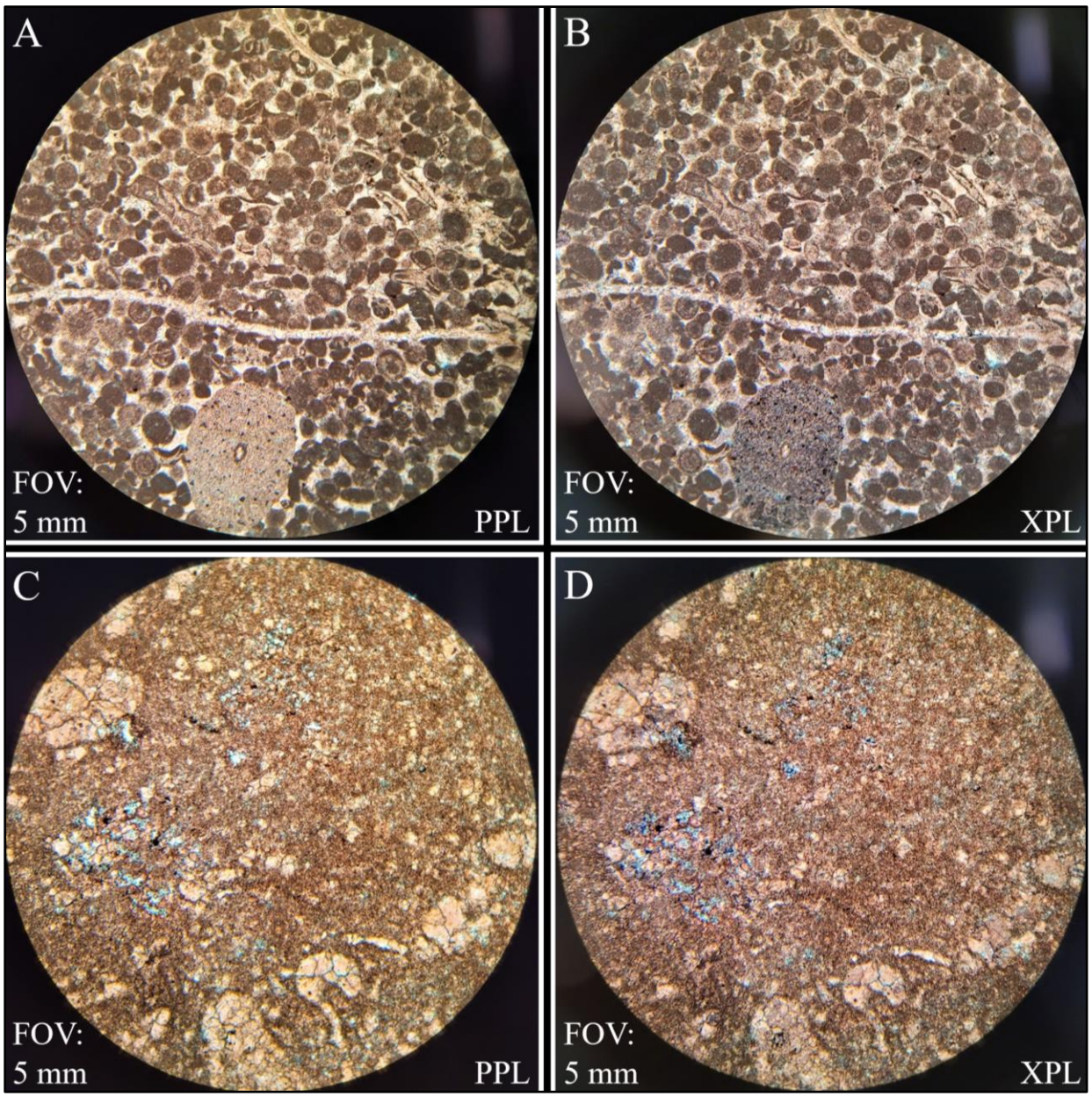

Figure 39: Photomicrographs of CGc fossiliferous carbonate clasts
Photomicrographs of CGc packstone and wackestone clasts. A) Plane-polarized light and B) cross-polarized light thin section photomicrographs of an oolitic packstone clast taken from CGc. Note large crinoid stem. C) Plane-polarized light and D) cross-polarized light thin section photomicrographs of a wackestone clast taken from CGc.

Interpretations: The fossiliferous carbonate lithology identified in CGc clasts is interpreted to have originated in a normal marine, shelf environment evidenced by the echinoderm and brachiopod skeletal grains that indicate normal marine salinity conditions (Wilson and Jordan,

1983). The presence of Chaetetid sponges, which were commonly patch reef formers in the Mississippian and early Pennsylvanian is further confirmation that this lithology was formed on an open shelf (Wilson and Jordan, 1983). The disarticulation and abrasion seen in some fossil grains suggests a moderately-high energy environment influenced by wave action. The fossiliferous nature of these clasts and lack of pyrite indicates oxidizing conditions.

While oolitic packstone appears as a facies (SLo) in the sandy limestone inclusions, and as clasts in CGc, they are not the same facies. The SLo facies is non-fossiliferous, contains large ooids, small quartz grains, and fabric-selective dolomitization. The oolitic packstones in fossiliferous carbonate clasts in CGc contain ooids that are smaller in size than those seen in SLo, do not contain quartz grains, contain fossil grains, and are not dolomitized. Thus, the oolitic packstones seen in the CGc fossiliferous carbonate clasts are not reworked SLo. Similarly, the sponge boundstone seen in the fossiliferous sandy limestone facies is different than sponge boundstones seen in CGc clasts. The sponge boundstone clasts in CGc experienced silica cementation (see chert clast composition below), while the sponge boundstone in the SLf facies did not experience silica cement in any analyzed sample. Additionally, the sponge boundstone in the SLf facies has quartz grains, which are not present in any CGc clast (Table 4).

Non-Fossiliferous Dolomicrite Clasts:

Observations: Non-fossiliferous dolomicrite clasts are light gray to dark gray on weathered and fresh surfaces and are pebble to boulder in size (Figs. 34, 40-A,B,C). Clasts are usually well-rounded to subrounded. Non-fossiliferous dolomicrite clasts are sometimes partially silicified (see chert clast composition below). Those that are not silicified all contain dolomitized micrite or microspar, and some contain dedolomite (occasionally ferroan; Fig. 41). In rare instances some calcite cement remains.

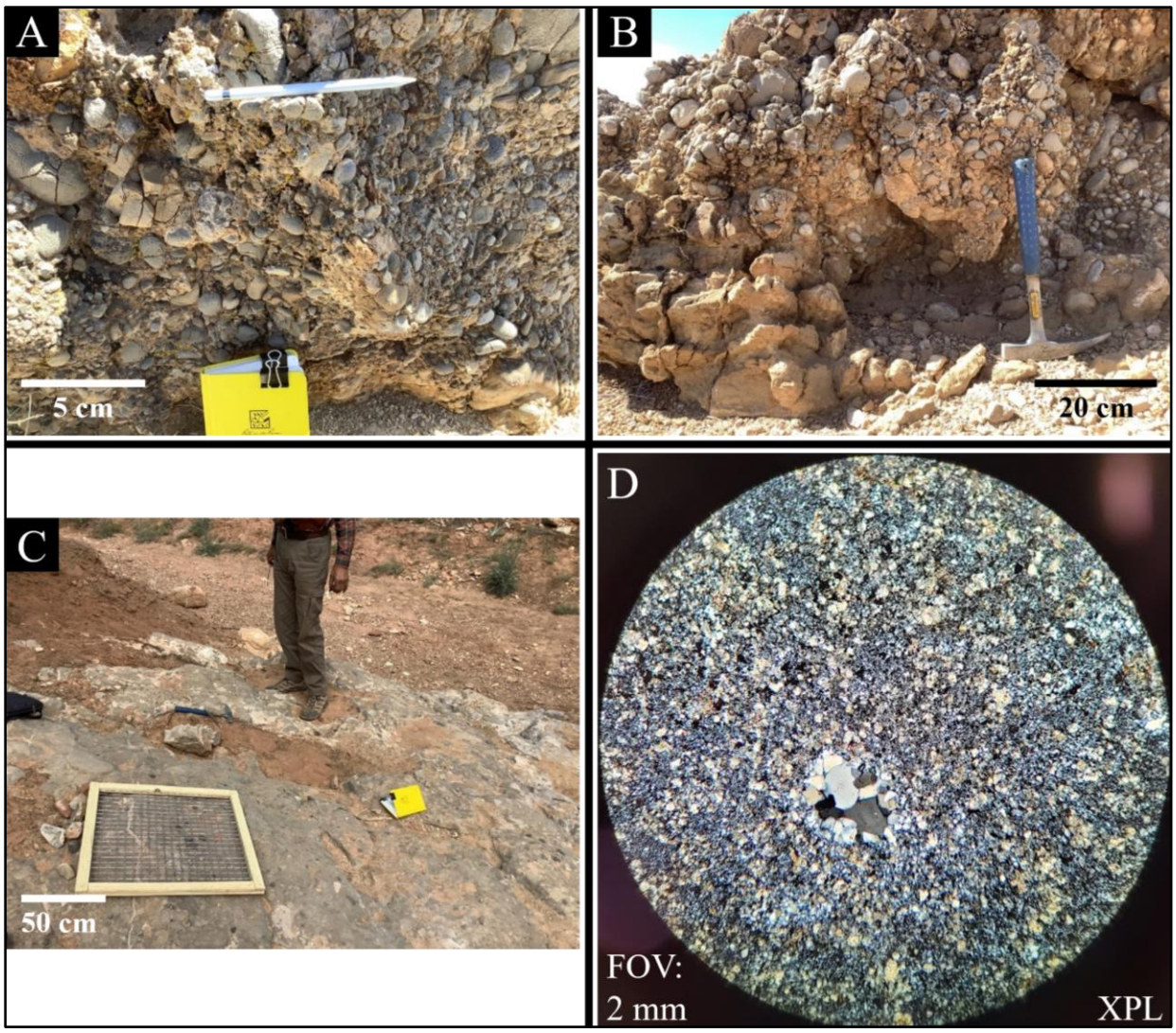

Figure 40: Outcrop images of CGc sample locations and photomicrograph of chert clast
A-B) Images of Salt Valley outcrops where CGc clast samples were gathered. C) Image of Sinbad Valley outcrop where CGc clast samples were gathered. D) Photomicrographs of the almost fully silicified endmember of non-fossiliferous chert clasts in CGc. Cross-polarized light thin section photomicrograph of a non-fossiliferous, almost fully silicified chert clast taken from CGc.

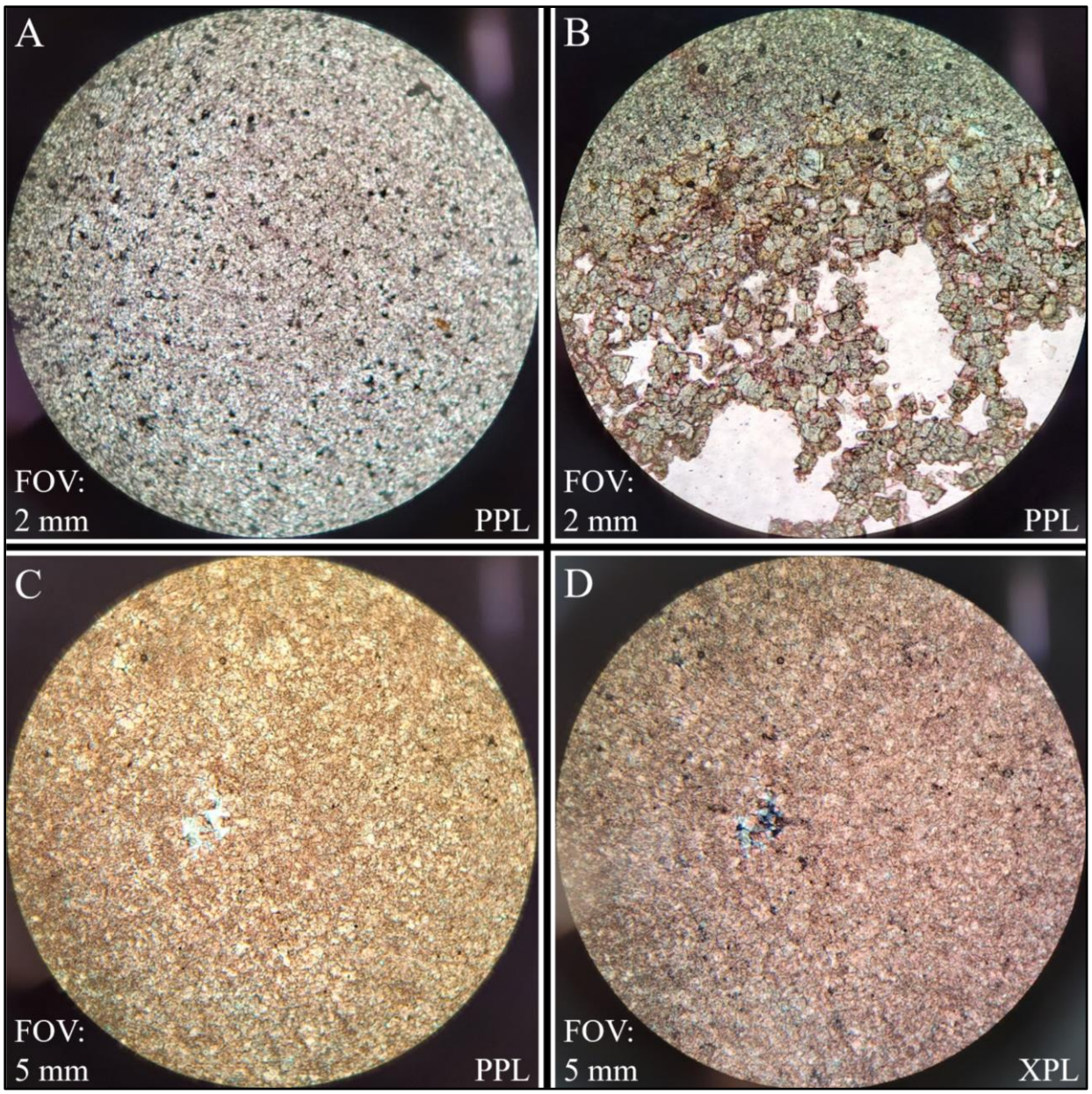

Figure 41: Photomicrographs of CGc non-fossiliferous carbonate clasts
A-B) Plane-polarized light thin section photomicrographs of partially dolomitized and dedolomitized carbonate clast taken from CGc. Note presence of rhombs and increase in size near porosity and presence of ferroan dedolomite. C) Plane-polarized light and D) cross-polarized light thin section photomicrographs of lightly dolomitized non-fossiliferous clast taken from CGc.

Interpretations: The non-fossiliferous dolomicrite lithology identified in CGc clasts is interpreted to have originated in a restricted marine environment in the middle shelf, perhaps close to the inner shelf in the tidal flat environment (Wilson and Jordan, 1983). The lack of fossils in

this lithology is indicative of an environmental stressor like a shelf barrier restricting water circulation and associated increasing salinity (Wilson and Jordan, 1983).

Chert Clasts:

Observations: Chert clasts are black (non-fossiliferous and less common; Fig. 14) and white (usually fossiliferous; Fig. 15) and subangular to subrounded (Figs. 15, 34, 40-A,B,C). Chert clasts represent either fully or partly silicified carbonate lithologies. Some chert clasts are non-fossiliferous, with chert replacing carbonate micrite and microspar (Fig. 40-D, 42). Those that are partly silicified have either silicification preferentially of the grains (fossils; Fig. 43) or the matrix (Fig. 44). In clasts where the matrix is silicified, some grains are partially silicified (Fig. 44). In clasts where the grains are silicified, the matrix is partially silicified (Fig. 43). In clasts that are almost fully silicified, some micrite and dolomite remains along with calcite cement. Sponge boundstones are completely silicified (Fig. 43-C,D). Fossils are evident and usually silicified, most are unidentifiable petrographically, crinoid fossils are identifiable and may or may not be silicified. Fossils identified in chert clasts include brachiopod, bryozoan, echinoderm, ostracod, and sponge. Fossils and ooids are generally well-preserved, with prevalent large, abraded crinoid plates (Fig. 44-C,D).

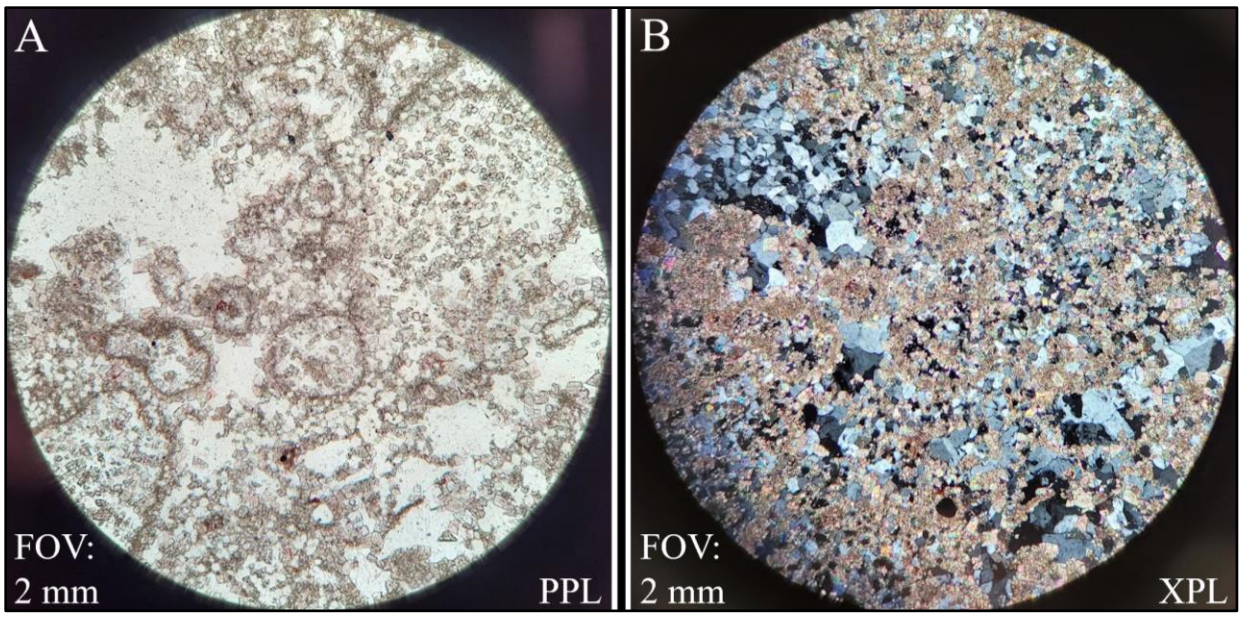

Figure 42: Photomicrographs of CGc non-fossiliferous chert clasts
Photomicrographs of the partially silicified endmember of non-fossiliferous chert clasts in CGc. A) Plane-polarized light and B) cross-polarized light thin section photomicrograph of a non-fossiliferous, partially silicified chert clast taken from CGc. Note remnant dedolomitized micrite envelopes.

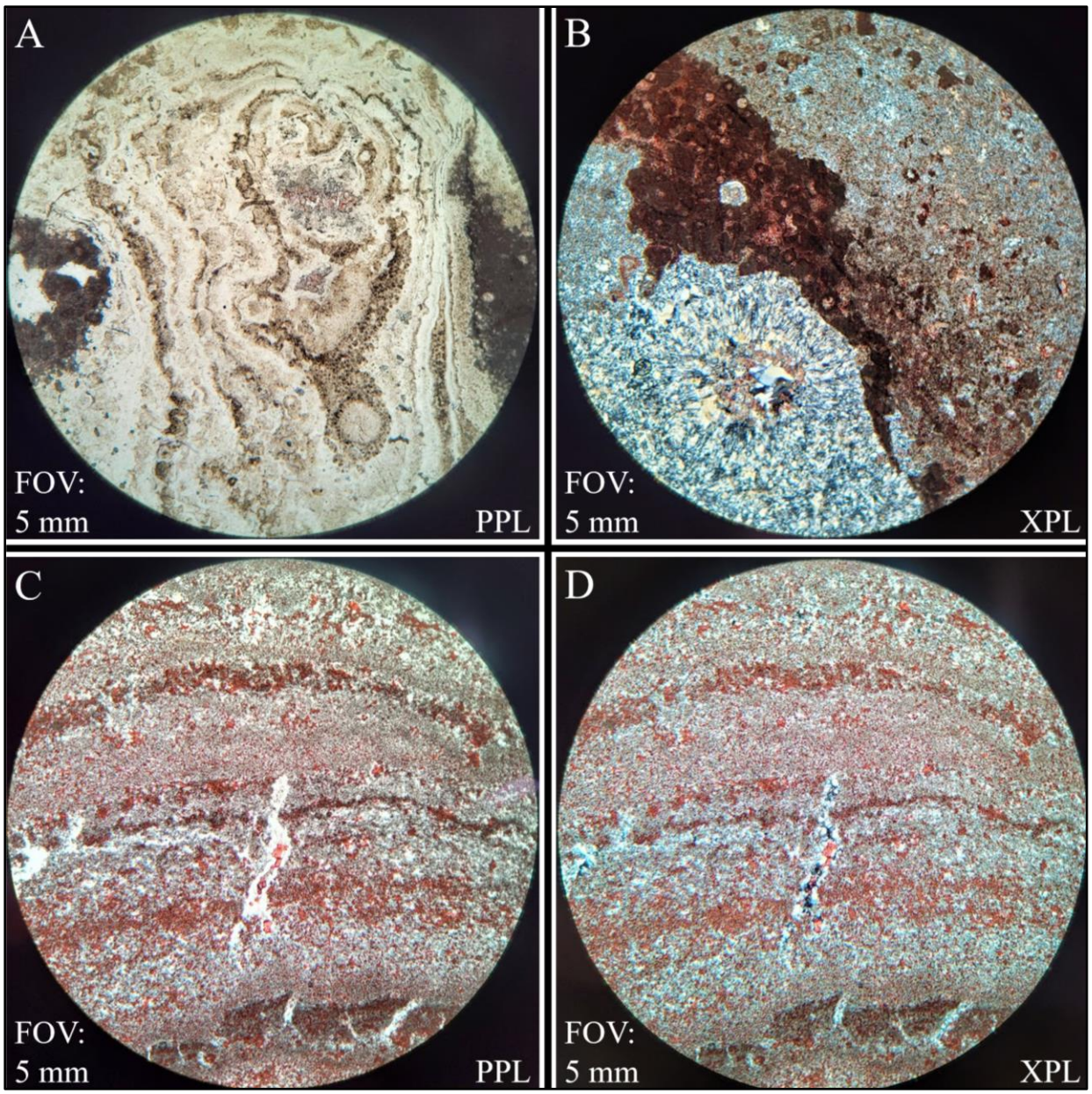

Figure 43: Photomicrographs of CGc fossiliferous chert clasts with silicification of grains
Photomicrographs of silicified fossil endmember of fossiliferous chert clasts in CGc showing preferential silicification of fossils, note micrite with partial silicification and preservation of original sponge fabric. A) Plane-polarized light and B) cross-polarized light thin section photomicrographs of almost fully silicified fossiliferous (sponge) chert clast taken from CGc. Note leftover micrite matrix. A) Plane-polarized light and B) cross-polarized light thin section photomicrographs of mostly silicified fossiliferous (sponge) chert clast taken from CGc.

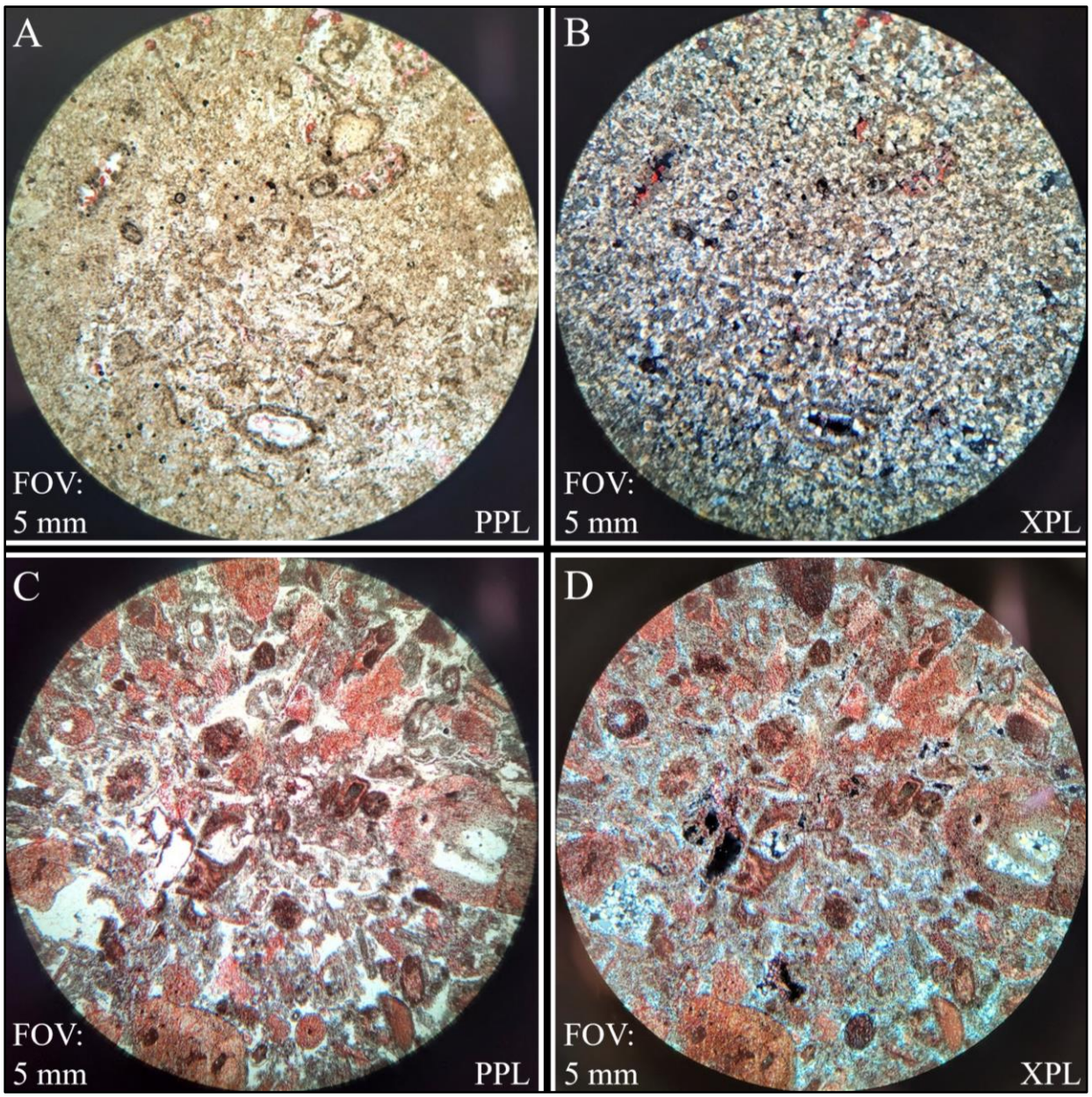

Figure 44: Photomicrographs of CGc fossiliferous chert clasts with silicification of matrix
Photomicrographs of silicified matrix endmember of fossiliferous chert clasts in CGc showing preferential silicification of matrix, fossil grains are micritic with partial silicification. A) Plane-polarized light and B) cross-polarized light thin section photomicrographs of partially silicified fossiliferous chert clast taken from CGc. Note minor calcite cement. A) Plane-polarized light and B) cross-polarized light thin section photomicrographs of partially silicified fossiliferous chert clast taken from CGc. Note well preserved mostly micritic fossil grains.

Interpretations: The chert lithology identified in CGc clasts is interpreted to have originated in a normal marine shelf environment (Wilson and Jordan, 1983). The presence of an

extremely similar fossil assemblage to the fossiliferous carbonate clast lithology found within CGc and the presence of leftover, non-silicified micritic grains indicates the chert clast lithology formed penecontemporaneous with the fossiliferous carbonate lithology. This limestone-chert syngenesis is supported by the preservation of fossil fabrics by chert, not dolomite, which formed later (Fig. 43-A; Tobin, 2004). Where chert is fossiliferous, it is likely the environment was oxidizing, whereas where chert is non-fossiliferous it is likely the environment was stressed. Altogether, this leads to the interpretation that the fossiliferous chert lithology formed alongside the fossiliferous carbonate lithology, and likewise the non-fossiliferous chert lithology formed alongside the non-fossiliferous dolomicrite lithology.

2.1.4.2 CGcs: Carbonate-Sandstone-Clast Conglomerate

Observations: Carbonate-Sandstone-Clast Conglomerate (CGcs) inclusions include clasts found in CGc but with the additional component of sandstone clasts and a red matrix (Table 2). CGcs are matrix-supported, usually with unsorted clasts that are pebble to boulder in size (carbonate clasts never larger than pebble size) in massive bedding with no sedimentary structures (Fig. 45). CGcs overlies tan sandstone beds (Fig. 45-A) that interfinger with reddish-pink sandy beds containing small, well-rounded clasts that are red or tan (Fig. 45-C,D). These reddish-pink sandy beds are matrix-rich pebble clast CGcs that are concordant with the matrix of CGcs (Figs. 45-D, 46-A,B).

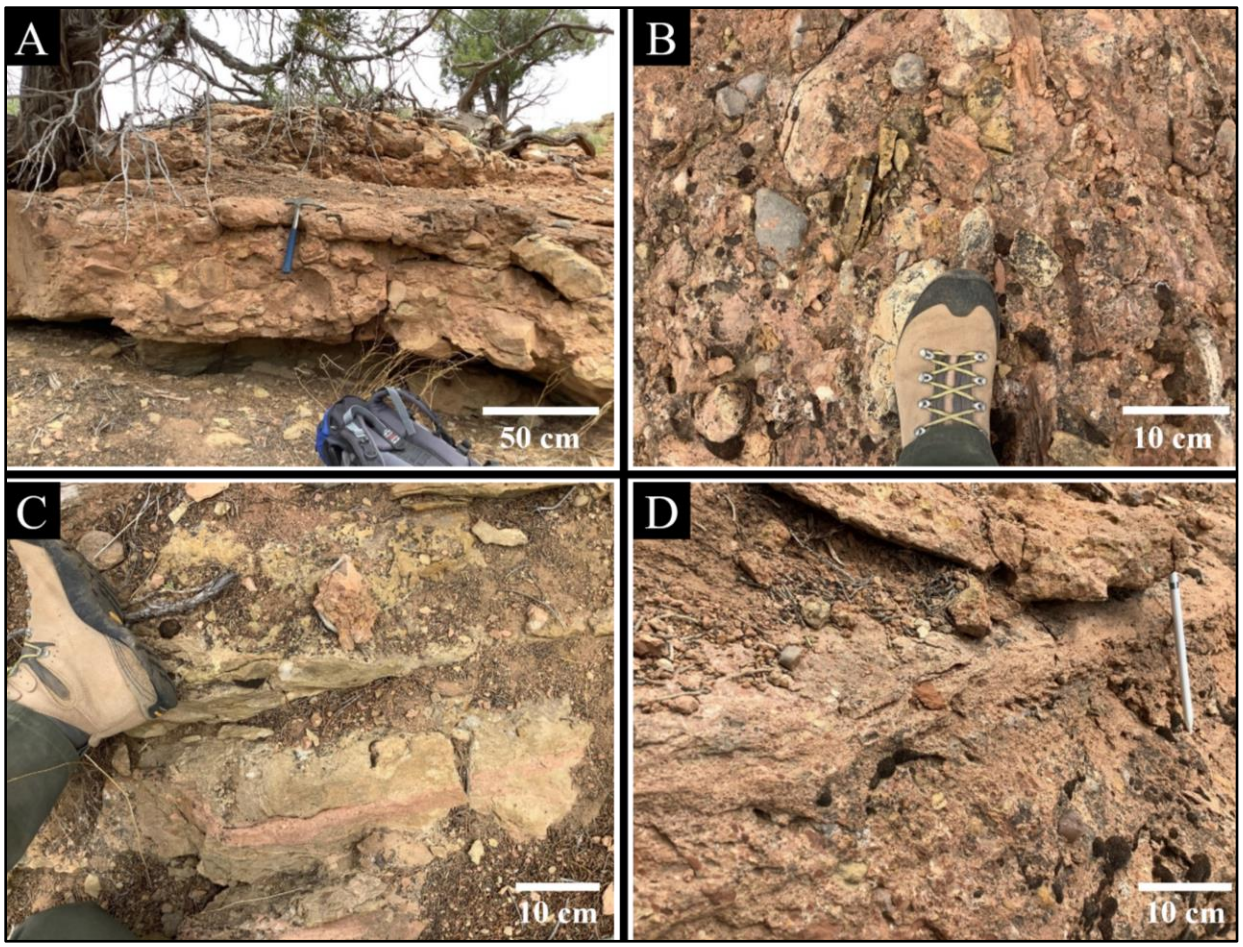

Figure 45: Carbonate sandstone clast conglomerate (CGcs) outcrop images
Images of Sinbad Valley outcrops where CGcs clast and matrix samples were gathered. A) Image shows main CGcs outcrop. B) Image shows angular sandstone clasts with bedding preserved among normal CGc clasts. C) Image of CGcs outcrop shows interfingering tan sandstone beds and reddish-pink sandy beds. D) Image shows gradational area between conglomerate and sandstone.

Matrix composition of CGcs (Fig. 46) was analyzed from samples taken from reddish-pink beds (matrix-heavy pebble-clast CGcs; Figs. 45-D, 46-A,B). The matrix contains subangular to subrounded, moderately-sorted, silt to medium sand size compacted quartz grains and fossil fragments (evident crinoids, other fragments unidentifiable; Fig. 46-C,D). Additionally, lightly dolomitized micrite peloids are common. The matrix is cemented by calcite and pyrite crystals are common.

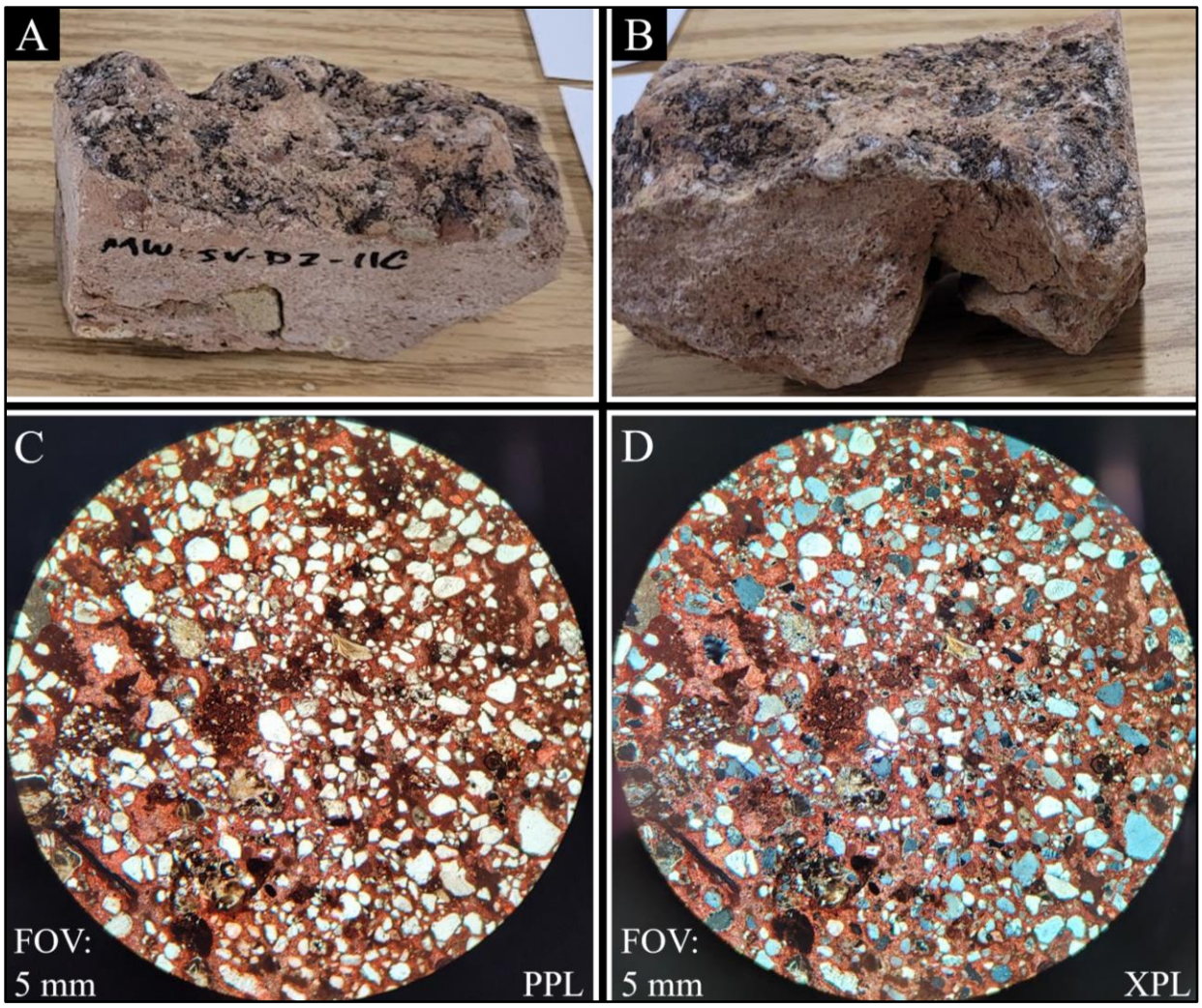

Figure 46: Hand sample images and photomicrographs of CGcs matrix
Hand samples and photomicrographs of CGcs matrix taken from gradational area between sandstone and conglomerate. A-B) Front and back images of CGcs matrix hand sample used for thin section. C) Plane-polarized light and D) cross-polarized light thin section photomicrographs of CGcs matrix. Note presence of fossil fragments.

Interpretations: CGcs is a petromictic, pebble-cobble, paraconglomerate (Boggs, 2006). Like CGc, CGcs is interpreted as a shallow subaqueous cohesive debris flow that originated from slope failure mass wasting clay to boulder sized grains/clasts (Rodine and Johnson, 1976; Enos, 1977; Lowe, 1982, Elverøi et al., 2000). The presence of sandstone clasts and the unique red matrix in addition to carbonate clasts implies that, unlike CGc, CGcs tapped multiple sediment sources.

Sandstone Clast Composition in CGcs:

Observations: Sandstone clasts are light red or tan on fresh surfaces and light reddish-tan or light brownish-tan on weathered surfaces (Figs. 45-A,B, 47-A,B). While carbonate clasts in CGcs are well-rounded, the sandstone clasts are often angular, especially on edges parallel with bedding planes (Fig. 45-B). Sandstone clasts are usually planar laminated, but occasionally display internal trough cross-bedding. They contain fine, well-sorted, subangular to subrounded, silt to fine sand size compacted quartz grains with some chert and dolomitized grains (Fig. 47-C,D,E,F). There is a small percentage of micritic matrix and light dolomitization. Calcite cement is minor (~5%) to ~25% of the composition. Glauconite can be rare or comprise ~5% of the composition. Pyrite crystals are abundant.

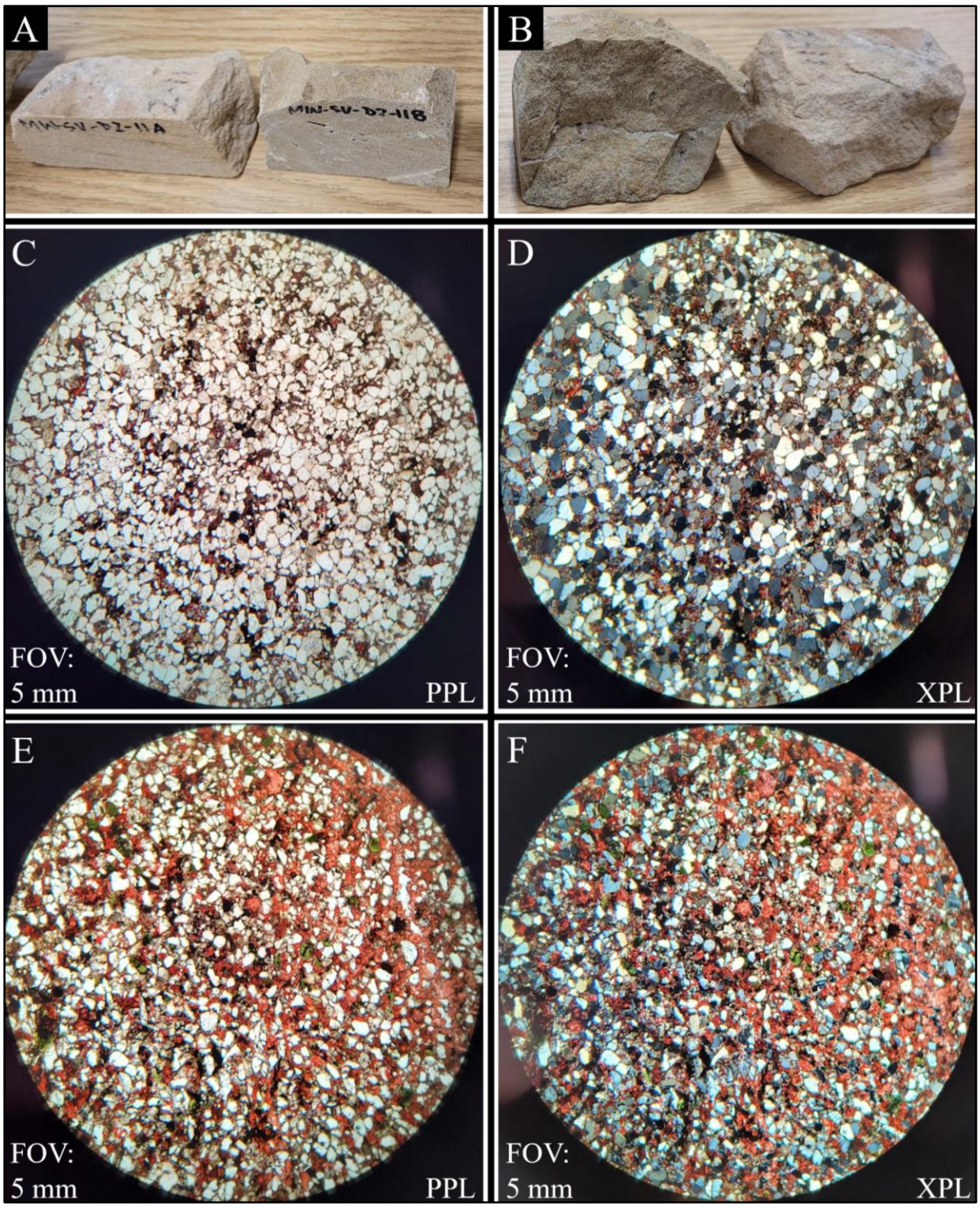

Figure 47: Hand sample images and photomicrographs of CGcs sandstone clasts
Hand samples and photomicrographs of endmembers of sandstone clasts in CGcs. A-B) Front and back images of CGcs sandstone clast hand samples used for thin sections. C) Plane-polarized light and D) cross-polarized light thin section photomicrographs of sandstone clast taken from CGcs.

Note minor amounts of glauconite. E) Plane-polarized light and F) cross-polarized light thin section photomicrographs of sandstone clast taken from CGcs. Note that glauconite comprises ~5% of the composition of this sandstone sample.

Interpretations: Sandstone clasts are interpreted to have originated in a shoreface environment based on planar laminated beds, and occasional crossbedding along with grain size, sorting, and roundness (Inden and Moore, 1983).

2.2 FIELD RELATIONSHIPS

The Sinbad Valley salt wall has the most rugged topography of the three field sites in this study. Likely, the significant topography seen at this site is caused by more intense rainfall and runoff, whereas the Salt Valley salt wall experiences far less annual rainfall and runoff. Furthermore, the inclusions exposed at Gypsum Valley salt wall margin are present as steep, near-vertical cliffs that can be attributed to erosion by the Dolores River that surges through the canyon after snowmelt events.

2.2.1 Sinbad Valley

The Sinbad Valley salt wall hosts inclusions that create significant topography on the breached anticline valley floor. The lithologies present in outcrop are ~85% CGc, ~10% SS, and ~5% SL (Tables 1-4). Figure 48 shows the distribution of these outcrops at the surface with respect to lithologies. Orientations are highly variable at this location and are often very difficult to attain on CG outcrops. CG outcrops often contain sandy interbeds providing surfaces for most orientation measurements taken near CG outcrops. These inclusions form large hills in the southeastern-portion of the valley. Outcrops are generally present only at the very top of hills with SS as ridge-formers (Fig. 49) and CG usually encircling the tops of the hills (Fig. 48). Occasionally, more resistant conglomeratic lithologies are present in valleys and streambeds. Outcrops are surrounded by modern Paradox gypsum caprock and Quaternary alluvium (Fig. 48).

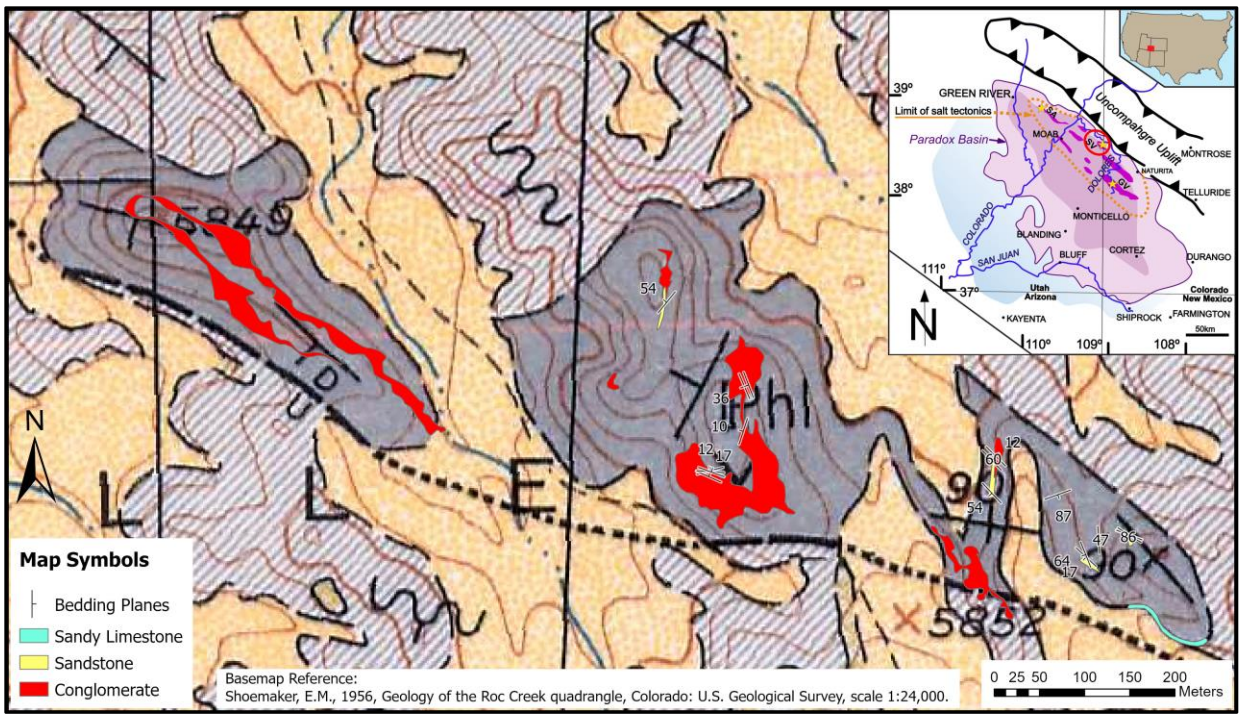

Figure 48: Geologic map of inclusions in Sinbad Valley
Geologic map showing exposure of inclusions in the southeastern quadrant of Sinbad Valley. Units mapped by Shoemaker (1956) were visited to identify inclusions and clarify lithologies at these previously mapped units (Map adapted from Shoemaker, 1956). The yellow unit is Quaternary alluvium (Shoemaker, 1956).

Figure 49: Sandstone outcrop at Sinbad Valley
Images of a sandstone inclusion of non-evaporite lithology outcrop in the southwestern quadrant of Sinbad Valley. Images display the strong resistance of these beds.

In one location, the CG is much different (CGcs), with a light red color, many sandy interbeds, and large sandstone clasts (Fig. 50). The regular CGc clasts in CGcs maintain the well-

rounded shape expected of conglomerate inclusion clasts in Sinbad Valley. SS are normally found close to CG exposures and often within CG outcrops as sandy interbeds. Where they are found alone, they can be small, low to the ground exposures, or near vertical and stand over 2 m above the ground (Fig. 49).

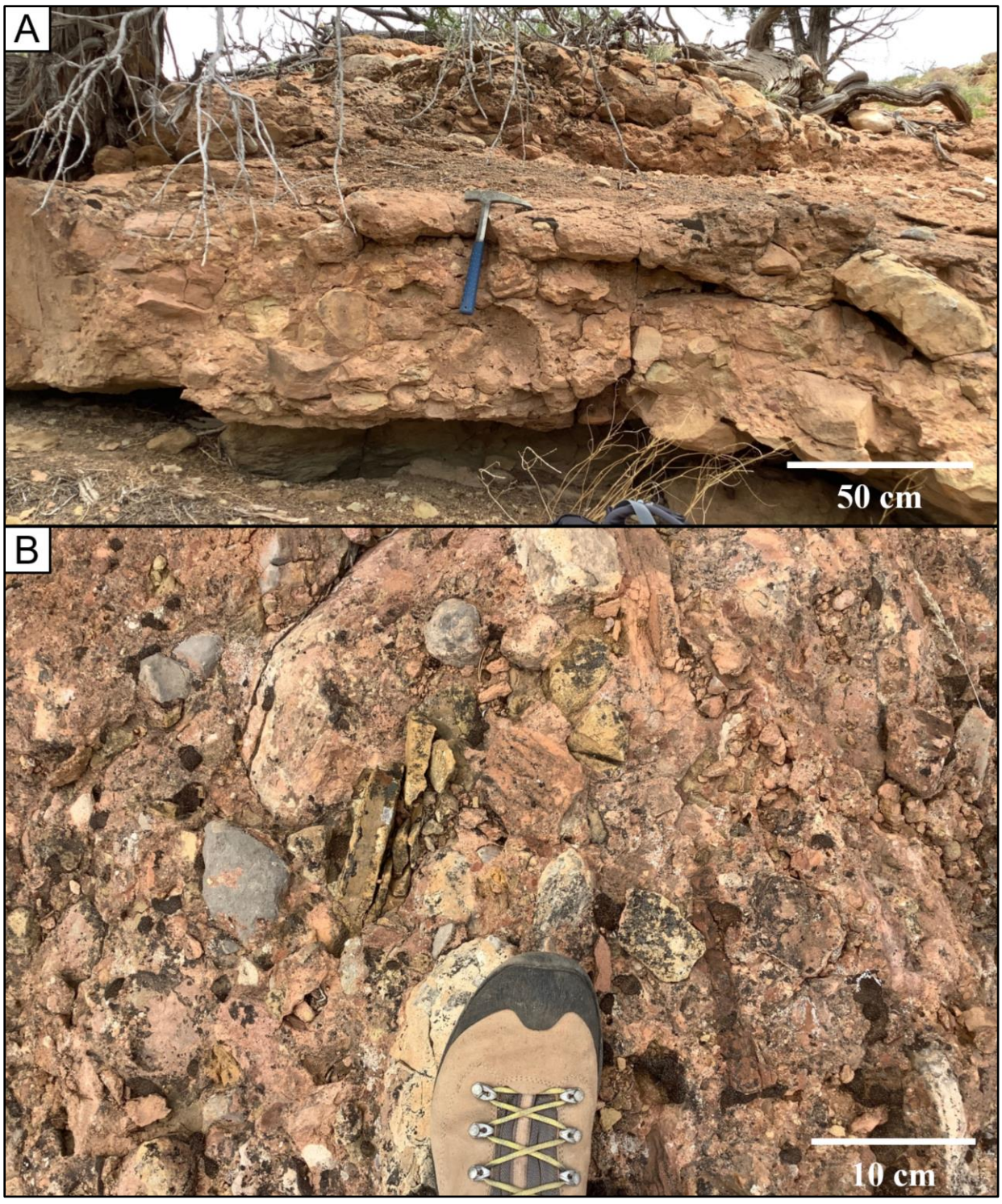

Figure 50: Sinbad Valley red conglomerate outcrop with sandstone clasts
Images show an unusual outcrop of red conglomerate in the southwestern quadrant of Sinbad Valley that contains sandstone clasts not seen in other conglomerate inclusions.

2.2.2 Salt Valley

The Salt Valley salt wall is home to numerous interesting CGc, SS, and SL inclusions that mainly outcrop in the northern portion of the valley, outside the Arches National Park boundary (Fig. 51). The lithologies present in outcrop are ~30% CGc, ~60% SS, and ~10% SL (Fig. 51; Tables 1-4). Outcrops of inclusions are mostly discrete, meter-scale blocks, with SL, SS, and CGc occasionally grading into each other. SL are never discrete, less common, and where present they grade into either SS or CGc (Fig. 51). Outcrops are arranged in snaking patterns defined by broken but coherent large blocks (Fig. 52).

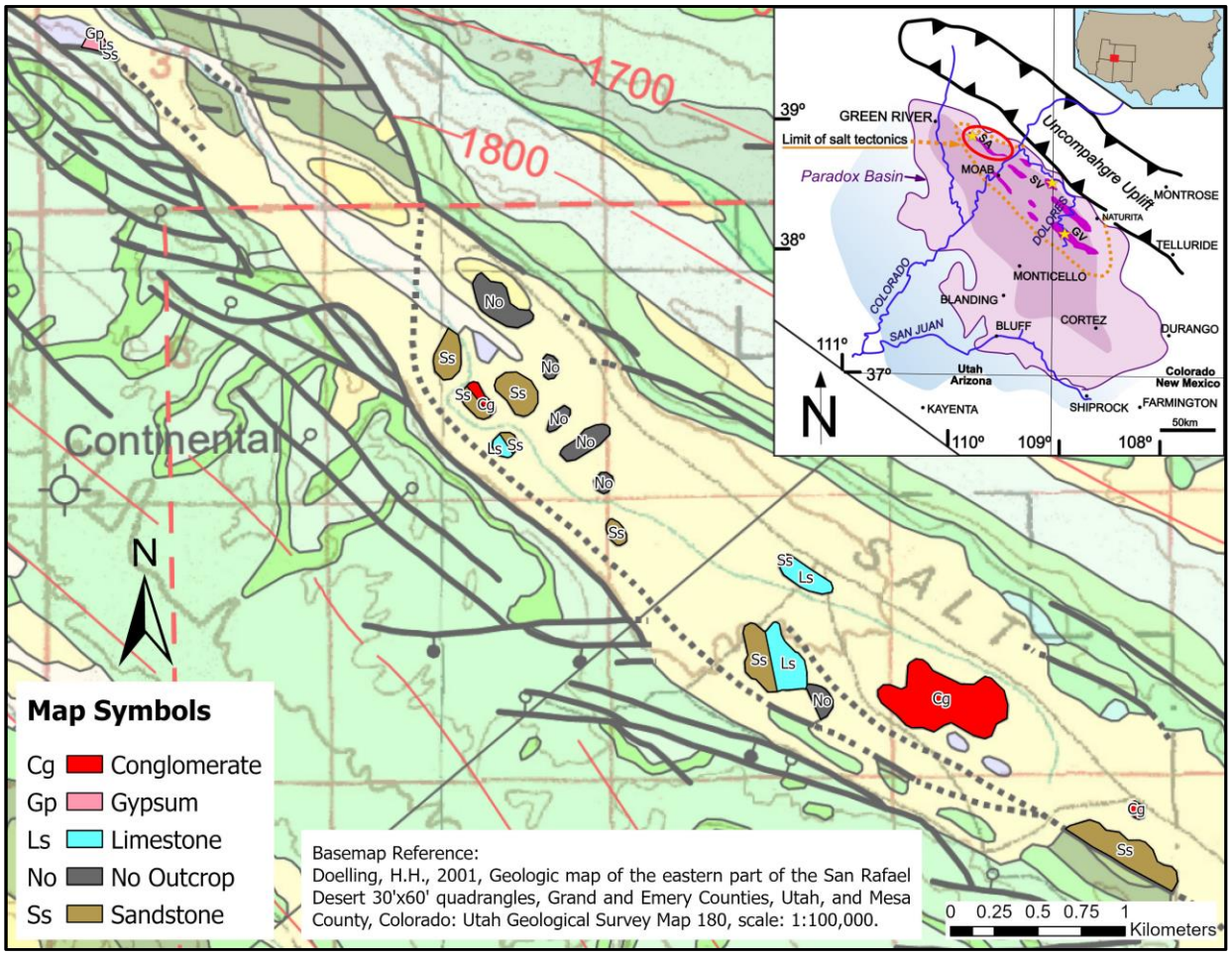

Figure 51: Geologic map of inclusions in Salt Valley
Geologic map showing ground-truthed locations of inclusions exposed in the northwest end of Salt Valley. Units mapped by Doelling (2001) were visited to ground truth and clarify lithologies at

these previously mapped units. These units are attributed based on presence of outcropping lithologies and lithology type (Map adapted from Doelling, 2001). Yellow unit is Quaternary alluvial mud, green units are various Jurassic rocks (Doelling, 2001).

Figure 52: Overview image of Salt Valley sandstone outcrop
Sandstone ridge-forming outcrop in northwestern Salt Valley showing the length and distortion of inclusions at the surface today (Image from Google Earth Pro).

Figure 53 shows the position of a mapped CGc outcrop that nicely displays the contorted and folded nature of the inclusion. Figure 51 shows the distribution of these outcrops at the surface with respect to lithology. In northern Salt Valley, within the valley floor, inclusions generate the main topography. CGc and SS are ridge formers on low hills and are continuous for long distances, sometimes over 100 m in length, with the SS outcrops displaying relatively undisturbed bedding and large-scale folding (Figs. 52, 53, 54). The carbonate outcrops which lie just inside the northernmost portion of Arches National Park are less prominent, but still produce readily recognizable topographic relief.

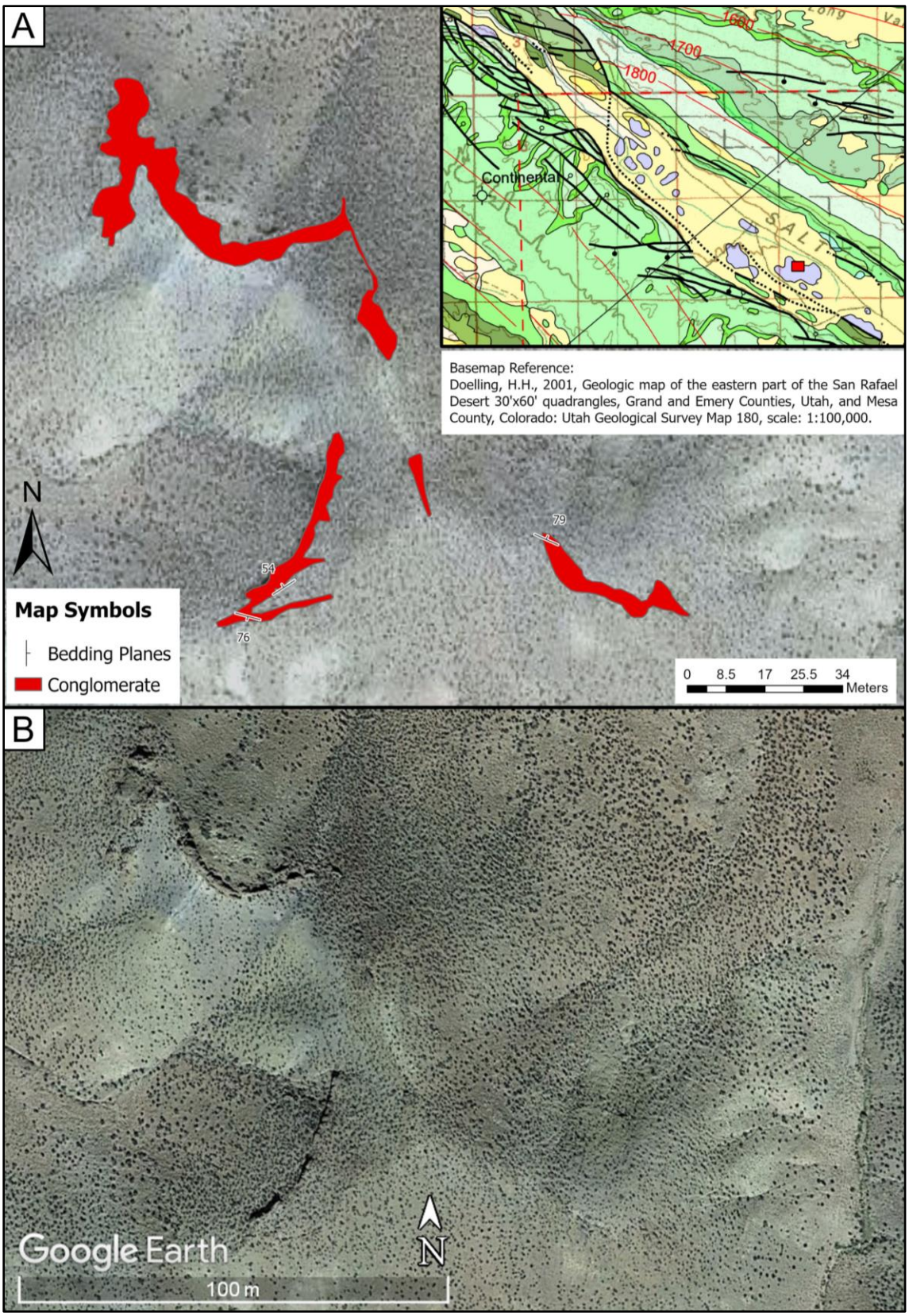

Figure 53: Prominent conglomerate outcrop in Salt Valley

Map of a prominent conglomerate outcrop in the northwestern section of Salt Valley showing large-scale folding common in inclusion outcrops (Location map after Doelling, 2001). Overview image of outcrop (Image from Google Earth Pro).

Figure 54: Salt Valley sandstone outcrop ridge former

Image showing large-scale outcrop of sandstone in northwestern Salt Valley (outcrop image of Figure 20 overview image). The image provides an example of how inclusions define the main topography in Salt Valley. Red dashed line outlines the inside of large-scale fold on the horizon.

Previously, inclusions in Salt Valley have been mapped as either the younger Honaker Trail Fm., Paradox gypsiferous exposures, or various Pennsylvanian rocks (Doelling, 1985). Generally, these do not include or account for the conglomerate lithologies widely present at this location. To clarify these exposures, previously mapped units were ground-truthed to detail the lithologies present at these mapped units (Fig. 51). This map shows the distribution of SL, SS, and CG outcrops throughout Salt Valley.

2.2.3 Gypsum Valley

The Gypsum Valley salt wall is host to a unique outcrop of inclusions bordering the Dolores River in Little Gypsum Valley (38° 9'30.48"N, 108°53'18.81"W). The lithologies present in outcrop are ~90% SL and ~10% BS (Figs. 18, 22, 23). This large outcrop is approximately 25 m long and 3 to 5 m tall (Fig. 55). It is a folded but coherent package displaying little variation in rock type, with the cohesive, SL beds displaying cyclic variations in color and sand content as well as variations in constituents (Table 1). Occasional plates of calcite crystals (sometimes displaying dogtooth calcite) between SL beds occur. The two BS beds are present at the southernmost portion of the outcrop. One (Lb3a) is squished into a thinly laminated, wedge-shape bed with the point of the wedge closer to the fold hinge, and the second (Lb3ai) is heavily compacted (Figs. 18, 23).

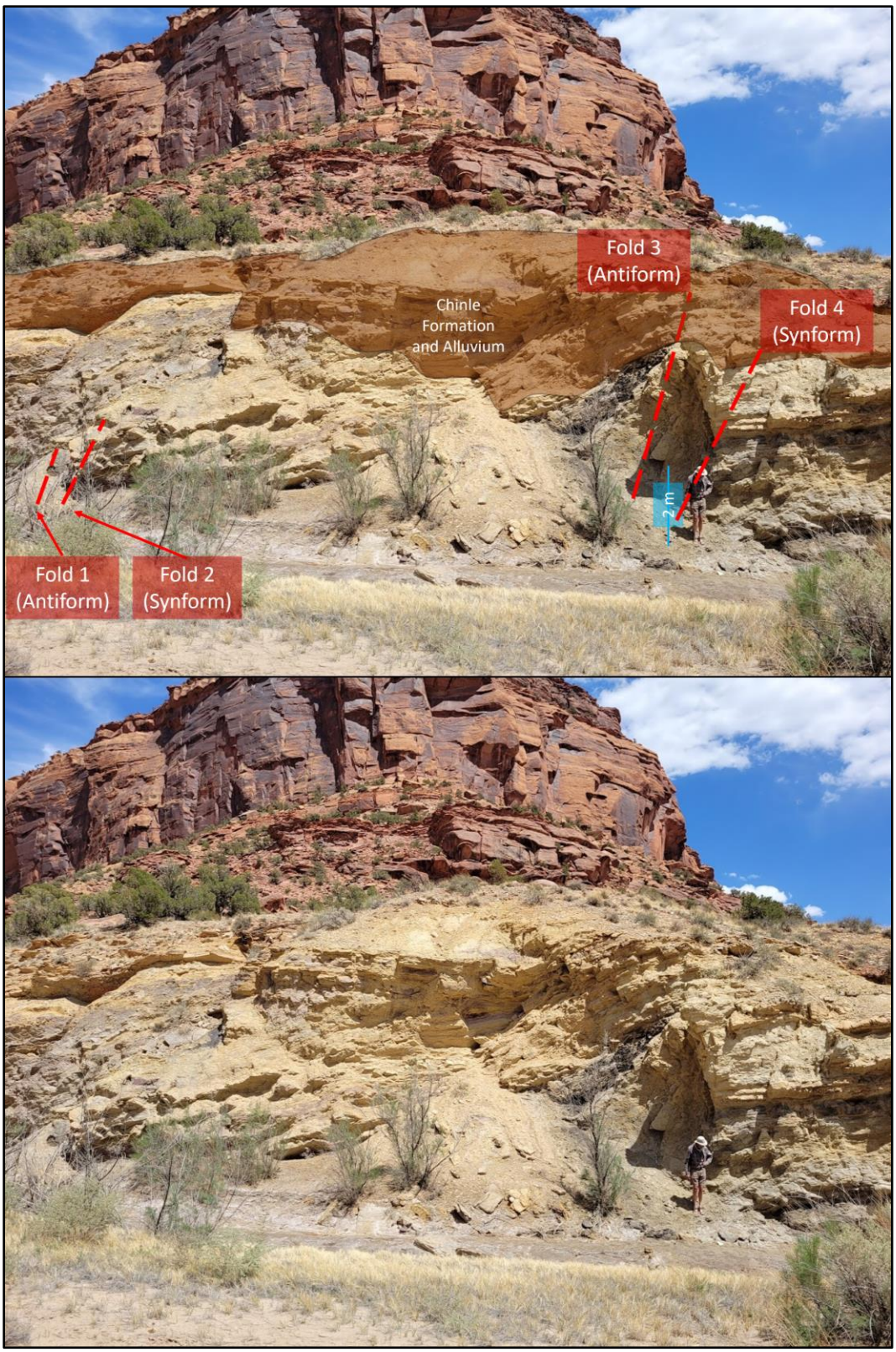

Figure 55: Overview of Gypsum Valley
Image of full Gypsum Valley outcrop with fold axes and overlapping Chinle Formation outlined.

At the hinge of folds, the lithologies tend to be more competent with some fold-plane parallel fracturing (Fig. 22). Moving away from the hinge, lithologies tend to become less competent except for more resistant beds. Due to the small scale and near-vertical exposure of this outcrop, annotated photographs were utilized over traditional mapping methods. Figures 18, 22, 23, and 55 show the mapped imagery of these folds with the various lithologies outlined; the SL lithologies are defined in Table 1. These photographs show the complex structures and lithologic interactions at outcrop scale. Stereonet analysis of the four folds present in the Gypsum Valley outcrop shows interlimb angles between 35.6° and 108.6° with all fold trends within 25° of North (Fig. 56). Additionally, I was able to measure a stratigraphic section and create a stratigraphic column from those measurements (Fig. 57).

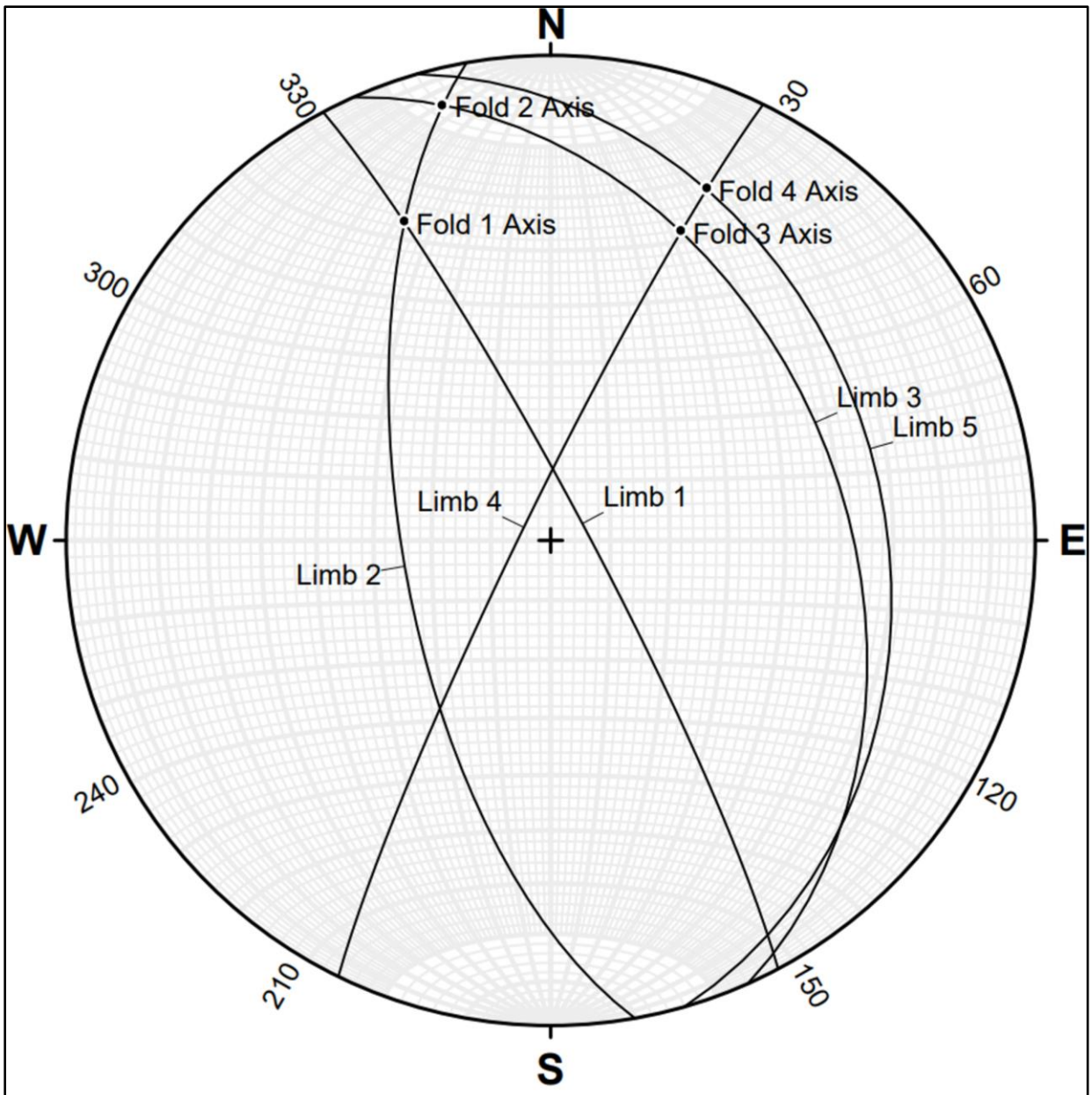

Fold (North to South)	Axial Trend and Plunge	Interlimb Angle
Fold 1	335.3°, 28.6°	35.6°
Fold 2	346.1°, 08.4°	104°
Fold 3	022.9°, 31.5°	69.8°
Fold 4	024.0°, 21.9°	108.6°

Figure 56: Stereonet and fold data from Gypsum Valley outcrop

Stereonet data simplified using average of orientations taken on beds in each fold limb. Limbs from north to south with limb 1 furthest north in outcrop and limb 5 furthest south in outcrop. Table of fold axial trends and plunges as well as interlimb angles.

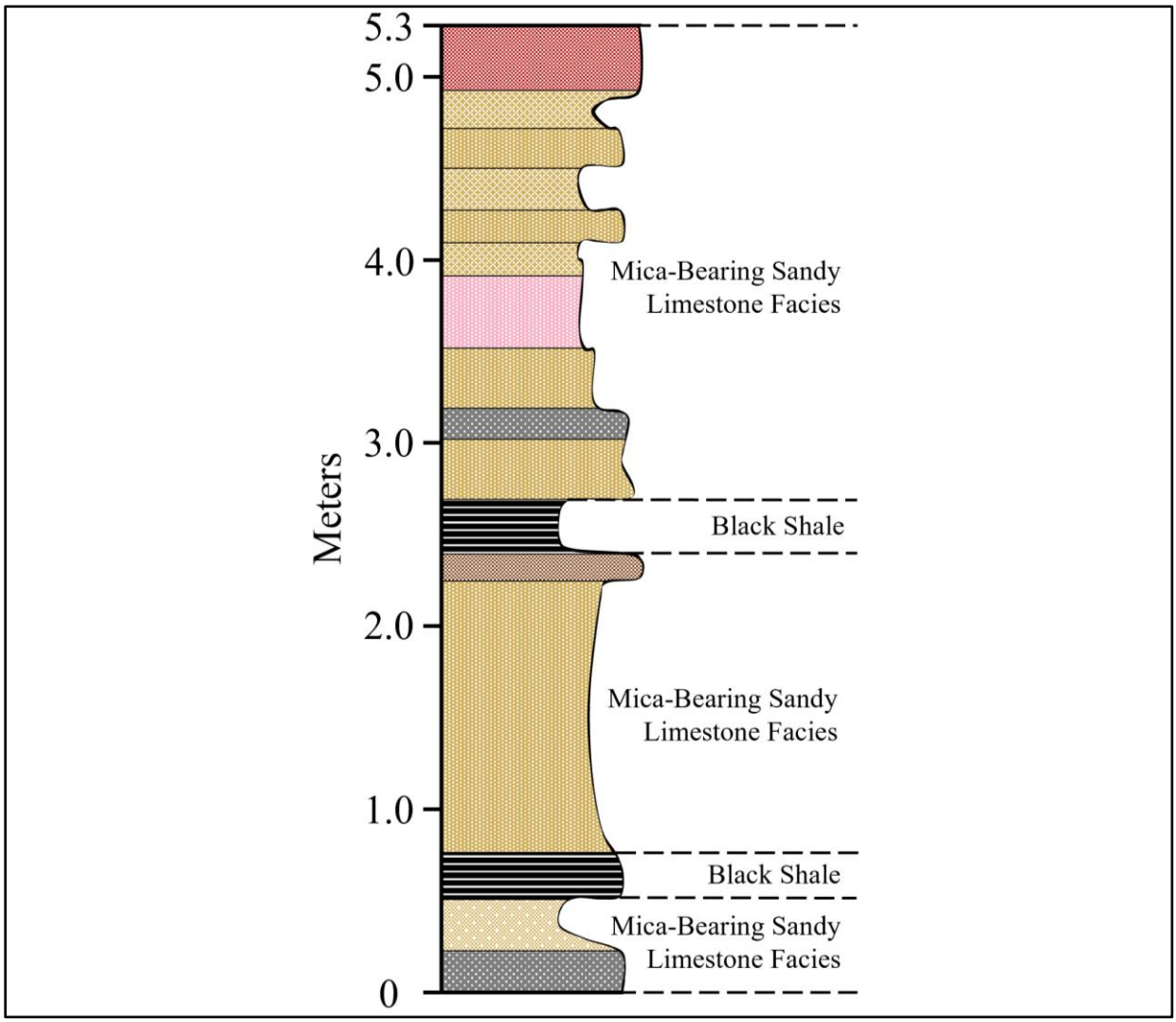

Figure 57: Gypsum Valley stratigraphic column of inclusion outcrop
Stratigraphic section showing thicknesses of individual beds within inclusions at Gypsum Valley. Individual facies labeled.

At the southernmost portion of the outcrop there is a colluvium hill that has two exposures of SL beds worth mentioning (Fig. 21-C,D). These beds are located south and topographically above the main inclusion outcrop and display some major differences from the other SL beds. The main difference in these lithologies is that these hillside beds do not contain the small mica flakes

present in all sandy limestone beds in the main outcrop. Additionally, they are composed mainly of calcite microspar and contain very little sand. It is likely that these beds are part of the onlapping Chinle Formation.

2.3 DIAGENESIS

Compaction and fracturing are seen in conglomerate clasts and quartz grains in sandstones and sandy limestones (e.g., Fig. 30-A,B). Cements were absent prior to compaction indicated by blocky calcite cements bridging boundaries where compaction is evident (e.g., Fig. 32). Grains and clasts show concavo-convex and occasional suture contacts, types of plastic deformation ultimately causing a compaction fabric (Scholle and Ulmer-Scholle, 2003).

Calcite cements are relatively imperfection-free and blocky (e.g., Fig. 19). Ferroan (Fe^{2+}) calcite cement, micritic matrix, and other constituents are present in many samples. Grains are sometimes replaced by calcite, dolomite, or silica. Silica replacement mainly occurs within conglomerate clasts, but silica replacement (in the form of chert) of a fossil (Sinbad Valley) and an ooid (Salt Valley; Fig. 33-C,D) in two sandstone samples was identified. Chert also occasionally replaces quartz grains within conglomerate matrix and sandstone at Sinbad Valley and Salt Valley.

Sinbad Valley, Salt Valley, and Gypsum Valley all have ^{18}O- and ^{13}C-depleted isotope signatures relative to the Vienna Pee Dee Belemnite (VPBD) standard. Isotope values of the various non-evaporite lithologies revealed a range of $\delta^{13}C$ and $\delta^{18}O$ values, from -8.33‰ to +3.01‰ for $\delta^{13}C$ and -15.93‰ to -0.93‰ for $\delta^{18}O$ (Plot 1). A strong meteoric diagenesis trend to isotopically lighter $\delta^{13}C$ and $\delta^{18}O$ values is observed at all three field sites (e.g., Fantle et al., 2020). Plot 1 shows the $\delta^{13}C$ and $\delta^{18}O$ values with respect to the various lithologies for each sample. The large arrows in this plot show the trend for each field site. Sandstones and sandy limestones tend to show lighter (more negative) $\delta^{13}C$ and $\delta^{18}O$ values which may be attributed to their higher

porosity allowing for more diagenetic overprinting. Overall, the Sinbad Valley samples had slightly lighter $\delta^{18}O$ values than the Salt Valley and Gypsum Valley samples. The $\delta^{13}C$ values from the three field sites fall into three different but overlapping groups: the Salt Valley samples display the heaviest $\delta^{13}C$ signatures, followed by Sinbad Valley and then Gypsum Valley where samples are relatively depleted in ^{13}C displaying the lightest $\delta^{13}C$ values from all three sites. All samples within the folded outcrop at Gypsum Valley experienced dolomitization (i.e., a strong replacement process) and were in proximity to organic-rich black shale (organic matter is isotopically light; Fry, 2006; Hoefs, 2021), which could be the reason for the more ^{13}C-depleted isotope signatures at this site., and all samples within the folded outcrop at Gypsum Valley experienced dolomitization. Cements, replacement, and isotope signatures all indicate classic meteoric diagenesis processes (Scholle and Ulmer-Scholle, 2003; Fantle et al., 2020).

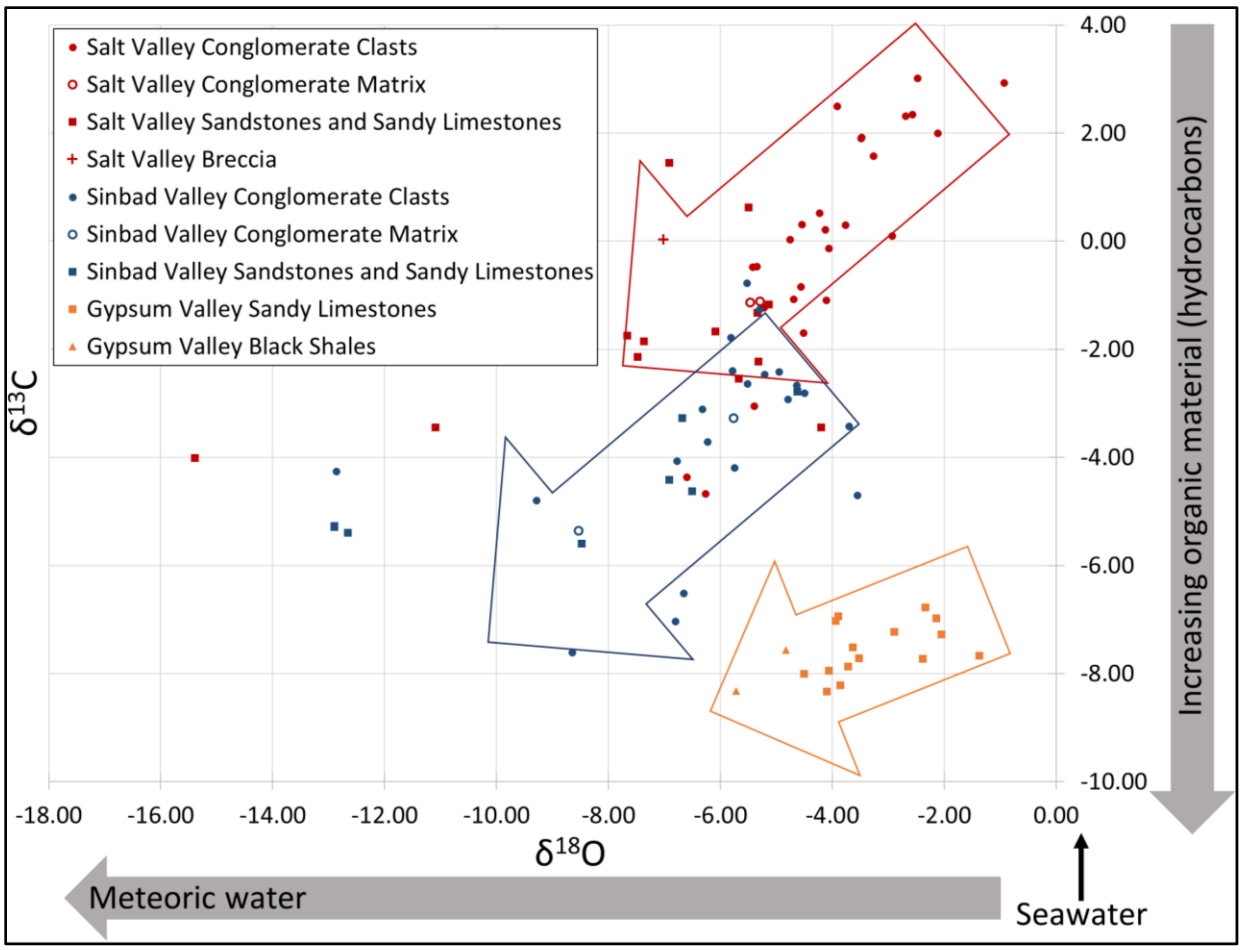

Plot 1: Isotope analysis of carbonates in inclusions
Plot compares $\delta^{13}C$ and $\delta^{18}O$ values for carbonate inclusions. Sinbad Valley data in blue, Salt Valley data in red, Gypsum Valley data in orange. Large arrows show data trends for each field site. Isotopically light $\delta^{13}C$ and $\delta^{18}O$ values generally belong to more porous sandstones and sandy limestones. Marker shape designates lithology of samples.

Chapter 3: Discussion

3.1 Where do Inclusions Come From?

The major lithologies that comprise inclusions are black shales (BS), sandy limestones (SL), sandstones (SS), and carbonate-clast conglomerates (CG; Fig. 17). Three of these four lithologies can be unequivocally considered Paradox Formation LES lithologies: BS, SL, and SS. These three lithologies have been previously identified and extensively studied in the context of the Paradox Formation LES (Herman and Sharps, 1956; Fetzner, 1960; Hite et al., 1984; Raup and Hite, 1992; Goldhammer et al., 1991; Grammer et al., 2000). In contrast, the CG inclusions found in the Sinbad Valley and Salt Valley salt walls are barely mentioned in the literature pertaining to the Paradox LES. These conglomerates have been previously identified and described, but mostly ignored due to their discordant nature with surrounding lithologies (Dane, 1935; Gard, 1976; Thompson Jobe et al., 2019). In this discussion, I will come to the conclusion that the most likely source for these carbonate clasts is the pre-salt Mississippian Leadville Limestone and that the most likely source area was the basement steps within the basin (Fig. 6).

3.2 Depositional Setting of Non-Evaporite Lithologies

3.2.1 Determination of Source of Inclusions

Black laminated mudstones, previously referred to as “black shales,” have been exhaustively characterized for the Paradox Formation because they are the source rocks for hydrocarbons in the PB (e.g., Hite et al., 1984; Raup and Hite, 1992; Goldhammer et al., 1991; Grammer et al., 2000; Rasmussen and Rasmussen, 2009). The BS were deposited during transitions from transgression to regression in low-salinity, oxygen depleted conditions when the water level was at a maximum (greater than 35 m depth; Hite et al., 1984). The BS were conclusively an original component of the PB LES. The origin of this lithology is uncontested and

provides initial evidence that the SL inclusions were also originally layered into the LES based on the presence of interbedded SL and BS seen in the inclusion outcrop at Gypsum Valley (Figs. 18, 22, 23, 55). This provides evidence to support the hypothesis that inclusions were derived from the Paradox Formation LES.

SL inclusions might be regarded as the Cambrian Ophir Formation, the Cambrian Lynch Dolomite, the Devonian Aneth Formation, or the Devonian Ouray Formation, but the limestones reported in these formations do not contain quartz grains and cannot account for the sandy composition of the SL inclusions (Parker and Roberts, 1966; Condon, 1995). This leaves the Pennsylvanian Paradox Formation or the late-Pennsylvanian Honaker Trail Formation as possible sources of the SL inclusions. The Honaker Trail Formation limestones are fossiliferous but include two common fossils that are not seen in the sandy limestone inclusions: fusulinid foraminifera and bivalves (Condon, 1997). Additionally, while the Honaker Trail Formation limestones commonly include chert concretions, there is no mention of quartz grains.

Conversely, the Paradox Formation contains sandy limestones that are described by Goldhammer et al. (1991) and by Pray and Wray (1963) who named them the intermediate facies of the Paradox Formation. This intermediate facies is defined by a wide variety of marine organisms of varying grain sizes and is noted to consist of up to 40% subangular quartz grains that are silt to very fine sand in size (Goldhammer et al., 1991). While quartz grains in SL inclusions are occasionally larger than very fine sand size, grains mostly fall between the classification of silt to very fine-grained sand size. Additionally, the marine fossils in the intermediate facies mentioned by Goldhammer et al. (1991) have all been identified petrographically in samples of SL inclusions except for fusulinids. While Goldhammer et al. (1991) does mention corals in the intermediate facies, they are clarified as Chaetetid, which are now known to be sponges (Scholle and Ulmer-

Scholle, 2003) and have been identified in SL inclusions. From this follows that the Paradox Formation LES is the only reasonable source of these SL inclusions further corroborating the hypothesis that inclusions originated from the Paradox LES.

SS inclusions could be attributed to several possible sources like the Devonian McCracken Sandstone Member of the Elbert Formation, the Pennsylvanian Paradox Formation, the late-Pennsylvanian Honaker Trail Formation sandstone facies, or the Permian Cutler Formation sandstones. The McCracken Sandstone Member is most often described as a white quartz arenite associated with silica cement; fine to coarse sand size grains – sourced from dunes – are very well-rounded and deposited through eolian processes (Condon, 1995; McBride, 2016). The SS inclusions identified and described at the Salt Valley and Sinbad Valley field sites are occasionally quartz sandstones, but with only one sample showing silica cement. Additionally, quartz grains in SS inclusions are never particularly well-rounded. The SSq facies has the most similar qualities to the McCracken Sandstone Member but does not display the same grain sizes. Honaker Trail Formation sandstones are described as having a wide variety of grain sizes from fine sand size to over 2 mm in diameter with a subarkosic to arkosic composition (Condon, 1997). While SS inclusions are variable in grain size, they never approach 2 mm in diameter, and they do not contain any feldspar. Cutler Group sandstones are defined as coarse-grained and arkosic and are interpreted as being deposited in a fluvial environment (Condon, 1997, Barbeau, 2003). The SS inclusions are of a finer grain size, do not contain feldspar, and are interpreted to have a shoreface origin. The transitional origin of SS inclusions is evidenced by the presence of glauconite peloids, fossils fragments, calcite cements, and significant amount of quartz grains most of which are not found in the Cutler Group sandstones.

Paradox Formation sandstones are described and named by Goldhammer et al. (1991) as a quartz sandstone facies that is calcareous, light in color, and contains fine-grained angular to subrounded quartz grains deposited in a shallow marine shoreface environment. Additionally, the calcareous material is clarified further as containing glauconite and carbonate peloids, ooids, and skeletal fragments. Each of these components is present in the SS inclusions and the depositional environment determined for SS inclusion facies fits that described by Goldhammer et al. (1991) for the quartz sandstone facies. Comparison of SS inclusions to the Paradox Formation and over- and underlying stratigraphy reveals the Paradox Formation is the most similar to SS inclusions both in constituents and depositional environment. From this follows that the SS inclusions are a known component of the Paradox Formation LES and that they did not originate as pre- or post-salt deposition from the previously discussed formations. This further affirms the hypothesis that inclusions were derived from the Paradox Formation LES.

CG inclusion clasts could be attributed to various sources within the under- and overlying stratigraphy of the Paradox Formation. What makes them unique from the BS, SL, and SS inclusions is that they could not have been derived from reworking the Paradox Formation itself, as the Paradox Formation does not contain the carbonate lithologies that make up clasts within the CG inclusions seen in Sinbad Valley and Salt Valley. Clasts within the CG inclusions are usually carbonate in nature and often fossiliferous, but there are also occasionally chert clasts with well-preserved fossils (Figs. 14, 15), and locally, sandstone clasts (Fig. 45).

The possible pre-salt sources for the clasts in CG inclusions could be the Cambrian Ophir Formation, the Devonian Elbert Formation, or the Devonian Ouray Formation, but these formations are far less likely sources due to the high abundance of crinoids found in CG inclusions, which suggest a Mississippian-aged origin. Possible post-salt sources for CG inclusion clasts are

the Late Pennsylvanian Honaker Trail Formation and the Permian Cutler Formation. The Mississippian Leadville Limestone, however, is the most probable source for CG inclusion clasts.

The Ophir Formation is composed primarily of shales and some sandstones, the middle member is a dark limestone that is interbedded with shales and occasionally contains trilobites, and the upper portion of the Ophir Formation contains some minor limestone with algae, oolites, brachiopods, and trilobites (Condon, 1995). While the carbonate clasts in the CG inclusions contain many of these fossils, they do not contain trilobites. Additionally, the Ophir Formation does not account for the fossiliferous chert clasts in CG inclusions. The Elbert Formation includes calcareous shale, limestone, and quartz sandstones, which all contain remains of Devonian fish (Condon, 1995). Not only do the clasts in CG inclusions not contain Devonian fish remains, but the Elbert Formation also does not account for the normal marine fossils or the chert clasts in these CG inclusions. The Ouray Formation, also known as the Ouray Limestone, contains abundant green shales, is a fossiliferous, brownish-gray limestone with a Devonian invertebrate assemblage and occasionally has crinoid fragments, oolites, and stromatolites (Condon, 1995). The Ouray Formation does not host sandstone, chert, or most of the fossils found in the CG inclusions (excepting crinoids and brachiopods, locally).

The Honaker Trail Formation is a fossiliferous limestone containing brachiopods, bryozoans, corals, crinoids, fusulinid foraminifera, gastropods, bivalves, and trilobites with occasional chert nodules (Doelling, 1988; Condon, 1997). The Honaker Trail Formation also contains sandstones that are subarkosic to arkosic. While the Honaker Trail Formation contains many of the elements found in CG inclusion clasts, the feldspar-rich sandstone composition does not match the composition of CG sandstone clasts (shoreface environment) and the chert nodules do not contain fossils. Additionally, CG inclusion clasts do not contain fusulinids, bivalves, or

trilobites, all of which are in the Honaker Trail Formation. The Cutler Formation, surmised by Elston et al. (1962) as a possible source for the Salt Valley CG inclusions, contains conglomerates with Proterozoic arkosic clasts and arkosic, coarse-grained sandstones (Doelling, 1988; Condon, 1997; Barbeau, 2003). The Cutler Group has a subarkosic to arkosic composition of the conglomerates and sandstones as well as a lack of fossiliferous chert. The abundant fossiliferous marine carbonate and chert clasts and lack of lithics in CG inclusions make the Cutler Group an unlikely source.

Dane (1935) summarized fossil assemblages from two prior studies pertaining to CG inclusions exposed in Salt Valley which reveal assemblages that are Mississippian in age and placed the Salt Valley CG inclusions as Early Pennsylvanian in age. Gard (1976) later concluded that the conglomerates in Salt Valley are turbidites and as such were deposited contemporaneously with the Middle Pennsylvanian Paradox Formation. I propose that CG inclusion clasts are most likely to have been sourced from the Leadville Limestone during shallow subaqueous debris flows resulting from slope failure mass wasting on active basement steps after initial turbulent flow (Rodine and Johnson, 1976; Enos, 1977; Lowe, 1982, Elverhøi et al., 2000). These mass wasting events are likely to have followed episodes of subaerial exposure of basement highs and subsequent weathering during fluvial transport (Fig. 58). While the fluvial transport distance may not have been great, it served as a mechanism to produce the rounded clasts found within CG inclusions.

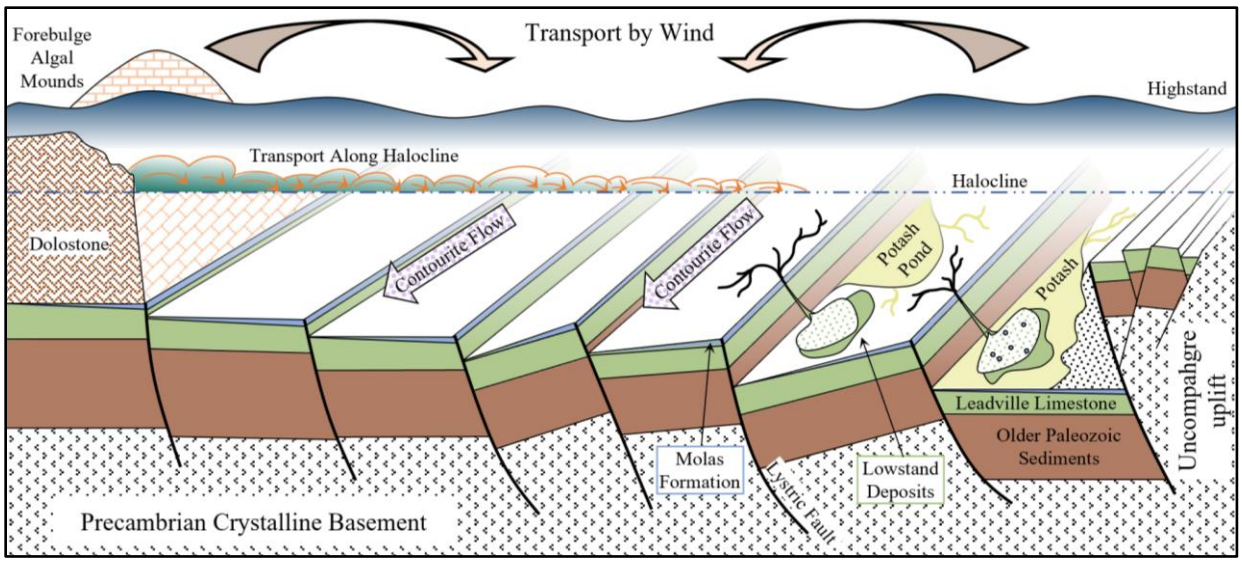

Figure 58: Sedimentary Processes in the Paradox Basin
Schematic reconstruction of the Paradox Basin during deposition of the Paradox Formation and inclusions. Sediment transport mechanisms shown include wind, dispersal along halocline, contourite flows along fault scarps (perpendicular to wind and halocline), precipitation of evaporite minerals, and riverine and mass wasting events during low sea levels. Interpreted reconstruction based on the assumption of active basement steps within the basin.

The Leadville Limestone, also known as the Madison Formation among other names, is gray and diversely fossiliferous (Condon, 1995; Chidsey, 2020). Most interestingly, the Leadville Limestone has an abundance of chert and is separated from the overlying Early Pennsylvanian Molas Formation by a major unconformity distinguished by a profusion of chert clasts and the chert is noted to preserve fossils much better than in the limestone or dolomite (Parker and Roberts, 1966; Chidsey, 2020). Additionally, the Deseret Limestone – a unit associated with the Leadville Limestone – has some sandstones that are fine to medium grained. As such, the Leadville Limestone is the only potential source that contains all elements of the clasts found in CG inclusions. The most telling component is the chert clasts that contain abundant, well-preserved fossils – present in both CG inclusions, and the Leadville Limestone.

While the sandstone clasts found at a CG inclusion outcrop in Sinbad Valley could be from the Deseret Limestone, it is more likely that they originated from the lower Coalbank Hill Member

and the middle member of the Molas Formation. The Coalbank Hill Member is a dissolution-formed, transition unit of the uppermost, karsted surface of the Leadville Limestone (Figs. 11, 12; Cross and Larsen, 1935; Merrill and Winar, 1958). These clasts could be sourced from the overlying Molas Formation unit itself, or from the Molas Formation material filling the karstic features in the Leadville Limestone (Figs. 11, 12). The Coalbank Hill Member likely provided the chert clasts and red siltstone clasts seen in CGcs (Fig. L11) with the middle member providing the sandstone clasts in CGcs. Additionally, the middle member is noted to contain black chert clasts, similar to those I identified in a streambed exposure of a CG inclusion in Sinbad Valley (Fig. 14). The sandstone clasts and associated outcrop of CGcs are stained red – the only instance of this identified for either Sinbad Valley or Salt Valley – which is a distinctive characteristic of the Molas Formation (Figs. 45, 50; Merrill and Winar, 1958).

CG inclusions contain abundant carbonate clasts, some with well-preserved fossils lending to the belief that they could not have originated from a distant source. The coarseness of the conglomerates and abundance of carbonate clasts suggests that there must have been a more proximal source for the detritus than the Uncompahgre uplift, which is over 15 kms away from the nearest diapir. The finding of marine fossils in the matrix of these conglomerates supports this interpretation as these fossil fragments would have been destroyed during transport. Additionally, some of these carbonate clasts are extremely large ranging just under 0.5 m in diameter (~45 cm) indicating that they could not have traveled far from their original source via debris flows. These findings provide evidence supporting the hypothesis that basement steps served as a local source of detritus.

In summary, BS inclusions are correlated with the black laminated mudstone facies of the Paradox Formation and were deposited under deep, calm, oxygen-depleted marine waters during

transgressive phases in the basin (Hite et al., 1984; Raup and Hite, 1992; Goldhammer et al., 1991; Grammer et al., 2000; Rasmussen and Rasmussen, 2009). The black shale and sandy limestone lithologies are facies of the Paradox Formation marking a change from maximum transgression to highstand, depositing black shales, to early regression phase, depositing sandy limestones. SL inclusions are correlated with the sponge to intermediate facies of the Paradox Formation and were deposited under fairly shallow waters during the shift from maximum transgression to early regression phases in the basin (Goldhammer et al., 1991). The sandstone and sandy limestone lithologies are facies of the Paradox Formation representing a change in conditions from early regressive phase, depositing sandy limestones, to a late regressive phase, depositing quartz to carbonate-quartz sandstones. SS inclusions are correlated with the quartz sandstone facies of the Paradox Formation. Goldhammer et al. (1991) proposed deposition in a shoreface setting where the sand was originally deposited under eolian conditions during lowstand and reworked under marine shoreface conditions during transgressive phases. I propose a shoreface depositional environment (Inden and Moore, 1983), but based on the less-sorted, up to medium sand size of grains, I do not think these sandstones experienced a precursor eolian depositional phase. This also explains the change in constituents from quartz (SSq) to carbonate-quartz (SScq) in different sandstone samples that were analyzed petrographically (Table 2).

CG inclusions include clasts that were sourced from the Leadville Limestone and Molas Formation (its lower member being formed by weathering and erosion of the Leadville Limestone; Fig. 6; Cross and Larsen, 1935; Merrill and Winar, 1958). The CG inclusions represent subaqueous debris flows into the Paradox evaporite basin resulting from local slope failure and mass wasting events most likely associated with steep local relief on basement steps during early transgressive

phases following periods of subaerial exposure (i.e., late regressive phase; Fig. 58; Rodine and Johnson, 1976; Enos, 1977; Lowe, 1982, Elverhøi et al., 2000).

3.2.2 Derivation of Anomalous Conglomerates from Basement Steps

The Leadville Limestone has been interpreted to have been deposited on a west facing shallow shelf with the Uncompahgre uplift area being depicted as either a subaerial highland constraining deposition (Blakey, 2009), or as submarine (Parker and Roberts, 1966).So, the Uncompahgre uplift area could have served as the source for Leadville Limestone-clast conglomerates in the Paradox Formation, however, carbonate rocks weather (both chemically and mechanically) and breakdown quickly during hydrologic transport (Folk, 1959). The finding of abundant carbonate clasts in CG inclusions, the large size of some carbonate clasts (up to 45 cm in diameter), and the presence of reworked calcareous fossils in the matrix of these CG inclusions suggest a more proximal source of detritus within the PB. Field, petrographic, and geochemical analyses were integrated to determine the possibility of local basement uplifts (basement steps) as the source of the anomalous CG by determining the history of inclusions from deposition to exhumation. From these analyses, evidence supporting the hypothesis that basement steps were active during deposition of the LES and locally contributed as a source of detritus challenges the previous paradigm that CG clasts originated predominantly from the Uncompahgre uplift.

The PB has been interpreted as a pull-apart basin and a flexural basin. While Barbeau (2003) supports the flexural basin model due to the size and aspect ratio of the PB and the lack of magmatism, it is possible that there are large-scale pull apart mechanisms that worked in conjunction with flexure (Trudgill and Arbuckle, 2009). Subsidence was rapid and differential, causing large offsets in basement steps due to basin-wide faults (Stevenson and Baars, 1986; Barbeau, 2003; Trudgill and Arbuckle, 2009). This ultimately resulted in the basement steps

resting at various levels within the basin (Fig. 5). The most vertically prominent steps were in the proximal basin with the vertical displacement decreasing toward the distal basin (Fig. 6). This vertical displacement could be why CG inclusion deposition varied at different salt walls. For instance, if the basement steps rose higher closer to the Uncompahgre uplift front (proximal basin), it could explain more deposition of conglomerate clasts at Sinbad Valley than Salt Valley, the deposition of larger clasts at Sinbad Valley than at Salt Valley, and no CG inclusions at Gypsum Valley, which is furthest from the Uncompahgre uplift front (more distal; Figs. 1, 17, 48, 51).

Salt walls are known to be defined in their shape by the underlying basement faults, which are progressively further apart moving towards the distal PB (Baars, 1966; Doelling, 2001; Trudgill and Arbuckle, 2009; Trudgill, 2011). This is seen at the surface in the distribution of salt walls in the PB with the most proximal to most distal stepping incrementally further from each other (Fig. 1). Additionally, the flexural history of the PB resulted in the deepest troughs in the most proximal parts of the basin. The area between the defining basement faults grows larger and shallower moving to the more distal areas of the PB. For a small, proximal diapir like Sinbad Valley, those basement steps would be very close to and high above the depocenter, while Salt Valley, a larger, more distal diapir, would have less vertically prominent basement steps resting further from the depocenter, and finally, Gypsum Valley, the largest, most distal of the three, would have low relief basement steps furthest from the depocenter and could be completely outside the range of conglomerate clast deposition.

Episodes of subaerial exposure of basement highs and subsequent chemical and mechanical weathering of the uppermost exposures during fluvial/shoreface transport are interpreted to have resulted in the production of rounded clasts derived from the Leadville Limestone (Fig. 58). CG inclusion facies were subsequently deposited as a result of remobilization of the fluvial/shoreface

rounded clasts in the subaqueous cohesive debris flow deposits during mass wasting events on active basement steps within the PB (Rodine and Johnson, 1976; Enos, 1977; Lowe, 1982, Elverhøi et al., 2000). From the basement step high, the flow would cascade down and then outwards toward the depocenter in the Paradox evaporite basin. In the more distal PB, where the steps are less vertically prominent, a mass wasting event off one of these low relief basement steps would be less climactic, resulting in minimal deposition and runout. This could help explain the lack of conglomerate inclusions at the more distal Gypsum Valley which is defined by the least vertically prominent basement steps of the three studied field areas (Fig. 58).

3.3 Using Inclusions to Determine the Timing and Evolution of the Paradox LES

3.3.1 Compaction and Diagenesis of Inclusions

Concavo-convex and occasional suture contacts in clasts and grains are a result of pressure solution (Scholle and Ulmer-Scholle, 2003). This is not common in quartz grains and most carbonate grains, which are resistant to this type of deformation, indicating that a deep burial depth is required to achieve this deformation (Scholle and Ulmer-Scholle, 2003). Concavo-convex deformation requires dissolution of the clasts and grains at boundaries. The lack of silica cements post-deformation indicates that the dissolved silica remained in solution and escaped, possibly via the basement steps as a pathway. Additionally, though quartz grains in inclusions show significant compaction features, the lack of silica cement in inclusions further evidences an absence of burial cements. The absence of cements prior to compaction lends to the inference that these sediments were weakly consolidated before entrainment. Further, the ferroan (Fe^{2+}) cement, matrix, and other constituents is indicative of reducing pore-fluids, and the soft-sediment deformation through "liquefication" supports lack of early cements (Scholle and Ulmer-Scholle, 2003; Cui et al., 2022).

Lithologies were deeply buried at some point, as evidenced by the compaction and fracturing seen in clasts and quartz grains. This challenges previous assumptions that inclusions either were part of the LES but were never deeply buried or that they were entirely post-Paradox Formation deposition, both of which imply they remained near the surface throughout their history (Elston, Shoemaker, and Landis, 1962; Doelling, 1988). These compaction fabrics tell a story of early, deep burial of inclusion strata. Thus, inclusions are most likely strata from the early depositional cycles of the Paradox LES that were subsequently buried by kilometers of younger Paradox Formation and Honaker Trail Formation strata prior to the onset of diapirism.

Relatively imperfection-free and blocky calcite cement is indicative of meteoric diagenesis (Scholle and Ulmer-Scholle, 2003) that occurred after deep burial compaction and subsequent entrainment of inclusions. A meteoric influence is also evidenced by observed trends in ^{18}O- and ^{13}C-depleted isotope signatures. Grain replacement by calcite occurs as recrystallization of micrite, a common diagenetic alteration. Due to the absence of burial cements, it can be inferred that this recrystallization occurred during meteoric diagenesis which is consistent with the meteoric diagenesis trends found in isotope analysis of these carbonates (Plot 1). Dolomite replacement requires a source of Mg and a large quantity of water moving through the original sediment (Scholle and Ulmer-Scholle, 2003). Organic material, in particular organic matter with carboxyl groups, originally present in samples could have catalyzed dolomitization (Kenward et al., 2013; Liu et al., 2020). Organic material, which captures high quantities of Mg from seawater, present within the sediment, resulted in the organogenesis of dolomite; water was readily available during meteoric diagenesis (Scholle and Ulmer-Scholle, 2003). Silica replacement in conglomerate clasts can be attributed to opaline silica spicules in siliceous sponges going into solution to form the chert concretions and silicify fossils within the Leadville Limestone (Chidsey, 2020). As such, it does

not infer anything about the diagenesis of these conglomerates. The silicified fossil and ooid identified in two samples are likely fragments from the chert clasts. The silicification in these clasts was in the form of chert, a common diagenetic alteration mineral, which is also observed in the chert replacement of quartz grains in inclusions.

Meteoric overprinting of carbon and oxygen isotope signatures is expected to occur in rocks exposed at the surface or in the shallow ground water realm. The strength of this imprint depends on several factors, including the permeability of the rocks, the abundance/supply of meteoric water, the relative difference between the isotope composition of the water and the original rock (the larger the offset, the higher the impact of overprinting), and the original amount of carbonate in the overprinted sample (the smaller the amount, the more strongly the water isotope signatures will be expressed). Sinbad Valley, Salt Valley, and Gypsum Valley all show meteoric diagenesis trends. This trend is caused by overprinting of carbonate isotope signatures by the oxygen isotope composition of meteoric water, which is depleted in ^{18}O relative to seawater, and overprinting by dissolved carbonate in meteoric water, which is derived from the oxidation of organic matter, and is depleted in ^{13}C relative to carbonate dissolved in seawater. The shift to light $\delta^{18}O$ values (i.e., relatively depleted in ^{18}O) is indicative that more meteoric water traveled through them; these samples are most often the higher permeability sandstones or sandy limestones.

A potential reason for samples from Sinbad Valley having slightly lighter $\delta^{18}O$ values is that Sinbad Valley receives more rainfall, thus a higher amount of meteoric water likely traveled through these lithologies over time. The distinct separation in $\delta^{13}C$ values from the three field sites may be explained by different organic matter content. Organic matter is strongly depleted in ^{13}C, overprinting the original values when the organic matter is oxidized during exposure to infiltrating meteoric water. This coincides with the observation that at Gypsum Valley, the samples showed a

much higher amount of organic material than those at Sinbad Valley, which in turn showed a higher amount of organic material than those at Salt Valley.

Finally, the $\delta^{18}O$ values for the three sites fall within the range of low and high temperature dolomite shown by Chidsey (2020) for the Leadville Limestone (also called the Madison Formation) isotopic data, thus inclusions and the Leadville Limestone are compatible (Plot 2). The $\delta^{13}C$ values of the Leadville Limestone, with a majority falling between -2‰ and -4‰, match with some conglomerate inclusion clasts at Sinbad Valley and Salt Valley, but the clasts show a wider range of values, particularly more $\delta^{13}C$ enrichment. This highlights the intriguing possibility that clasts from the Leadville Limestone may have preserved original isotope signatures better than the rocks that are still in place.

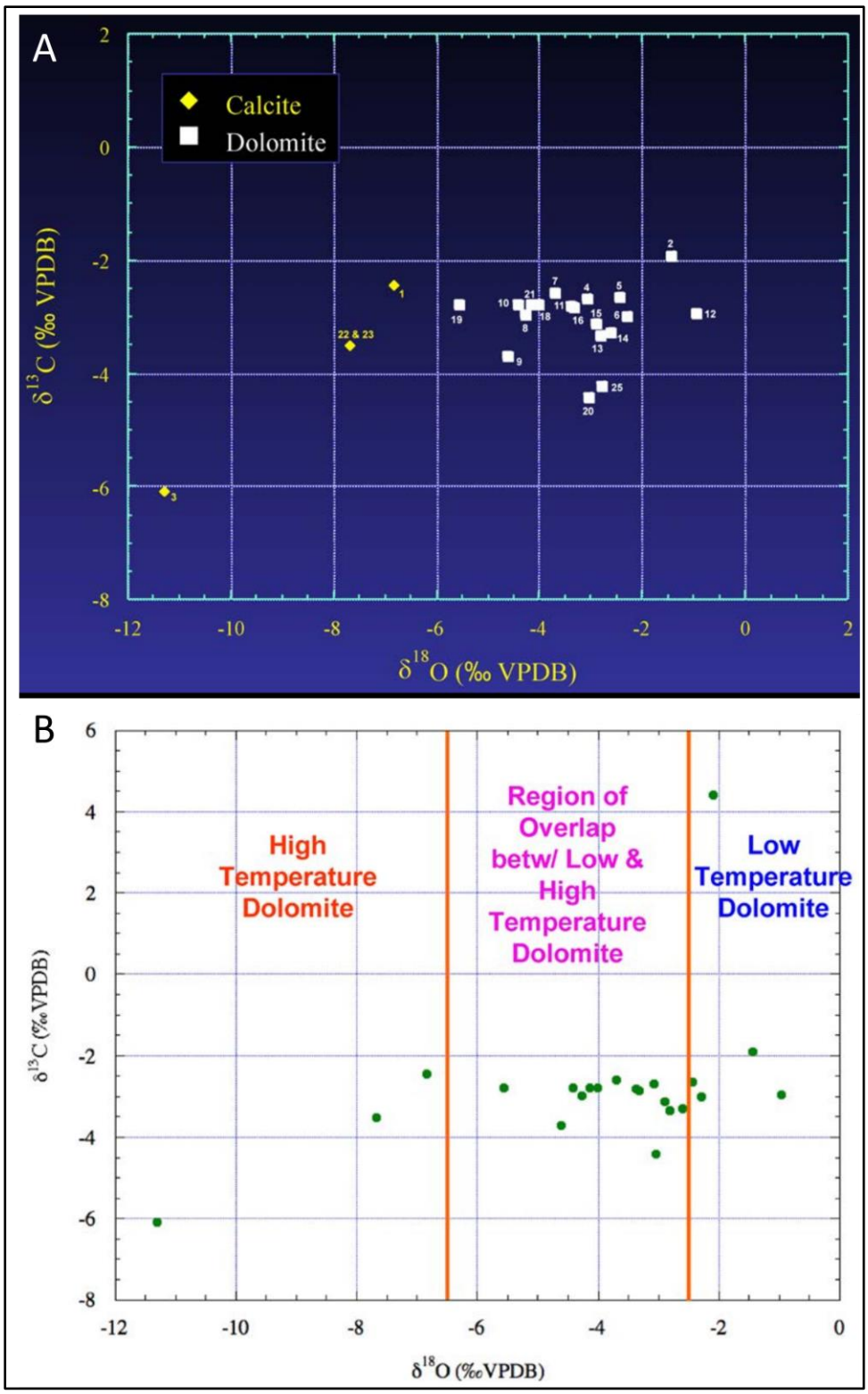

Plot 2: Isotopic composition data for the Leadville Limestone
Plots show comparison of $\delta^{13}C$ and $\delta^{18}O$ values for the Leadville Limestone. A) isotopic compositions for dolomite and calcite Leadville Limestone samples, B) regions of temperatures

for dolomite formation suggested by Allan and Wiggins (1993) for Leadville Limestone (Figure after Chidsey, 2020).

3.3.2 History of the Deposition and Entrainment of Inclusions

The history of inclusions is discussed to understand how these lithologies interact with the Paradox Formation salt from post-deposition to entrainment in the salt during diapirism. The entrainment of these inclusions provides a glimpse into salt mechanics by looking at the deformation, placement, and diagenesis of inclusions, which cannot be determined by analyzing Paradox Formation rock salt.

One of the black shale beds (Lb3b) at Gypsum Valley is heavily compacted and the other (Lb3a) is squished into a wedge-shape with the point of the wedge closer to the fold hinge suggesting that the folding event likely contributed to lithification through compression (Figs. 18, 23). While the black shales are perhaps more easily distorted during these processes, the sandy limestones would be more durable if the lithologies were lithified. The finding of a competent, sandy limestone bed (Lt3a) also displaying a wedge-shape with the point closest to the fold hinge further evidences this soft sediment (weakly consolidated) deformation (Figs. 18, 23). If these lithologies were deposited atop the LES either syn- or post-depositionally and did not sink into the LES, they would not experience the burial deformation (compaction, fracturing of grains/clasts) or entrainment deformation (folding, squishing, and disarticulation of individual units) seen in inclusions at Sinbad Valley, Salt Valley, and Gypsum Valley.

Further supporting this assertion is the mechanics of saturated, soft sediment deformation. Subsequent to the deposition of the Paradox Formation, salt became mobile due to differential loading by overlying strata. There is evidence that some water still existed in the Paradox Formation at the end of the Pennsylvanian from brines found in the younger Honaker Trail Formation sourced from evaporation from the Paradox Formation (Kim et al., 2022). If so, these

fluids could have partially saturated the soft sediments. The differential loading would have then also caused the soft sediments underlying the Paradox Formation to become mobile as well by creating pore fluid pressure between the sediment grains and water, resulting in the "liquefication" of the salt sediments (Cui et al., 2022). These sediments would then be either entrained in the salt or act as a type of sedimentary dyke.

Ductile deformation would induce folding rather than fracturing or faulting, which is evidenced in the substantial folding, often squished nature, and minimal fracturing of the inclusion outcrop at Gypsum Valley (Figs. 18, 22, 23) as well as the large-scale folds seen at Salt Valley (Figs. 52, 53). Additionally, supporting the notion that these sediments were rather weakly consolidated is the lack of significant radial fracturing on folds and the lack of metamorphism present in the Gypsum Valley inclusion outcrop which suggests that these rocks were not completely lithified as they were folded nor were they experiencing intense heat. Lithified, brittle rocks will display fractures radiating around the hinge line of a fold due to the brittleness of such rocks, while soft sediment would be squished and compacted (Ramsay, 1967, Cui et al., 2022). Due to pore fluid pressure in these saturated soft, or weakly-consolidated sediments, stresses acted to fold these sediments rather than fracture of fault them (Cui et al., 2022). This raises the intriguing perspective that the inclusion facies in the Paradox Formation were entrained in the mobile salt after burial as weakly lithified sediments and only fully lithified at a later stage during meteoric diagenesis, potentially with contribution from compression in entrainment as they were folded. If true, this could challenge previous theories as to the timing of diapirism in the Paradox Basin, placing it much closer to the end of Paradox Formation deposition.

Chapter 4: Conclusions

Non-evaporite lithologies originally interlayered in the Paradox LES and exposed at breached salt walls today provide information that elucidates the history of salt basin evolution and subsequent diapirism in the PB. This study provides context for potential modes of deposition of inclusions, and how those inclusions interact with the LES not only for the PB, but for diapirs across the globe. This study examines and explains inclusion deposition in evaporite basins, the relative timing of that deposition, and how they come to be exposed in outcrop at the surface today. Additionally, this study explores the diagenesis of inclusions, hinting at the possibility that salt may preserve the early history of these anomalous rocks.

The inclusions at Sinbad Valley, Salt Valley, and Gypsum Valley fall into four distinct lithologies: black shales (organic-rich, laminated dolomudstones), sandy limestones, sandstones, and carbonate-clast conglomerates. The BS, SL, and SS inclusions are typical of those described for the Paradox Formation LES (e.g., Goldhammer et al., 1991). The CG inclusions, however, had a different mode of deposition originating from mass wasting off basement highs into the Paradox LES. These shallow subaqueous cohesive debris flows followed episodes of subaerial exposure of basement highs which provided rounded clast material for these flows (Fig. 58). This supports deposition of the CG inclusions in the LES cycle between late regression and early transgression in the basin.

In the framework of this study, no additional information could be gained on the provenance of the detritus that makes up the black shales, sandstones, and sandy limestones, but all evidence suggests they are facies of the Paradox Formation LES (e.g., Goldhammer et al., 1991). Based on the fossil content of the carbonate clasts and their association with fossil-rich chert clasts, it is concluded that clasts in the conglomerate inclusions are sourced from the

Leadville Limestone, which exhibits the same features. It is also likely that the Molas Formation (its lower member being a dissolution-formed unit from the Leadville Limestone; Cross and Larsen, 1935; Merrill and Winar, 1958) contributed paleosol clasts in Sinbad Valley. On its own, this insight does not preclude the Uncompahgre uplift as the source – the Leadville Limestone has been both assumed to have been deposited across a region that encompasses both the PB and the Uncompahgre uplift (Parker and Roberts, 1966) as well as with the Uncompahgre uplift depicted as a subaerial highland limiting deposition of the Leadville Limestone (Blakey, 2009). However, the fact that the clasts are predominantly carbonates, which are prone to rapid degradation by weathering and erosion, and the remarkable size of boulders of up to 45 cm in diameter, emphasizes a very short travel distance between source and deposition of clasts, challenging the notion of the Uncompahgre uplift as the primary source of CG inclusions. Moreover, a simple flexural foreland basin geometry with a static load – as proposed for the PB – would have resulted in the deepest trough right next to the uplift, precluding sediment that does not travel in suspension (i.e., grain sizes larger than silt) from reaching depocenters in more distal portions of the basin. This, in combination with the insight that when modeled as a single block, the Uncompahgre uplift would be submerged for most of the duration of the deposition of the Paradox Formation, is problematic for its interpretation as a source of detritus (Trudgill and Arbuckle, 2009). It follows that sources more local must be considered.

It is accepted that the PB hosts basement steps, that those steps appear to be the locus for the formation of salt walls, and that their development pre-dates the deposition of the Paradox Formation (Trudgill and Arbuckle, 2009). In seismic interpretations, the offset at some of these basement steps is such that Precambrian basement is juxtaposed to Paradox LES (Fig. 6), making it plausible that debris from the Leadville Limestone exposed at basement highs could have been

incorporated as CG inclusions in evaporite sequences in basement lows. This interpretation calls for a more complex geometry of the PB, with steep gradients between elevated and subsiding blocks. Such features would be more typical for a system with strike-slip components, forming pull-apart basins. Indeed, the PB has been considered a pull-apart (flower-structure type) basin (Stevenson and Baars, 1986) before being reinterpreted as flexural foreland basin (Barbeau, 2003), and it has been noted that neither interpretation matches all observations, leading to the conclusion that it is a combination of the two (Trudgill and Arbuckle, 2009; Trudgill, 2011). Tectonic features that could accommodate strike-slip components and point to more complex kinematics than the formation of a flexural foreland basin are known: it is assumed that vertical and lateral movement during the Phanerozoic followed ancient fracture systems in the Precambrian basement, discerned as lineaments with two intersecting trends: an east-west and north-south, and a orthogonal northwest and northeast trend (Maughan and Perry, 1986). Moreover, the geometry of the Uncompahgre uplift front to the southeast from the Utah/Colorado state line contrasts to the single large fault in Utah. It is a stack of southwest directed thrust faulted basement blocks that also carry Mississippian and older pre-salt rocks (Kluth and DuChene, 2009), pointing to a detachment between those provinces. The carbonate-clast conglomerate inclusions found at Sinbad Valley and Salt Valley add strong evidence in favor for the interpretation of basement steps in the PB as important local detritus sources for the Paradox Formation LES.

A second insight from this study pertains to the burial and entrainment of inclusions after deposition in the Paradox LES. Intense compaction of grains is ubiquitous for sandstone, sandy limestone, and carbonate-clast conglomerate inclusions. This observation indicates that before entrainment and subsequent exhumation, these lithologies were deeply buried (i.e., they are not lithologies that, from the moment of deposition, ‘floated atop the salt’ during diapirism, nor are

these lithologies that were deposited only toward the final stages of the deposition of the LES). Further, the lack of burial cements and evidence of reducing pore fluids in some inclusions suggests that they may have been entrained as weakly lithified sediments that experienced further lithification near the surface during meteoric diagenesis

Chapter 5: Future Outlook

I believe this work demonstrates the value of using diapiric inclusions in the reconstruction of the paleogeography and early history of the PB. Further, I believe that this study can be used as a model to study non-evaporite lithologies incorporated in other salt basins across the globe. While this research is on the forefront of evaluating and determining the utility of investigating inclusions, there is much yet to be explored. For the future, I envision inclusions being researched in other salt basins to constrain modes of deposition and further elucidate basin formation and history, the mechanics of salt flow, and subsequent deformation of more competent lithologies within the salt. These inclusions offer a window into much more than underlying lithologies, they hold a record of the basin's salty past and may reveal answers to questions that have eluded basin research for decades.

A critical component is the identification of the source of inclusions. Current evidence from this study supports the hypothesis that inclusions are facies of the Paradox LES and that conglomerate inclusions are sourced from the Mississippian Leadville Limestone and overlying Early Pennsylvanian Molas Formation. To constrain and add further relevance to this hypothesis, biostratigraphic dating is critical. Therefore, conodont extraction (from clasts in conglomerate inclusions) and analysis would be the next step to constrain accurate age dates for biostratigraphy.

The observation that fossil and rock fabrics appear pristine in inclusion outcrops and hand samples sparked the question of how well original properties of inclusion lithologies are preserved. The diagenetic analysis performed on inclusion samples in this study can be compared to the outboard Paradox Formation outcrops in the future. I hypothesize that while diapiric inclusions are deformed during salt diapirism, they preserve lithological and geochemical information better than equivalent lithologies accessible by drilling. The inclusions are protected and essentially

"mummified" by the encasing salt preserving the diagenetic history of inclusion facies by preventing overprinting during later events. A comprehensive test of this hypothesis would require the comparison of carbonate inclusions to exposures of Paradox carbonates that are not part of diapirs, which is beyond the scope of this master's project. If "mummification" by salt encasement occurred, fracturing and healing of carbonate rocks by vein formation should take place in a closed system. This means that the inventory of carbon (i.e., its carbon isotope composition) within a fractured rock package should be reflected in the vein material. Oxygen isotopes, on the other hand, should vary from each other, as they are influenced by formation temperatures and the presence of salt brines. By comparing the carbon and oxygen isotope composition of carbonate inclusions to the composition of associated carbonate veins, one could assess if the expected pattern of invariant carbon and variable oxygen isotope composition holds.

The encasement by salt is important for the chemical inventory of inclusions as it indicates a lack of percolating water. It is expected that inclusions did not experience burial diagenesis because they were protected by the encasing salt. Petrographic and carbon and oxygen isotope analyses can be employed to verify this.

References

Ala, M.A., 1974, Salt diapirism in Southern Iran: AAPG Bulletin, v. 58, p. 1758–1770, doi:https://doi.org/10.1306/83D919A2-16C7-11D7-8645000102C1865D.

Allan, J.R., and Wiggins, W.D., 1993, Dolomite Reservoirs: Geochemical Techniques for Evaluating Origin and Distribution: Tulsa, Oklahoma, American Association of Petroleum Geologists, v. 36, 129 p., https://doi.org/10.1306/CE36576.

Baars, D.L., 1966, Pre-Pennsylvanian Paleotectonics—Key to Basin Evolution and Petroleum Occurrences in Paradox Basin, Utah and Colorado: AAPG Bulletin, v. 50, p. 2082–2111, doi:https://doi.org/10.1306/5D25B70D-16C1-11D7-8645000102C1865D.

Baars, D.L., and See, P.D., 1968, Pre-Pennsylvanian Stratigraphy and Paleotectonics of the San Juan Mountains, Southwestern Colorado: GSA Bulletin, v. 79, p. 333–350, doi:https://doi.org/10.1130/0016-7606(1968)79[333:PSAPOT]2.0.CO;2.

Baars, D.L., and Ellingson, G.M., 1984, Geology of the Western San Juan Mountains, *in* Brew, D.C., ed., Field Trip Guidebook, Geological Society of America, Rocky Mountain Section 37th Annual Meeting, p. 1–45.

Barbeau, D.L., 2003, A flexural model for the Paradox Basin: implications for the tectonics of the Ancestral Rocky Mountains: Basin Research, v. 15, p. 97–115, doi:10.1046/j.1365-2117.2003.00194.x.

Black, R.A., 1953, A Magnetic Investigation of the Round Mountain Plug, Castle Valley, Grand County, Utah: United States Department of the Interior, Geological Survey Trace Elements Investigations Report 342, 1–25 p.

Blakey, R.C., 2009, Paleogeography and Geologic History of the Western Ancestral Rocky Mountains, Pennsylvanian-Permian, Southern Rocky Mountains and Colorado Plateau, *in* Houston et al., The Paradox Basin Revisited – New Developments in Petroleum Systems and Basin Analysis, Rocky Mountain Association of Geologists, Special Publication, p. 222–264.

Boggs, S., 2006, Principles of Sedimentology and Stratigraphy: Hoboken, New Jersey, Pearson Prentice Hall, 662 p.

Brunner, B. et al., 2019, Synthesizing Old Questions with New Developments in Caprock Research: Is it Time to Abandon Well-Trodden Paths?, *in* Fiduk, J.C., Norman, C.R., Salt Tectonics, Associated Processes, and Exploration Potential: Revisited 1989-2019, SEPM Publications, Gulf Coast Section SEPM Special Publication, p. 100–141.

Byers, C.W., 1977, Biofacies Patterns in Euxinic Basins: A General Model, *in* Cook, H.E., Enos, P., Deep-Water Carbonate Environments, Society of Economic Paleontologists and Mineralogists, SEPM Special Publication 25, p. 5–17, https://doi.org/10.2110/pec.77.25.0005.

Cater, F.W., and Craig, L.C., 1970, Geology of the Salt Anticline Region in Southwestern Colorado, With a Section on Stratigraphy: U.S. Geological Survey Professional Paper 637, 80 p.

Chidsey, T.C., Jr., 2020, The Mississippian Leadville Limestone Oil and Gas Play, Paradox Basin, Southeastern Utah and Southwestern Colorado-Lisbon Field, Regional, and Analog Studies: Utah Geological Survey Bulletin 139, 1–246 p., https://doi.org/10.34191/B-139.

Choquette, P.W., and Traut, J.D., 1963, Pennsylvanian Carbonate Reservoirs, Ismay Field Utah and Colorado, *in* Bass, R.O., Sharps, S.L., Shelf Carbonates of the Paradox Basin, Four Corners Geological Society, Fourth Field Conference, p. 157–184.

Condon, S.M., 1995, Geology of Pre-Pennsylvanian Rocks in the Paradox Basin and Adjacent Areas, Southeastern Utah and Southwestern Colorado: Evolution of Sedimentary Basins-Paradox Basin U.S. Geological Survey Bulletin 2000-G, G1–G53 p.

Condon, S.M., 1997, Geology of the Pennsylvanian and Permian Cutler Group and Permian Kaibab Limestone in the Paradox Basin, Southeastern Utah and Southwestern Colorado: Evolution of Sedimentary Basins-Paradox Basin U.S. Geological Survey Bulletin 2000-P, P1–P46 p.

Cross, W., and Larsen, E.S., 1935, A Brief Review of the Geology of the San Juan Region of Southwestern Colorado: U.S. Geological Survey Bulletin 843, 1–138 p.

Cui, M., Peng, N., Liu, Y., Wang, Z., Li, C., Xu, K., and Kuang, H., 2022, Recognizing deformation origins: a review of deformation structures and hypothesis on the perspective of sediment consolidation: International Geology Review, p. 1–24, doi:https://doi.org/10.1080/00206814.2022.2094840.

Dane, C.H., 1935, Geology of the Salt Valley Anticline and Adjacent Areas, Grand County, Utah: U.S. Geological Survey Bulletin 863, 1–184 p., https://doi.org/10.3133/b863.

Deatrick, K.T., 2019, Sequence Stratigraphy, Diagenesis, and Depositional Facies of an Exposed Megaflap: Pennsylvanian Hermosa Group, Gypsum Valley Salt Wall, Paradox Basin, Colorado [M.S. thesis]: The University of Texas at El Paso, 199 p., https://www.utep.edu/science/its/about/Kyle-Deatrick-Thesis-2019.pdf (accessed August 2022).

Doelling, H.H., 1985, Geology of Arches National Park, with accompanying text: Utah Geological and Mineral Survey, Map 74, 1–15 p.

Doelling, H.H., 1988, Geology of the Salt Valley Anticline and Arches National Park, Grand County, Utah, *in* Doelling, H.H., Oviatt, C.G., and Huntoon, P.W., Salt Deformation in the Paradox Region Utah Geological and Mineral Survey Bulletin B-122, 1–58 p.

Doelling, H.H., 2001, Geologic map of the eastern part of the San Rafael Desert 30'x60' quadrangles, Grand and Emery Counties, Utah, and Mesa County, Colorado: Utah Geological Survey Map 180, scale 1:100,000.

Elston, D.P., Shoemaker, E.M., and Landis, E.R., 1962, Uncompahgre Front and Salt Anticline Region of Paradox Basin, Colorado and Utah: AAPG Bulletin, v. 46, p. 1857–1878, doi:https://doi.org/10.1306/BC7438F7-16BE-11D7-8645000102C1865D.

Elverhøi, A., Harbitz, C.B., Dimakis, P., Mohrig, D., Marr, J., and Parker, G., 2000, On the dynamics of subaqueous debris flows: Oceanography, v. 13, p. 109–117.

Enos, P., 1977, Flow regimes in debris flow: Sedimentology, v. 24, p. 133–142, doi:https://doi.org/10.1111/j.1365-3091.1977.tb00123.x.

Escosa, F.O., Rowan, M.G., Giles, K.A., Deatrick, K.T., Mast, A.M., Langford, R.P., Hearon, T.E., and Roca, E., 2019, Lateral terminations of salt walls and megaflaps: An example from Gypsum Valley Diapir, Paradox Basin, Colorado, USA: Basin Research, v. 31, p. 191–212, doi:10.1111/bre.12316.

Fantle, M.S., Barnes, B.D., and Lau, K.V., 2020, The Role of Diagenesis in Shaping the Geochemistry of the Marine Carbonate Record: Annual Review of Earth and Planetary Sciences, v. 48, p. 549–583, doi:https://doi.org/10.1146/annurev-earth-073019-060021.

Fetzner, R.W., 1371, Pennsylvanian Paleotectonics of Colorado Plateau: AAPG Bulletin, v. 44, p. 1960, doi:https://doi.org/10.1306/0BDA61B2-16BD-11D7-8645000102C1865D.

Fry, B., 2006, Stable Isotope Ecology: New York, NY, Springer, 308 p., https://doi.org/10.1007/0-387-33745-8.

Gard, L.M., 1976, Geology of the north end of the Salt Valley Anticline, Grand County, Utah: U.S. Geologic Survey Open-File Report 76–303, 35 p., https://doi.org/10.3133/ofr76303.

Gianniny, G.L., and Miskell-Gerhardt, K.J., 2009, Progradational Mixed Siliciclastic/Carbonate Sequence Sets on the Tectonically Active Eastern Margin of the Pennsylvanian Paradox Basin, Southwestern Colorado, *in* Houston et al., The Paradox Basin Revisited – New Developments in Petroleum Systems and Basin Analysis, Rocky Mountain Association of Geologists, Special Publication, p. 310–380.

Giles, K. and Brunner, B., personal communication, 2021, in the framework of visiting field sites in the Paradox Basin in November 2021.

Girty, G.H., 1903, The Carboniferous formations and faunas of Colorado: U.S. Geological Survey Series C, Systematic Geology and Paleontology, 63, U.S. Geological Survey Professional Paper 16, 533 p., https://doi.org/10.3133/pp16.

Goldhammer, R.K., Oswald, E.J., and Dunn, P.A., 1991, Hierarchy of stratigraphic forcing: Example from Middle Pennsylvanian shelf carbonates of the Paradox basin: Sedimentary Modeling: Computer Simulations and Methods for Improved Parameter Definition Kansas Geological Survey, Bulletin 233, 361–413 p.

Grammer, G.M., Eberli, G.P., Van Buchem, F.S.P., Stevenson, G.M., and Homewood, P.W., 2000, Application of high resolution sequence stratigraphy in developing an exploration and

production strategy for a mixed carbonate/siliciclastic system (Carboniferous) Paradox Basin, Utah, USA, *in* P. W. Homewood and G. P. Eberli, eds., Genetic stratigraphy on the exploration and production scales: Case studies from the Pennsylvanian of the Paradox Basin and the Upper Devonian of Alberta, Elf Aquitaine Memoir 24, p. 29–69.

Hintze, L.F., and Kowallis, B.J., 2009, Geologic history of Utah; a field guide to Utah's rocks: Brigham Young University Geology Publications, Special Publication 9, 225 p.

Hite, R.J., and Buckner, D.H., 1981, Stratigraphic Correlations, Facies, Concepts, and Cyclicity in Pennsylvanian Rocks of the Paradox Basin, *in* Wiegand, D.L., ed., Geology of the Paradox Basin, Rocky Mountain Association of Geologists, 1981 Field Conference, p. 147–159.

Hite, R.J., Anders, D.E., and Ging, T.G., 1984, Organic-rich source rocks of Pennsylvanian age in the Paradox basin of Utah and Colorado, *in* Woodward, Jane, Meissner, F.F., and Clayton, J.L., eds., Hydrocarbon source rocks of the greater Rocky Mountain region, Rocky Mountain Association of Geologists, p. 255–274.

Hoefs, J., 2021, Stable Isotope Geochemistry: Cham, Switzerland, Springer Nature Switzerland AG, 504 p., https://doi.org/10.1007/978-3-030-77692-3.

Hsu, K.J., 1959, Flute- and groove-casts in the Prealpine Flysch, Switzerland: American Journal of Science, v. 257, p. 529–536, doi:https://doi.org/10.2475/ajs.257.7.529.

Hudson, S.M., Tuttle, T., and Wood, M., 2017, Source Within the Seal—Distribution and Implications of Organic Shale-Bearing Stringers within the Onion Creek Diapir, Northern Paradox Basin, Utah: Geology of the Intermountain West, v. 4, p. 215–229, doi:10.31711/giw.v4i0.15.

Huffman, A.C., and Condon, S.M., 1993, Stratigraphy, Structure, and Paleogeography of Pennsylvanian and Permian Rocks, San Juan Basin and Adjacent Areas, Utah, Colorado, Arizona, and New Mexico: Evolution of Sedimentary Basins-San Juan Basin: U.S. Geological Survey Bulletin 1808-O, O1–O44 p., doi:10.3133/b1808O.

Inden, R.F., and Moore, C.H., 1983, Beach Environment, *in* Scholle, P.A., Bebout, D.G., Moore, C.H., eds., Carbonate Depositional Environments, American Association of Petroleum Geologists, Memoir 33.

Kenward, P.A., Ueshima, M., Fowle, D.A., and Goldstein, R.H., 2013, Ordered low-temperature dolomite mediated by carboxyl-group density of microbial cell walls: AAPG Bulletin, v. 97, p. 2113–2125, doi:10.1306/05171312168.

Kernen, R.A., 2019, Origin And Characterization Of Intrasalt Non-Halite Lithologies Of The Neoproterozoic Patawarta Diapir, Central Flinders Ranges, South Australia [Ph.D. thesis]: The University of Texas at El Paso, 138 p., https://scholarworks.utep.edu/cgi/viewcontent.cgi?article=3866&context=open_etd (accessed August 2022).

Kim, J.-H. et al., 2022, Hydrogeochemical evolution of formation waters responsible for sandstone bleaching and ore mineralization in the Paradox Basin, Colorado Plateau, USA: GSA Bulletin, v. 134, p. 2589–2610, doi:https://doi.org/10.1130/B36078.1.

Kim, N., 1996, Sedimentology of Cross-Stratified Carbonate Grainstone Facies of the Honaker Trail Formation (Permo-Pennsylvanian), Southeastern Utah [Ph.D. thesis]: University of Nebraska, 175 p., https://www.proquest.com/docview/304273933?pq-origsite=gscholar&fromopenview=true (accessed April 2023).

Kluth, C.F., and Coney, P.J., 1981, Plate tectonics of the Ancestral Rocky Mountains: Geology, v. 9, p. 10–15, doi:10.1130/0091-7613(1981)9<10:PTOTAR>2.0.CO;2.

Kluth, C.F., 1986, Plate Tectonics of the Ancestral Rocky Mountains: Part III. Middle Rocky Mountains, *in* Peterson, J.A., Paleotectonics and Sedimentation in the Rocky Mountain Region, United States, American Association of Petroleum Geologists, Memoir 41, p. 353–369, doi:10.1306/M41456C17.

Kluth, C.F., and DuChene, H.R., 2009, Late Pennsylvanian and Early Permian Structural Geology and Tectonic History of the Paradox Basin and Uncompahgre Uplift, Colorado and Utah, *in* Houston et al., The Paradox Basin Revisited – New Developments in Petroleum Systems and Basin Analysis, Rocky Mountain Association of Geologists, Special Publication, p. 178–197.

Kukla, P.A., Reuning, L., Becker, S., Urai, J.L., and Schoenherr, J., 2011, Distribution and mechanisms of overpressure generation and deflation in the late Neoproterozoic to early Cambrian South Oman Salt Basin: Geofluids, v. 11, p. 349–361, doi:https://doi.org/10.1111/j.1468-8123.2011.00340.x.

Labrado, A.L., 2021, Geological Problems with Microbiological Solutions: Deciphering the Authigenesis of Calcite, Dolomite, and Native Sulfur in Salty Environments [Ph.D. thesis]: The University of Texas at El Paso, 326 p., https://www.proquest.com/docview/2546079021/fulltextPDF/8E6834856EF74033PQ/1?accountid=7121 (accessed August 2022).

Langford, R.P., Giles, K.A., Rowan, M.G., McFarland, J., Heness, L., Lankford-Bravo, D., Thompson Jobe, J., Soltero, A., and Bailey, C., 2022, Burial wedges—Evidence for

prolonged progressive burial of the Paradox Basin salt walls—With a detailed example from Gypsum Valley, Colorado: Basin Research, v. 34, p. 1244–1267, doi:10.1111/bre.12658.

Lankford-Bravo, D.F., 2021, Structural and Stratigraphic History of a Deformed Diapir Margin, Onion Creek Salt Diapir, Paradox Basin, Utah [Ph.D. thesis]: The University of Texas at El Paso, 273 p., https://www.proquest.com/docview/2621045817/fulltextPDF/2AE32204FD8F4C06PQ/1?accountid=7121 (accessed August 2022).

Lerer, K., 2017, Gypsum, Calcite, And Dolomite Caprock Fabrics And Geochemistry From The Gypsum Valley Salt Diapir, Paradox Basin, Southwestern Colorado [M.S. thesis]: The University of Texas at El Paso, 178 p., https://scholarworks.utep.edu/cgi/viewcontent.cgi?article=1478&context=open_etd (accessed August 2022).

Liu, D., Xu, Y., Yu, Q., Yu, N., Qiu, X., Wang, H., and Papineau, D., 2020, Catalytic effect of microbially-derived carboxylic acids on the precipitation of Mg-calcite and disordered dolomite: Implications for sedimentary dolomite formation: Journal of Asian Earth Sciences, v. 193, p. 1–13, doi:https://doi.org/10.1016/j.jseaes.2020.104301.

Lowe, D.R., 1982, Sediment Gravity Flows: II. Depositional Models with Special Reference to the Deposits of High-Density Turbidity Currents: Journal of Sedimentary Petrology, v. 52, p. 279–297, doi:https://doi.org/10.1306/212F7F31-2B24-11D7-8648000102C1865D.

Mast, A.M., 2016, The origin of anomalous carbonate units outcropping at the salt sediment interface of the southern end of Gypsum Valley Salt Wall, Paradox Basin, southwest Colorado [M.S. thesis]: The University of Texas at El Paso, 201 p.,

https://www.proquest.com/docview/1876050813?parentSessionId=iaiD6LF1gMDDzPRRyeoIOkaSx1rmhEao5dvWvGQR%2FKA%3D (accessed August 2022).

Maughan, E.K., and Perry, W.J., Jr., 1986, Lineaments and Their Tectonic Implications in the Rocky Mountains and Adjacent Plains Region, *in* Peterson, J.A., Paleotectonics and Sedimentation in the Rocky Mountain Region, United States, American Association of Petroleum Geologists, Memoir 41, p. 41–53, doi:10.1306/M41456C17.

McBride, E.F., 2016, Stratigraphy, petrography, and depositional history of the Ignacio Quartzite and McCracken Sandstone Member of the Elbert Formation, southwestern Colorado, U.S.A.: Rocky Mountain Geology, v. 51, p. 23–68, doi:doi:10.2113/gsrocky.51.2.23.

Mcfarland, J.C., 2016, Structural and stratigraphic development of a salt-diapir shoulder, Gypsum Valley, Colorado [M.S. thesis]: The University of Texas at El Paso, 108 p., https://www.proquest.com/docview/1803590334?pq-origsite=gscholar&fromopenview=true (accessed August 2022).

Nuccio, V.F., and Condon, S.M., 1996, Burial and Thermal History of the Paradox Basin, Utah and Colorado, and Petroleum Potential of the Middle Pennsylvanian Paradox Formation: Geology and Resources of the Paradox Basin U.S. Geological Survey Bulletin 2000-O, 57–76 p., doi:10.3133/b00O.

Ohlen, H.R., and McIntyre, L.B., 1965, Stratigraphy and Tectonic Features of the Paradox Basin, Four Corners Area: AAPG Bulletin, v. 49, p. 2020–2040, doi:https://doi.org/10.1306/A6633880-16C0-11D7-8645000102C1865D.

Parker, J.WM., and Roberts, J.W., 1966, Regional Devonian and Mississippian Stratigraphy, Central Colorado Plateau: AAPG Bulletin, v. 50, p. 2404–2433, doi:https://doi.org/10.1306/5D25B76D-16C1-11D7-8645000102C1865D.

Penge, J., Munns, J.W., Taylor, B., and Windle, T.M.F., 1999, Rift–raft tectonics: examples of gravitational tectonics from the Zechstein basins of northwest Europe: Geological Society, London, Petroleum Geology Conference Series, v. 5, p. 201–213, doi:10.1144/0050201.

Peterson, J.A., and Hite, R.J., 1969, Pennsylvanian Evaporite-Carbonate Cycles and Their Relation to Petroleum Occurrence, Southern Rocky Mountains: AAPG Bulletin, v. 53, p. 884–908, doi:https://doi.org/10.1306/5D25C807-16C1-11D7-8645000102C1865D.

Poe, P.L., 2018, Characterization And Geochemistry Of Carbonate Caprock Associated With The Gypsum Valley Salt Wall, Paradox Basin, Colorado: Implications For Understanding Lateral Caprock Emplacement [M.S thesis.]: The University of Texas at El Paso, 120 p., https://scholarworks.utep.edu/cgi/viewcontent.cgi?article=1147&context=open_etd (accessed August 2022).

Posey, H.H., and Kyle, J.R., 1988, Fluid-rock interactions in the salt dome environment: An introduction and review: Chemical Geology, v. 74, p. 1–24, doi:https://doi.org/10.1016/0009-2541(88)90143-X.

Pratt, B.R., 2002, Storms versus tsunamis: Dynamic interplay of sedimentary, diagenetic, and tectonic processes in the Cambrian of Montana: Geology, v. 30, p. 423–426, doi:10.1130/0091-7613(2002)030<0423:SVTDIO>2.0.CO;2.

Pratt, B.R., 2010, Peritidal Carbonates, *in* James, N.P., and Dalrymple, R.W., eds., Facies Models 4, Geological Association of Canada, p. 401–419.

Pray, L.C., and Wray, J.L., 1963, Porous Algal Facies (Pennsylvanian) Honaker Trail, San Juan Canyon, Utah, *in* Bass, R.O., Sharps, S.L., Shelf Carbonates of the Paradox Basin, Four Corners Geological Society, Fourth Field Conference, p. 204–234.

Ramsay, J.G., 1967, Folding and Fracturing of Rocks: New York, NY, McGraw-Hill, 568 p.

Raup, O.B., and Hite, R.J., 1992, Lithology of Evaporite Cycles and Cycle Boundaries in the Upper Part of the Paradox Formation of the Hermosa Group of Pennsylvanian Age in the Paradox Basin, Utah and Colorado: Evolution of Sedimentary Basins-Paradox Basin U.S. Geological Survey Bulletin 2000-B, B1–B37 p.

Rasmussen, L., and Rasmussen, D.L., 2009, Burial History Analysis of the Pennsylvanian Petroleum System in the Deep Paradox Basin Fold and Fault Belt, Colorado and Utah, *in* Houston et al., The Paradox Basin Revisited – New Developments in Petroleum Systems and Basin Analysis, Rocky Mountain Association of Geologists, Special Publication, p. 24–94.

Rodine, J.D., and Johnson, A.M., 1976, The ability of debris, heavily freighted with coarse clastic materials, to flow on gentle slopes: Sedimentology, v. 23, p. 213–234, doi:https://doi.org/10.1111/j.1365-3091.1976.tb00047.x.

Rowan, M.G., 2019, Conundrums in loading-driven salt movement: Journal of Structural Geology, v. 125, p. 256–261, doi:10.1016/j.jsg.2018.04.010.

Rowan, M.G., Urai, J.L., Fiduk, J.C., and Kukla, P.A., 2019, Deformation of intrasalt competent layers in different modes of salt tectonics: Solid Earth, v. 10, p. 987–1013, doi:https://doi.org/10.5194/se-10-987-2019.

Scholle, P.A., and Ulmer-Scholle, D.S., 2003, A Color Guide to Petrography of Carbonate Rocks: Grains, textures, porosity, diagenesis: American Association of Petroleum Geologists, Memoir 77, 474 p.

Scott, D.T., 2022, Characterization and Evolution of the Professor Valley Pennsylvanian Salt Body (Paradox Basin, UT) Using Gravity and Magnetotellurics [M.S. thesis]: The University of Texas at El Paso, 84 p., https://scholarworks.utep.edu/cgi/viewcontent.cgi?article=4582&context=open_etd. (accessed August 2022).

Shinn, E.A., 1983, Tidal Flat Environment, *in* Scholle, P.A., Bebout, D.G., Moore, C.H., eds., Carbonate Depositional Environments, American Association of Petroleum Geologists, Memoir 33.

Soreghan, G.S., Keller, G.R., Gilbert, M.C., Chase, C.G., and Sweet, D.E., 2012, Load-induced subsidence of the Ancestral Rocky Mountains recorded by preservation of Permian landscapes: Geosphere, v. 8, p. 654–668, doi:https://doi.org/10.1130/GES00681.1.

Stern, R.J., Anthony, E.Y., Minghua, R., Lock, B.E., Norton, I., Kimura, J.-I., Miyazaki, T., Hanyu, T., Chang, Q., and Hirahara, Y., 2011, Southern Louisiana salt dome xenoliths: First glimpse of Jurassic (ca. 160 Ma) Gulf of Mexico crust: Geology, v. 39, p. 315–318, doi:https://doi.org/10.1130/G31635.1.

Stevenson, G.M., and Baars, D.L., 1986, The Paradox: A Pull-Apart Basin of Pennsylvanian Age, *in* Peterson, J.A., Paleotectonics and Sedimentation in the Rocky Mountain Region, United States, American Association of Petroleum Geologists, Memoir 41, p. 513–539.

Strozyk, F., 2017, The Internal Structure of the Zechstein Salt and Related Drilling Risks in the Northern Netherlands, *in* Soto, J.I., Flinch J.F., Tari, G., eds., Permo-Triassic Salt

Provinces of Europe, North Africa and the Atlantic Margins: Tectonics and Hydrocarbon Potential, Elsevier, p. 115–128, https://doi.org/10.1016/B978-0-12-809417-4.00006-9.

Szabo, E., and Wengerd, S.A., 1975, Stratigraphy and Tectogenesis of the Paradox Basin, *in* Fassett, J.E. and Wengerd, S.A., Canyonlands Country, Four Corners Geological Society, 8th Field Conference, Guidebook, p. 193–210.

Thomas, W.A., 2007, Pennsylvanian sinistral faults along the southwest boundary of the Uncompahgre uplift, Ancestral Rocky Mountains, Colorado: Geosphere, v. 3, p. 119–132, doi:https://doi.org/10.1130/GES00068.1.

Thompson Jobe, J.A., Giles, K.A., Hearon, T.E., Rowan, M.G., Trudgill, B., Gannaway Dalton, C.E., and Jobe, Z.R., 2020, Controls on the structural and stratigraphic evolution of the megaflap-bearing Sinbad Valley salt wall, NE Paradox Basin, SW Colorado: Geosphere, v. 16, p. 297–328, doi:10.1130/GES02089.1.

Trudgill, B.D., 2011, Evolution of salt structures in the northern Paradox Basin: controls on evaporite deposition, salt wall growth and supra-salt stratigraphic architecture: Basin Research, v. 23, p. 208–238, doi:10.1111/j.1365-2117.2010.00478.x.

Tobin, K.J., 2004, A survey of paleozoic microbial fossils in chert: Sedimentary Geology, v. 168, p. 97–107, doi:https://doi.org/10.1016/j.sedgeo.2004.03.006.

Trudgill, B.D., and Arbuckle, W.C., 2009, Reservoir Characterization of Clastic Cycle Sequences in the Paradox Formation of the Hermosa Group, Paradox Basin, Utah: Utah Geological Survey Open-File Report 543, https://doi.org/10.34191/ofr-543.

Warner, L.A., 1978, The Colorado Lineament: A middle Precambrian wrench fault system: GSA Bulletin, v. 89, p. 161–171, doi:https://doi.org/10.1130/0016-7606(1978)89%3C161:TCLAMP%3E2.0.CO;2.

Wengerd, S.A., and Matheny, M.L., 1958, Pennsylvanian System of Four Corners Region: AAPG Bulletin, v. 42, p. 2048–2106, doi:https://doi.org/10.1306/0BDA5BA9-16BD-11D7-8645000102C1865D.

Wengerd, S.A., 1963, Stratigraphic Section at Honaker Trail, San Juan Canyon San Juan County, Utah, *in* Bass, R.O., Sharps, S.L., Shelf Carbonates of the Paradox Basin, Four Corners Geological Society, Fourth Field Conference, p. 235–243.

Williams-Stroud, S.C., 1994, Solution to the Paradox? Results of some chemical equilibrium and mass balance calculations applied to the Paradox Basin evaporite deposit: American Journal of Science, v. 294, p. 1189–1228, doi:10.2475/ajs.294.10.1189.

Williams-Stroud, S.C., 1994, The Evolution of an Inland Sea of Marine Origin to a Non-Marine Saline Lake: The Pennsylvanian Paradox Salt, *in* Renaut, R.W., Last, W.M., Sedimentology and Geochemistry of Modern and Ancient Saline Lakes Models, Society for Sedimentary Geology, SEPM Special Publication, v. 50, p. 293–306, https://doi.org/10.2110/pec.94.50.0293.

Wilson, J.L., and Jordan, C., 1983, Middle Shelf Environment, *in* Scholle, P.A., Bebout, D.G., Moore, C.H., eds., Carbonate Depositional Environments, American Association of Petroleum Geologists, Memoir 33.

Vita

Madison Clare Woelfel, the second of five siblings, was born and raised in Española, New Mexico. After graduating as valedictorian of McCurdy High School in 2012 and completing an internship with Los Alamos National Laboratories, she began her undergraduate studies at New Mexico State University. After a year at NMSU, she transferred schools looking for a more challenging and rewarding STEM-oriented experience. She ultimately attained her B.S. in Earth Sciences with the Geology Option and a Minor in Mathematics from New Mexico Institute of Mining and Technology in May 2017. While at NMT, she participated in many clubs, worked for the New Mexico Bureau of Geology and Mineral Resources, and completed field camp.

After graduating with her B.S., she took a break from academia that ended when she began pursuing her Master of Science degree in Geological Sciences at The University of Texas at El Paso in August 2021. At UTEP, Madison explored her geologic passion – carbonate diagenesis. She also worked as a teaching assistant for Historical Geology lectures and labs, leaving her mark when she created a suite of laboratory activities that emphasized hands-on, collaborative activities. She even helped inspire an undergraduate student that changed their major to geology.

While conducting research at UTEP, Madison was awarded research grants from AAPG, GSA, and SEPM as well as the George B. McBride Graduate Fellowship Endowment. She was awarded scholarships from the West Texas Geological Society (E. Russell Lloyd Memorial and WinGS Scholarships), Permian Basin Section of SEPM, and the Southwest Section of AAPG. She received awards at the 36th and 37th annual DEERS Colloquiums, a research award at the HGS Student Expo, and the John and Vida White Endowment Award. After attending the HGS Student Expo, she became a member of the committee to help promote future geoscientists. At the end of her M.S. studies, she began an internship with ExxonMobil working in unconventional reservoirs.

Contact Information: woelfel.madison@gmail.com

This thesis was typed by Madison Woelfel.